Work Order No. 582-20-12109-016
Contract No. 582-19-90500
Tracking No. 2020-07
Task 7.2

Prepared for:

Texas Commission on Environmental Quality
12100 Park 35 Circle MC 164
Austin, TX 78753

Prepared by:

Ramboll US Corporation
7250 Redwood Blvd., Suite 105
Novato, California 94945

November 13, 2020

Near-Real Time Exceptional Event Modeling

Final Report

PREPARED UNDER A CONTRACT FROM THE
TEXAS COMMISSION ON ENVIRONMENTAL QUALITY

The preparation of this document was financed through a contract from the State of Texas through the Texas Commission on Environmental Quality.
The content, findings, opinions and conclusions are the work of the author(s) and do not necessarily represent findings, opinions or conclusions of the TCEQ.

RAMBOLL

Near-Real Time Exceptional Event Modeling

Ramboll
7250 Redwood Boulevard
Suite 105
Novato, CA 94945
USA

T +1 415 899 0700
https://ramboll.com

Contents

Table of Figures

Table of Tables

LIST OF ACRONYMS AND ABBREVIATIONS

AIRS	Atmospheric Infrared Sounder
AOD	Aerosol optical depth
AQRP	Air Quality Research Program
ARL	Air Resources Laboratory
BCs	Boundary Conditions
CAMS	Continuous Air Monitoring Station
CAMx	Comprehensive Air quality Model with extensions
CMAQ	Community Multiscale Air Quality Model
CO	Carbon Monoxide
CST	Central Standard Time
DFW	Dallas-Fort Worth Area
EBI	Euler Backward Iterative method
EDGAR	Emissions Database for Global Atmospheric Research
EOSDIS	Earth Observing System Data and Information System
EPA	Environmental Protection Agency
EPS3	Emissions Processing System version 3
FAIRMODE	Forum for Air quality Modelling in Europe
FIM	Fire Impact Modeling
FINN	Fire INventory from NCAR
GEOS	Goddard Earth Observing System
GEOS-5	Goddard Earth Observing System Version 5
GDAS	GFS Data Assimilation System
GFS	Global Forecasting System
GOES	Geostationary Operational Environmental Satellite
HGB	Houston-Galveston-Brazoria Area
HMS	Hazard Mapping System
HTAP	Hemispheric Transport of Air Pollution
HYSPLIT	Hybrid Single-Particle Lagrangian Integrated Trajectory Model
ICs	Initial Conditions
IGBP	International Geosphere Biosphere Programme
ISD	Integrated Surface Data
km	kilometer
LAI	Leaf Area Index
LI	Local Increment
LSM	Land Surface Model
m	meter
mb	millibars
MB	Mean Bias

MDA1	daily maximum 1-hour average
MDA8	daily maximum 8-hour average
ME	Mean Error
MEGAN	Model of Emissions of Gases and Aerosols from Nature
MM5	Fifth-Generation Penn State/NCAR Mesoscale Model
MODIS	Moderate Resolution Imaging Spectroradiometer
MPI	Message Passing Interface
mph	miles per hour
MQI	Model Quality Indicator
MQO	Model Quality Objective
MSKF	Multi-Scale Kain Fritsch
NAAQS	National Ambient Air Quality Standard
NAM	North American Model
NASA	National Aeronautics and Space Administration
NCAR	National Center for Atmospheric Research
NCDC	National Climatic Data Center
NCEP	National Centers for Environment Prediction
NCL	NCAR Command Language
NDAS	NAM Data Assimilation System
NMB	Normalized Mean Bias
NME	Normalized Mean Error
NO	Nitric Oxide
NOAA	National Oceanic and Atmospheric Administration
NOx	Oxides of Nitrogen
NRT	Near Real-Time
NRTEEM	Near-Real Time Exceptional Event Modeling
OMP	Open Multi-Processing
OMPS	Ozone Mapping and Profiler Suite
PBL	Planetary Boundary Layer
PM	Particulate Matter
$PM_{2.5}$	Particulate Matter < 2.5 ug m^{-3}
ppb	parts per billion
PPM	Piecewise Parabolic Method
PVU	potential vorticity unit
Q/D	Emissions/Distance
QAS	Quality control audit in progress
Q-Q	Quantile-Quantile
RAMS	Regional Atmospheric Modeling System
RAP	WRF-based Rapid Refresh model

RAQMS	Real Time Air Quality Monitoring System
READY	Real-time Environmental Applications and Display sYstem
RMS	Root Mean Square
RMSE	Root Mean Squared Error
RPO	Regional Planning Organization
RRTMG	Rapid Radiative Transfer Model for GCM applications
RV	Reference Value
SIP	State Implementation Plan (for the ozone NAAQS)
TCEQ	Texas Commission on Environmental Quality
TCs	Top Conditions
tpd	tons per day
TUV	Tropospheric UltraViolet radiative transfer model
ug	micrograms
US	United States
UTC	Coordinated Universal Time
UTEP	University of Texas El Paso
VOC	Volatile Organic Compound
WACCM	Whole Atmosphere Community Climate Model
WRF	Weather Research and Forecast model
WSM6	WRF Single-Moment 6-Class Microphysics Scheme
YSU	Yonsei University WRF planetary boundary layer parameterization

EXECUTIVE SUMMARY

Ramboll assisted the TCEQ by deploying a Near-Real Time Exceptional Event Modeling (NRTEEM) system that estimates ozone impacts for three potential sources of background ozone in Texas: (1) biomass burning in Mexico and Central America; (2) stratospheric ozone intrusion; (3) anthropogenic emissions in Mexico.

The NRTEEM system uses the Weather, Research and Forecasting (WRF) meteorological model, the Comprehensive Air Quality Model with Extensions (CAMx) air quality model, biomass burning emissions from Fire INventory of NCAR (FINN) and anthropogenic emissions data provided by the TCEQ. Model configurations are similar to those used for the TCEQ's State Implementation Plan (SIP) modeling. This report describes the implementation of the 2020 NRTEEM system and our evaluation of system performance. We provide specific recommendations for future NRTEEM system improvements.

We operated the NRTEEM system during March 15-October 15, 2020 and delivered model results via a website. The NRTEEM system delivers results with a 1-day lag to acquire biomass burning emissions that are derived from satellite observations of Earth.

Our goal is to make NRTEEM a useful tool for TCEQ to quickly identify potential exceptional events.

Updates from 2019 NRTEEM System

- Added new 4 km WRF and CAMx domains encompassing the El Paso region.
- Implemented a new way of summarizing model performance that incorporates measurement uncertainty through the use of "target plots".
- We used a new Sensitivity Testing Phase during March 15-April 15, 2020 to determine the best configuration for the Operational Modeling Phase during April 15-October 15, 2020. Specific goals of the Sensitivity Testing Phase were to:
  - More easily identify fires associated with a potential exceptional event; and
  - Improve simulation of ozone in the upper troposphere and lower stratosphere

Main Findings

- Using WRF's hybrid sigma-pressure vertical coordinate and a new CAMx 32-layer vertical layer mapping better resolves the upper troposphere and lower stratosphere. This new vertical layer structure results in a geographic distribution of stratospheric ozone impacts that is more consistent with the conceptual model of stratospheric ozone intrusions having a greater influence on high elevation areas like El Paso than on low elevation areas like Houston.
- Our model performance evaluation finds that 2020 NRTEEM does not agree with observations as well as the 2019 model. COVID-related changes in activity may reduce the correspondence of actual emissions to modeled emissions and may explain some of this discrepancy.
- Analysis of NRTEEM-diagnosed stratospheric intrusion events in 2019 and 2020 suggests that NRTEEM is able to indicate the influence of these events on surface ozone and can be used to identify events where a diagnostic exceptional event analysis is warranted.
- Overall, we find model performance is acceptable and that NRTEEM was able to identify potential exceptional events and instances of Texas ozone impacts from Mexico anthropogenic emissions in 2020.

Recommendations

We provide the following recommendations to improve the usefulness of the modeling system:

- Develop a method to identify fires responsible for potential exceptional events by tracking tracers associated with fire emissions across multiple days. These fires can later be tagged for source apportionment analysis to quantify ozone impacts at specific locations.
- Provide Q/D plots through the NRTEEM website for fires above a defined Q/D threshold
- Investigate methods to improve persistent negative biases found on the highest observed ozone days
- Investigate alternate methods of model performance evaluation that incorporate measurement uncertainty
- Investigate alternate sources of near real-time fire emissions if available
- Use the latest available versions of WRF and CAMx model code
- Use an updated emissions inventory from TCEQ if available
- Work with TCEQ to refine the Mexico emission inventory used in the NRTEEM modeling
- Other improvements proposed by TCEQ

In addition, we recommend that TCEQ investigate using WRF’s hybrid vertical coordinate system along with increased vertical resolution in the upper troposphere/lower stratosphere for their SIP modeling efforts.

1.0 BACKGROUND

The purpose of this study is to implement and refine the photochemical grid model system used by the TCEQ for the State Implementation Plan (SIP) planning by modelling ozone in a near real-time (NRT) mode in order to identify potential exceptional event impacts. We evaluate ozone impacts from fires, Mexican anthropogenic emissions and stratospheric ozone and evaluate model performance statistics to measure the impacts of different model configurations and identify areas for improvement.

The 2020 NRTEEM system is based on the 2019 NRTEEM project which was developed from the 2018 NRTEEM, 2017 FIM and 2013-2016 NRT projects. Lessons learned from the NRTEEM system and sensitivity simulations run in previous NRT projects have aided us in our design of the 2020 base model run configuration, in terms of performance and reliability.

We presented a complete overview of the 2013 project in Johnson et al. (2013). We found that the ozone model performed well when high ozone was observed. A general lack of cloud cover and stagnant conditions from WRF meteorology led to ozone over-predictions when observed ozone was low to moderate. Johnson et al. (2015) provides a summary of the 2014 project. The 2014 modeling improved overall ozone bias and error relative to the 2013 modeling, despite much lower observed ozone overall. In the 2015 project, we found improvement in reducing persistent positive ozone bias and discovered that choice of analysis fields in WRF has a substantial impact on ozone (Johnson et al., 2016a). Finally, the 2016 project found further improvement in reducing positive ozone bias, though background ozone was still consistently overestimated in Houston and, to a lesser extent, Dallas. We constructed an ensemble model by averaging together results from five simulations to investigate whether a forecast ensemble could demonstrate greater skill than the individual simulations that go into the ensemble. Lack of sufficient ensemble member diversity hampered our ability to produce a useful ensemble prediction (Johnson et al., 2016b). The 2017 Fire Impact Modeling (FIM) system demonstrated usefulness by identifying potential days when exceptional events may be responsible for ozone exceedances (Johnson et al., 2017). In 2018, we developed and deployed the NRTEEM system which expanded upon the FIM system by adding two new potential sources of exceptional events: 1) stratospheric ozone intrusion and 2) Mexican anthropogenic emissions (Johnson et al., 2018). In 2019, the NRTEEM system added a methodology to mask out industrial flares from the NRT wildfire emissions by removing all wildfire emissions for locations with urban landcover and added a cap to lateral boundary conditions for ozone in the top two model layers in the base model to provide a better estimate of stratospheric ozone at the surface (Johnson et al., 2019).

This report describes the various components of the development of the NRTEEM system and presents an evaluation of potential exceptional event impacts and other model results.

First, we detail our modeling cycle in Section 2.1, including information about run schedule and data sources used. We then specify our WRF and CAMx configurations in Section 2.4 and 2.5 and describe our sensitivity tests and why they were selected in Section 2.6. Next, we present our model evaluation results in Section 3, including potential exceptional events. Finally, in Section 4 we discuss various recommendations as improvements to the 2020 NRTEEM system.

2.0 NEAR-REAL TIME EXCEPTIONAL EVENT MODELING SYSTEM

This section describes the components of the NRTEEM system. We detail our modeling cycle, including information about run schedule and data sources used. We then describe our WRF and CAMx configurations, CAMx sensitivity tests and finally, features of the NRTEEM website.

2.1 Modeling Cycle

We utilize the modeling system as developed for the 2019 NRTEEM project which was developed from the 2018 NRTEEM, 2017 FIM and 2013-2016 NRT projects. Ramboll runs the NRTEEM system for 24 simulation hours (1 full day from midnight to midnight in CST). The term initialization is used because the meteorological simulation is started from initial conditions at this time. Ramboll uses 0.25 degree Global Forecasting System (GFS) data assimilation system (GDAS) analysis data (Ek et al., 2014) as initial conditions for the WRF meteorological model. This GDAS data is also used for boundary conditions and data assimilation. Because the NRTEEM system runs a modeling cycle with at least a 1-day lag, observations and analyses are available to the WRF model for the entire modeling cycle and therefore no GFS forecast data needs to be used. We are not able to utilize the NAM (North American Mesoscale) data assimilation system (NDAS) analysis data because it does not cover our expanded 36 km domain used in the NRTEEM system.

Model images were uploaded to the NRTEEM website as model results were processed. Images for the entire modeling period (March 15-October 15, 2020) were generated for:

- Hourly ozone, NO, NOx, CO concentrations
- Daily maximum 1-hour and 8-hour average ozone concentrations
- Hourly 2-m temperature, PBL height, wind speed, wind vectors, incoming solar radiation
- Hourly formaldehyde/NO_2 indicator ratio for VOC or NOx sensitivity of ozone formation

Users can select images for any modeling cycle for the base case and all sensitivity simulations.

As in previous projects, Ramboll delivered zoom-able, interactive statistics and time series charts to the site which use observations from the TCEQ Continuous Air Monitoring Station (CAMS) and other monitors in Arkansas, Oklahoma, Louisiana and Colorado. We added statistics and time series charts for New Mexico observations in 2020 due to their proximity to El Paso. Normalized Mean Bias (NMB), Normalized Mean Error (NME) and correlation coefficient (r) statistics are available for ozone, NO, NOx, CO, 2-meter temperature, wind speed, wind direction and solar radiation.

2.2 Modeling Domains

Figure 2-1 presents the 36/12/4 km CAMx modeling domains used for the NRTEEM system, including the 4 km CAMx domain over El Paso (orange) that is new for 2020 NRTEEM. The WRF domains are excluded from this figure for clarity. The 36 km CAMx modeling domain (black) includes all of Mexico, the Yucatan Peninsula, Belize and much of Guatemala. The 12 km (blue) and East Texas 4 km (green) domains are the TCEQ SIP modeling domains.

Figure 2-2 shows the El Paso WRF (brown) and CAMx (orange) 4 km domains in detail. The CAMx domain is centered over El Paso and includes nearby cities Juarez, Mexico and Sunland Park and Las

Cruces in New Mexico. This domain was originally developed by TCEQ for modeling the El Paso near-non attainment area under the Rider 7/8 Program, but this modeling was never performed[1].

In Table -2-1, we present the vertical layer mapping tables used for 2019 NRTEEM (28 CAMx layers) and the 2020 NRTEEM operational phase (32 CAMx layers). Both sets of vertical layer structures use the same 43 WRF layers. We provide more information about the testing of the two vertical layer structures, the new WRF hybrid vertical coordinate and our rationale for choosing the 32-layer structure with the hybrid coordinate in Section 2.6.

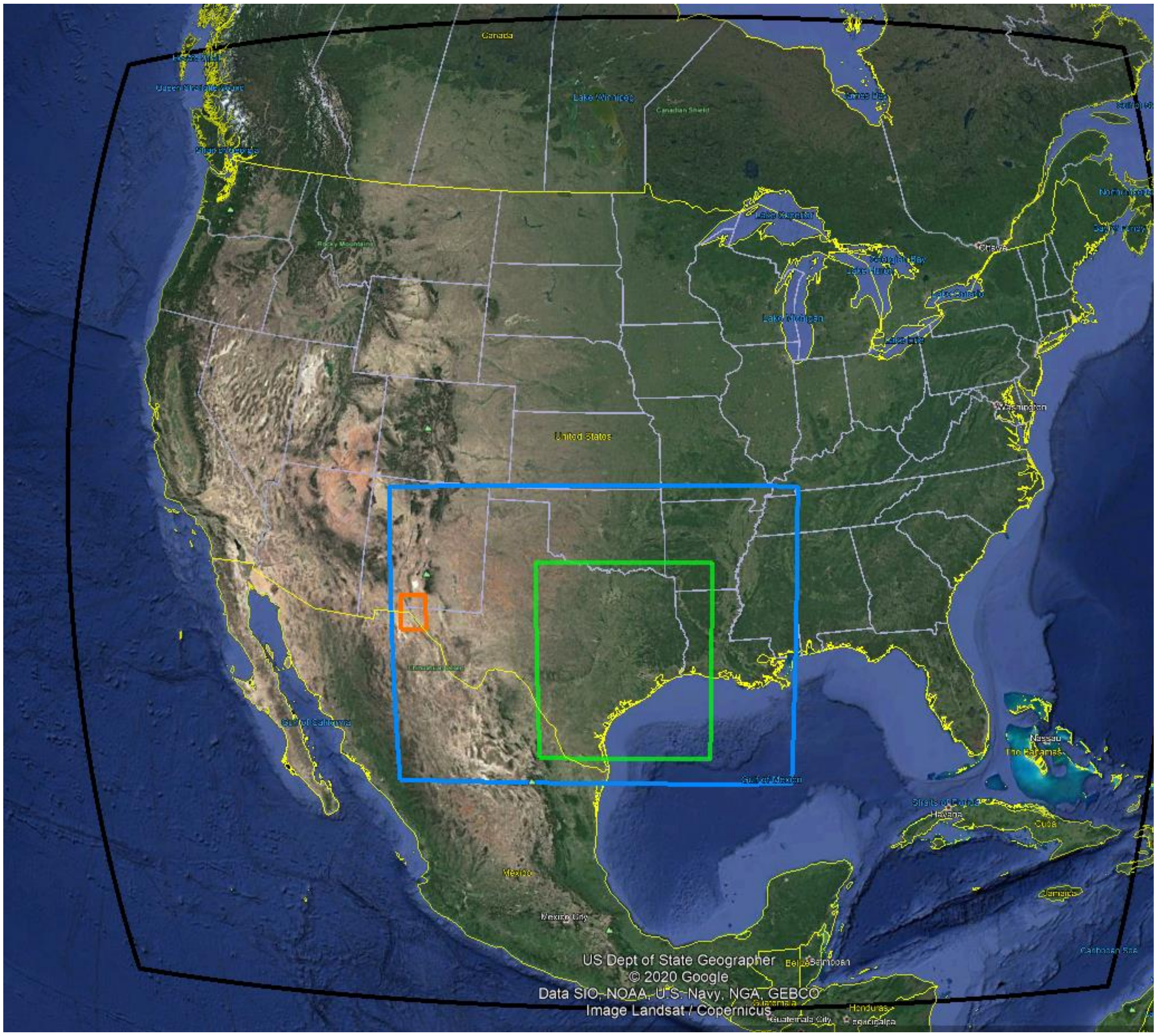

CAMx Domain	Range (km)		Number of Cells		Cell Size (km)	
	Easting	Northing	Easting	Northing	Easting	Northing
RPO 36km Domain	(-2736, 2592)	(-2808, 1944)	148	132	36	36
Texas 12km Domain	(-984, 804)	(-1632, -312)	149	110	12	12

[1] Personal communication, Doug Boyer, TCEQ.

Texas 4km Domain	(-328, 436)	(-1516, -644)	191	218	4	4
El Paso 4km Domain	(-940, -824)	(-940, -788)	29	38	4	4

Figure 2-1. WRF and CAMx 36/12/4 km modeling domains used in the NRTEEM system.

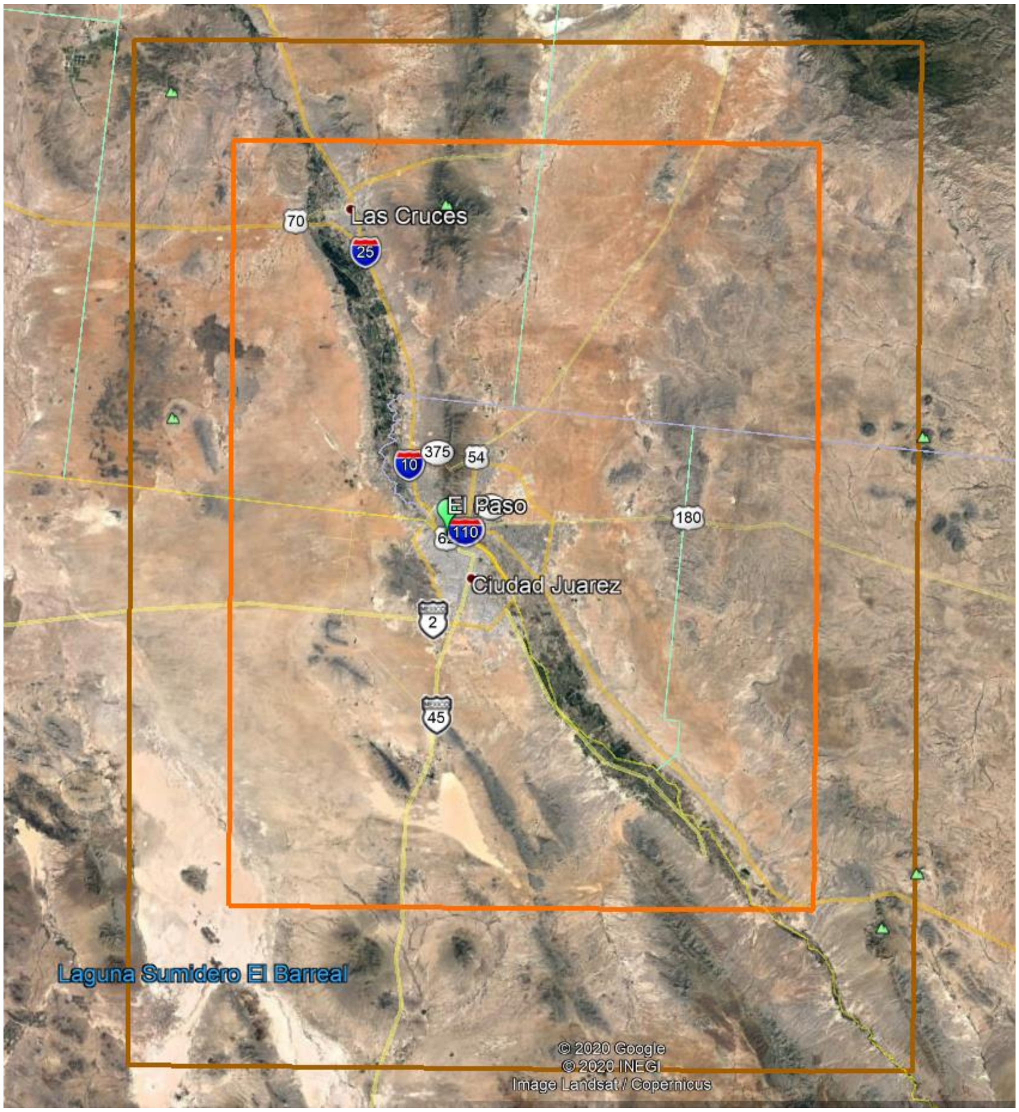

Figure 2-2. Horizontal extents of the WRF (brown) and CAMx (orange) 4 km domains (map from Google Earth).

Table -2-1. Vertical layer mapping from 43 WRF layers to 28 CAMx layers (2019 NRTEEM) and 32 CAMx layers (2020 NRTEEM).

WRF				CAMx 28-layer			CAMx 32-layer		
Layer	Eta	Pressure (mb)	Top (m)	Layer	Top (m)	Thickness (m)	Layer	Top (m)	Thickness (m)
43	0.0000	50.00	20576				32	20576	2494
42	0.0100	59.63	19458						
41	0.0250	74.08	18082				31	18082	2656
40	0.0450	93.35	16616						
39	0.0650	112.61	15427				30	15427	2258
38	0.0900	136.69	14198	28	14198	2077			
37	0.1150	160.77	13169				29	13169	1948
36	0.1450	189.67	12120	27	12120	3586			
35	0.1750	218.57	11221				28	11221	1849
34	0.2100	252.28	10304						
33	0.2500	290.81	9372				27	9372	1599
32	0.2900	329.34	8534	26	8534	2030			
31	0.3300	367.87	7773				26	7773	1269
30	0.3700	406.40	7073						
29	0.4050	440.12	6504	25	6504	1040	25	6504	1040
28	0.4400	473.83	5969						
27	0.4750	507.54	5464	24	5464	870	24	5464	870
26	0.5100	541.26	4985						
25	0.5400	570.16	4594	23	4594	737	23	4594	737
24	0.5700	599.05	4219						
23	0.6000	627.95	3857	22	3857	684	22	3857	684
22	0.6300	656.85	3509						
21	0.6600	685.75	3174	21	3174	324	21	3174	324
20	0.6900	714.64	2849	20	2849	314	20	2849	314
19	0.7200	743.54	2535	19	2535	304	19	2535	304
18	0.7500	772.44	2231	18	2231	247	18	2231	247
17	0.7750	796.52	1984	17	1984	241	17	1984	241
16	0.8000	820.60	1743	16	1743	235	16	1743	235
15	0.8250	844.68	1508	15	1508	230	15	1508	230
14	0.8500	868.76	1279	14	1279	135	14	1279	135
13	0.8650	883.21	1144	13	1144	134	13	1144	134
12	0.8800	897.66	1010	12	1010	132	12	1010	132
11	0.8950	912.11	878	11	878	130	11	878	130
10	0.9100	926.56	748	10	748	86	10	748	86
9	0.9200	936.19	662	9	662	85	9	662	85
8	0.9300	945.82	577	8	577	84	8	577	84
7	0.9400	955.46	493	7	493	84	7	493	84
6	0.9500	965.09	409	6	409	83	6	409	83
5	0.9600	974.72	326	5	326	82	5	326	82
4	0.9700	984.35	243	4	243	82	4	243	82
3	0.9800	993.99	162	3	162	81	3	162	81
2	0.9900	1003.62	80	2	80	48	2	80	48
1	0.9960	1009.40	32	1	32	32	1	32	32
0	1.0000	1013.25	0	0	0		0	0	

2.3 Models, Configurations, and Data

We present a general overview of the input/output and processing streams for the NRTEEM system in Figure 2-3. A description of the inputs used and configuration of the WRF and CAMx models follows.

	Emissions	Geography	Meteorology	Photolysis	Air Quality
Data	TCEQ EI & FINN fires	LULC	NOAA/NCEP GFS analysis	Ozone column	NCAR WACCM global forecast
Pre-processing	EPS3 & MEGAN		WRF v4.1.4 WRFCAMx v4.8	TUV	WACCM2CAMx
Core Model			CAMx version 7.0		
Post-processing			NCL NRTEEM website		

Figure 2-3. CAMx flow chart detailing input/output and processing streams for the NRTEEM system.

2.4 Meteorology

We are utilizing WRF v4.1.4 (released February; Skamarock et al., 2019) for the NRTEEM system, the latest version of the model available at the start of the project. We provide the WRF physics options in Table 2-2. This configuration is similar to that used for the TCEQ SIP modeling. We are using MPI (Message Passing Interface) for our WRF simulations, utilizing 28 cores. Previous experience with WRF guided us to this configuration, as performance gains from either increasing the number of cores or using a hybrid MPI/OMP (Open Multi-Processing) approach were found to be minimal for WRF, in contrast to CAMx.

Table 2-2. WRF v4.1.4 physics options used in the NRTEEM system.

WRF Physics Option	Option Selected	Notes
Vertical Coordinate System	Hybrid Sigma-Pressure	Replaced eta vertical coordinate used in 2019 NRTEEM; WRFCAMx updated to account for Hybrid Sigma-Pressure coordinate
Microphysics	WRF Single-Moment 6-class (WSM6)	A scheme with ice, snow and graupel processes suitable for high-resolution simulations.
Longwave Radiation	RRTMG	Rapid Radiative Transfer Model. An accurate scheme using look-up tables for efficiency. Accounts for multiple bands, and microphysics species.
Shortwave Radiation	RRTMG	Rapid Radiative Transfer Model. An accurate scheme using look-up tables for efficiency. Accounts for multiple bands, and microphysics species.
Surface Layer Physics	MM5 similarity	Based on Monin-Obukhov with Carslon-Boland viscous sub-layer and standard similarity functions from look-up tables
LSM	Noah	NCEP/NCAR land surface model with soil temperature and moisture in four layers, fractional snow cover and frozen soil physics.
PBL scheme	Yonsei University (YSU)	Non-local-K scheme with explicit entrainment layer and parabolic K profile in unstable mixed layer
Cumulus parameterization	MSKF WRF	Multi-Scale Kain-Fritsch (MSKF) cumulus parameterization includes feedback of subgrid cloud information to the radiation schemes.

2.5 CAMx Configuration

Ramboll selected CAMx version 7.00 (released June 2020; Ramboll 2020) for the NRTEEM system, the latest version of the model at the start of the project. The 2019 NRTEEM system used CAMx version 6.50.

Table 2-3 gives the CAMx configuration options that are currently in use. We utilize a hybrid MPI/OMP configuration for CAMx. We determined from model benchmarking that 14 MPI slice x 4 OMP thread setup was the optimum configuration for this application.

Table 2-3. CAMx v7.00 options used for the NRTEEM system.

Science Options	Configuration	Comments
Model Code	CAMx Version 7.00	Released June 2020
Time Zone	Central Standard Time (CST)	
Vertical Layers	28 layers (model top approximately 100 mb)/32 layers (model top approximately 50 mb)	Both vertical layer structures testing during Sensitivity Testing Phase; Lowest 21 CAMx layers match lowest 21 WRF layers in each
Chemistry Gas Phase Chemistry Aerosol Chemistry	 CB6r4 None	 CB6r4 combines a condensed set of reactions involving ocean-borne inorganic iodine from the CB6r2h full halogen mechanism with the temperature- and pressure-dependent organic nitrate branching ratio introduced in CB6r3. Primary PM smoke tracers from NRT FINN fire emissions are inert
Plume-in-Grid	None	Turned off; run-time consideration for NRTEEM modeling
Photolysis Rate Adjustment	In-line TUV	Adjust photolysis rates for each grid cell to account for clouds and primary PM smoke tracers. Certain photolysis rates adjusted for temperature and pressure.
Meteorological Processor Subgrid Cloud Diagnosis	WRFCAMx CMAQ-based	Sub-grid clouds diagnosed from WRF grid-resolved thermodynamic properties.
Horizontal and Vertical Transport Eddy Diffusivity Scheme Diffusivity Lower Limit	 K-Theory Kz_min = 0.1 m^2/s	Vertical diffusivity (Kv) fields patched to enhance mixing: 1. over urban areas in lowest 100 m (OB70 or “Kv100” patch) 2. in areas where convection is present, by extending the daytime PBL Kv profile through capping cloud tops (cloud patch)
Dry Deposition	Wesely (1989)	Utilizes 11 landuse categories and does not use LAI
Numerical schemes Gas Phase Chemistry Solver Horizontal Advection Scheme	 Euler Backward Iterative (EBI) Piecewise Parabolic Method (PPM) scheme	As used in TCEQ SIP modeling

We are using the following CAMx inputs for the NRTEEM system:

- Initial conditions and boundary conditions extracted from NRT Whole Atmosphere Community Climate Model (WACCM) chemical forecasts from NCAR (https://www.acom.ucar.edu/waccm/forecast/). Chemical forecasts are run each day using WACCM, driven by GEOS-5 meteorology and including the standard (100 species) chemical mechanism.
- Initial conditions were extracted only for the initialization of the February 14, 2019 modeling cycle; subsequent cycles restarted from the previous cycle.
- 2020 day-of-week specific anthropogenic emissions inventory provided by the TCEQ
- Month-specific elevated point source emissions provided by the TCEQ
- 2010 EDGAR global 0.1 degree emissions based on EPA's HTAP emissions modeling platform used outside TCEQ 36 km domain.
- MEGAN v3.1 biogenic emissions using current WRF modeling cycle meteorology (A bug was recently discovered that slightly reduces soil NO emissions at night. We do not expect that this bug had a substantial impact on model performance.)
- WRFCAMx v4.8 using YSU Kv methodology
- Kv landuse patch up to 100 m and Kv cloud patch applied
- O3MAP: 2018 monthly averages from 1 degree Ozone Mapping and Profiler Suite (OMPS) satellite ozone column data
- Photolysis rates files generated using O3MAP 2018 monthly averages
- Land use / land cover inputs from TCEQ's HGB SIP modeling database; MODIS IGBP (International Geosphere Biosphere Programme) land use / land cover used outside TCEQ 36 km
    - NRT FINN fire emissions using more realistic (rapid) NOx to NOy conversion in smoke plumes using vegetation type dependent species mapping factors (see Table 2-4) as developed for 2018 NRTEEM (Johnson et al., 2018)

Table 2-4. NOx-to-NOy FINN fire emissions species mapping factors by vegetation type. Factors obtained from 2015 Texas Air Quality Research Program (AQRP) Fires project (McDonald-Buller et al., 2015).

		Vegetation Type Scale Factor		
Species	**FINN**	**A**	**B**	**C**
NO	NOx	0.000	0.000	0.000
NO2	NOx	0.736	0.421	0.451
PAN	NOx	0.056	0.144	0.128
PANX	NOx	0.008	0.104	0.072
NTR2	NOx	0.020	0.050	0.050
HNO3	NOx	0.180	0.280	0.300

A: Grasslands/Savanna/Woody Savanna/Shrublands/Croplands
B: Tropical Forest
C: Temperate Forest

2.6 Sensitivity Testing Phase

The NRTEEM operating schedule for 2020 was as follows:

- March 15 – April 15, 2020: Sensitivity testing phase
- April 15 – October 15, 2020: Operational modeling phase

This section summarizes the NRTEEM system's performance during the testing phase, describes the sensitivity tests performed during the sensitivity testing phase and includes justification for configurations chosen for the operational modeling phase.

2.6.1 CAMx Sensitivity Simulations

The testing phase consisted of a Base run and 5 sensitivity runs. Table 2-5 shows the CAMx sensitivity simulations performed for the NRTEEM testing phase. The goals of the sensitivity testing phase were:

- More easily identify fires associated with a potential exceptional event
- Improve simulation of ozone in the upper troposphere and lower stratosphere

Table 2-5. List of CAMx sensitivity simulations performed for the NRTEEM testing phase, March 15 – April 15, 2020.

Number	Run	Description
1	Base	Includes NRT FINN fire emissions and fire tagging with 5 km fire grouping threshold No capping Top Conditions/Boundary Conditions (TCs/BCs) Hybrid 28-layer vertical layer mapping
2	32 Layers	Same as Base, but use 32 vertical layers to improve model representation of upper troposphere and lower stratosphere
3	Group Fires 10 km	Same as Base, but extend fire grouping threshold from 5 to 10 km
4	No Fires	Same as Base, but exclude FINN fire emissions
5	Stratospheric Ozone	Cap ozone TCs at 60 ppb; cap ozone for BC layers aloft at 60 ppb
6	Stratospheric Ozone 32 Layers	Same as Stratospheric Ozone run, but use 32 vertical layers

2.6.1.1 Fire Tagging Procedure

The purpose of the fire tagging procedure is to more easily identify fires associated with a potential exceptional event. EPA Guidance[2] suggests that a Q/D (emissions/distance) metric be used to conduct a screening assessment of potential ozone impacts from fires. Specifically, Q/D is calculated as the sum of wildfire NOx and VOC emissions in tons per day divided by the distance from the wildfire to a monitoring site in kilometers. EPA's Q/D criterion for a Tier II exceptional event is 100 tpd/km.

FINN fire inventories consist of fires that are always less than or equal to 1 km^2 in size because of the pixel size of the MODIS instrument. If these fire points are treated as separate fires, the Q/D metric will be underestimated for large wildfires that consist of multiple FINN fire points. Therefore, fire points that are within 5 km (or 10 km in the Group Fires 10 km sensitivity run) of one another are assumed to be part of the same fire; the virtual areas of each of these points are added together so they have characteristics of a larger fire.

The fire tagging procedure associates an inert smoke tracer species with each fire group. The addition of the fire tracer species imposes a computational burden on the NRTEEM system. CAMx timing tests found an upper limit of 200 fire groups for operational feasibility within NRTEEM.

The procedure for tagging fire emissions in the model is described below:

[2] https://www.epa.gov/sites/production/files/2018-10/documents/exceptional_events_guidance_9-16-16_final.pdf

1. Group FINN fires into groups within 5 or 10 km threshold
2. Tag all FINN fire groups in Texas
3. Calculate Q/D for fire groups outside Texas at all 100 Continuous Air Monitoring Stations (CAMS)
4. Find maximum Q/D across all CAMS for each fire group and rank from largest to smallest
5. Tag all fire groups in 2 and then 4 until 200 fire groups are reached

2.6.1.2 Vertical Layer Structure Comparison

All CAMx simulations performed for the sensitivity testing phase are driven by meteorological inputs produced from the same WRF configuration. Since its inception, WRF has used the eta (sometimes called sigma or "terrain-following") vertical coordinate system. One weakness of the eta coordinate is that variations in terrain (especially steep topography) can increase numerical errors in the model. To reduce these errors, Park et al., (2018) developed a hybrid sigma–pressure coordinate that is now included as the default vertical coordinate system for the WRF model (Skamarock et al., 2019). The 2020 NRTEEM configuration has been updated to include the hybrid sigma-pressure vertical coordinate system.

<u>Comparison of Eta and Hybrid Vertical Coordinate Systems</u>

In Figure 2-4, we present vertical cross sections of layer interface heights over the Rocky Mountains during a strong near-surface wind event (Park et al., 2018). The left panel shows the results using the eta or terrain-following vertical coordinate and the right panel shows the same results but using the hybrid vertical coordinate. The eta coordinate cross-sections show the influence of terrain extending high into the stratosphere. This is a representation of numerical noise and results in erroneous vertical motion in the model. In CAMx, erroneous vertical motion can help transport stratospheric ozone toward the surface. Park et al., (2018) found that the simulation using the eta vertical coordinate produced high turbulence forecasts aloft which were not observed by pilots or soundings. In contrast, the same simulation using the hybrid vertical coordinate produced lower turbulence forecasts that agreed more closely with observations. The hybrid vertical coordinate cross-sections show a gradual damping of terrain effects with increasing altitude until the layer interfaces are flat aloft. The purpose of using the hybrid vertical coordinate in the NRTEEM system is to better represent ozone in the upper troposphere and lower stratosphere. Eliminating this source of numerical noise reduces spurious downward transport of stratospheric ozone.

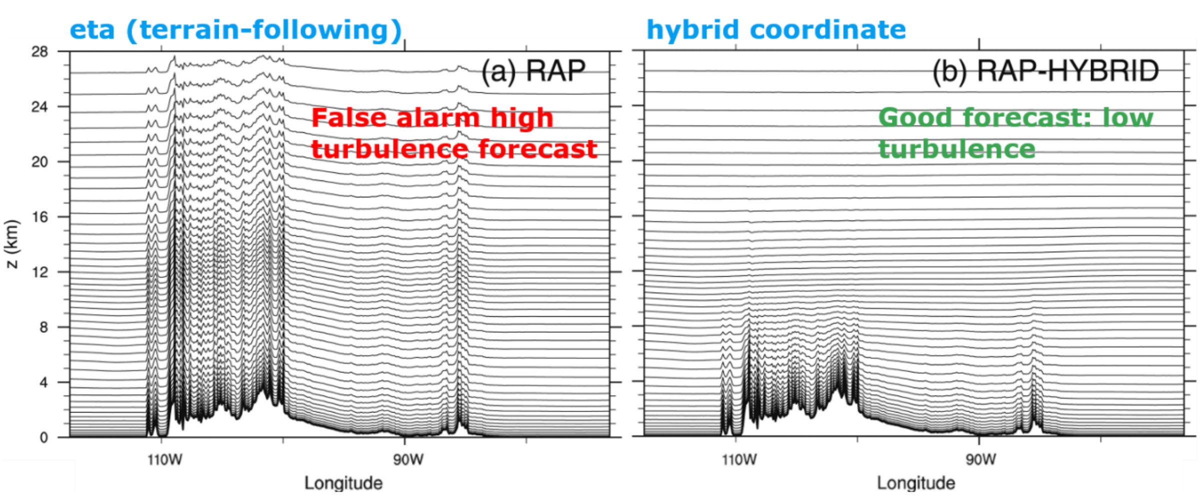

Figure 2-4. Cross-sections of layer interface heights over the Rocky Mountains for the eta (left panel) and hybrid (right panel) vertical coordinates for the WRF-Based Rapid Refresh (RAP) model. Adapted from Park et al., (2018).

Figure 2-5 shows the vertical layer structure mapping from WRF to CAMx for the Base (28 layer) and 32 Layer model configurations. The green boxes highlight differences in how the WRF layers are collapsed differently between the two models. All layers from the surface to 440 mb are identical between the two models. Above 440 mb, the 32-layer mapping has finer vertical resolution. The 32-layer configuration also extends to the top of the WRF model (50 mb), where the 28-layer model top is about 137 mb. Using thick layers in the upper troposphere and lower stratosphere leads to high ozone biases in the troposphere. The purpose of using more layers aloft is to better resolve the upper troposphere and lower stratosphere, so that these ozone biases are reduced.

WRF				28-Layer CAMx			32-Layer CAMx		
Layer	Eta	Pressure (mb)	Top (m)	Layer	Top (m)	Thickness (m)	Layer	Top (m)	Thickness (m)
43	0.0000	50.00	20576				32	20576	2494
42	0.0100	59.63	19458						
41	0.0250	74.08	18082				31	18082	2656
40	0.0450	93.35	16616						
39	0.0650	112.61	15427				30	15427	2258
38	0.0900	136.69	14198	28	14198	2077			
37	0.1150	160.77	13169				29	13169	1948
36	0.1450	189.67	12120	27	12120	3586			
35	0.1750	218.57	11221				28	11221	1849
34	0.2100	252.28	10304						
33	0.2500	290.81	9372				27	9372	1599
32	0.2900	329.34	8534	26	8534	2030			
31	0.3300	367.87	7773				26	7773	1269
30	0.3700	406.40	7073						
29	0.4050	440.12	6504	25	6504	1040	25	6504	1040
28	0.4400	473.83	5969						
27	0.4750	507.54	5464	24	5464	870	24	5464	870
26	0.5100	541.26	4985						
25	0.5400	570.16	4594	23	4594	737	23	4594	737
24	0.5700	599.05	4219						
23	0.6000	627.95	3857	22	3857	684	22	3857	684
22	0.6300	656.85	3509						
21	0.6600	685.75	3174	21	3174	324	21	3174	324

Figure 2-5. Vertical layer structure comparison for the 28-layer (Base) and 32-layer configurations used in the NRTEEM testing phase. Green boxes show WRF layers collapsed differently in the two models.

2.6.2 Analysis of Sensitivity Simulations

The sensitivity testing phase (March 15 – April 15, 2020) was a period of relatively low observed ozone in Texas. In fact, there were no ozone exceedances at any CAMS in 2020 prior to April 20. Therefore, we evaluated the sensitivity runs through comparison of results in a set of case studies. For the fire emissions group threshold sensitivity, we selected two fires for further investigation: the Walker Fire in California in September 2019 and smaller fires in rural Comanche County, Texas in April 2020. For the vertical layer structure sensitivity, we examined stratospheric ozone for episodes in June 2019 and April 2020.

2.6.2.1 Fire Emissions Group Threshold

The Walker fire burned 221 km^2 from September 4-25, 2019 and was the second largest California wildfire of 2019. Figure 2-6 shows a map of FINN fire pixels within the burned area of the Walker Fire complex on September 15, 2019. The groups of blue (2 pixels), red (6) and green (2) pixels each represent different fire groups using the 5 km group threshold. All 10 FINN fire pixels are combined into a single fire group using the 10 km group threshold.

Figure 2-7 shows Q/D for all California FINN fire groups for the 5 km group threshold (left) and the 10 km group threshold (right) for September 15, 2019 at the Skyline Park C72 monitor in El Paso. Walker fire groups are highlighted with green boxes. Paddles are color-coded to match 5 km fire groupings shown in Figure 3. The Q/D for the 10 km group threshold is the sum of the Q/D for each of the three fire groups.

For the Walker Fire (and likely other large wildfires), the 10 km group threshold is more appropriate than 5 km for grouping FINN fire pixels that are part of the same fire. As shown in the next example, this conclusion may not be appropriate for smaller fires.

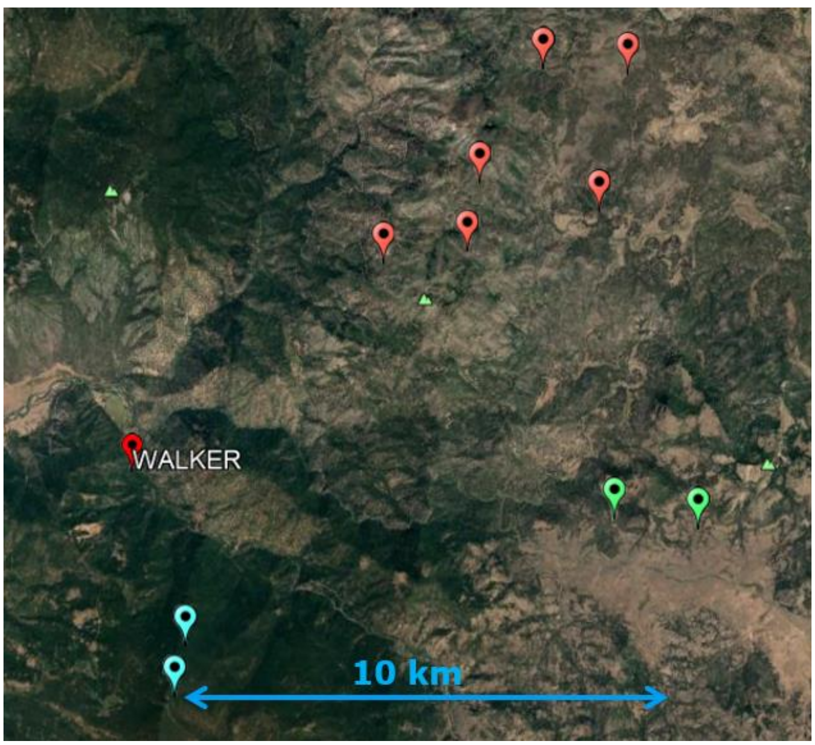

Figure 2-6. Map showing FINN fire pixels in the vicinity of the Walker Fire complex on September 15, 2019. Each color represents a different fire group using the 5 km group threshold. All 10 pixels are combined into a single fire group using the 10 km group threshold.

Group ID	State	Q/D
G000004	CA	0.1144
G000006	CA	0.0988
G000008	CA	0.0773
I000046	CA	0.0564
G000005	CA	0.0093
G000012	CA	0.0069
G000010	CA	0.0864
G000003	CA	0.0770

5 km threshold

Group ID	State	Q/D
G000004	CA	0.1144
G000006	CA	0.0988
G000008	CA	0.0773
I000046	CA	0.0564
G000005	CA	0.0093
G000003	CA	0.1704

10 km threshold

Figure 2-7: Q/D for all California FINN fire groups for 5 km group threshold (left) and 10 km group threshold (right) for September 15, 2019 at the Skyline Park C72 monitor in El Paso. Walker fire groups are highlighted with green boxes. Paddles are color coded to match 5 km fire groupings shown in Figure 2-6. The Fire IDs that start with an "I" denote individual fires. Fire IDs that start with a "G" have multiple fire pixels that have been grouped into a single fire.

Next, we show a fire grouping example for two FINN fire pixels in rural Comanche County, Texas on April 15, 2020. Figure 2-8 shows a map with two FINN fire pixels (green paddles) and Granbury C73 monitor (red paddle). The map is zoomed out to show proximity to the monitor and the Dallas-Fort Worth metropolitan area. Granbury C73 is about 70 km from the nearer FINN fire pixel. Figure 2-9 shows a close-up view of the two FINN fire pixels, which are separated by about 7 km. Therefore, the pixels are treated as two different fires for the Base run (5 km group threshold). For the Group Fire 10 km run, the two pixels are treated as a single fire.

Table 2-6 shows wildfire emissions (NOx+VOC in tons per day), distance (km) and Q/D at Granbury C73 for the 5 and 10 km fire group thresholds for the FINN fire pixels shown in Figure 2-7. The Fire IDs for the 5 km group thresholds start with an "I", which means they are treated as individual fires. These two fires are grouped ("G") into a single fire for the 10 km group threshold. The Q/D for the single grouped fire (10 km group threshold) equals the sum of the Q/D for the two individual fires (5 km group threshold).

In contrast with the 2019 Walker Fire, the terrain and obstacles between the two fire pixels in Comanche County suggest that they are not part of the same fire. This example shows that while a 10 km group threshold may be appropriate for large wildfire complexes like the 2019 Walker Fire, it may not be suitable for smaller fires like the Comanche County fires in April 2020. More work is needed to better refine the fire grouping procedure. It is important to adjust the method so that it doesn't inappropriately group smaller fires given the prevalence of smaller agricultural fires in the central and eastern US during the ozone season. For the operational phase, we will continue to process separate fire emissions processing streams for both 5 and 10 km group thresholds so that we can compare both sets of Q/D for fires that may be associated with exceptional events. However, the operational phase cannot support the computational demands from two separate fire tracking runs. Therefore, we will use only the 10 km group threshold for the operational phase. We can re-run a particular day with 5 km group threshold if warranted by examination of fires associated with a potential exceptional event.

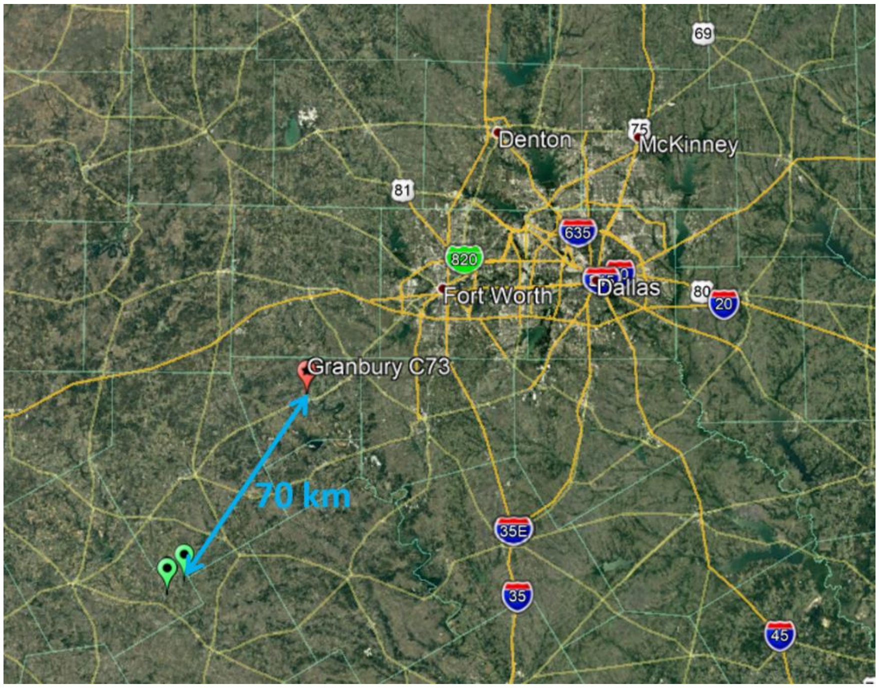

Figure 2-8. Context map for FINN fire pixels. The nearest fire pixel is about 70 km from Granbury C73.

Figure 2-9. Closeup map for FINN fire pixels. The fire pixels are about 7 km apart.

Table 2-6. Fire emissions (NOx+VOC in tons per day) , distance (km) and Q/D at Granbury C73 for 5 and 10 km fire group thresholds for the FINN fire pixels shown in Figure 2-9.

Fire Grouping Threshold	Fire ID	Emissions (Q)	Distance (D) to C73	Q/D for C73
5 km				
	I001294	6.7	78.2	0.086
	I001295	6.6	71.4	0.093
10 km				
	G000400	13.4	74.8	0.179

2.6.2.2 Vertical Layer Structure

For the vertical layer structure sensitivity test, we examined ozone vertical profiles and stratospheric ozone impacts at the surface for episodes in June 2019 and April 2020.

<u>June 11-12, 2019</u>

The 2019 NRTEEM modeling indicated a regional, multi-day stratospheric impact on western US and Texas surface ozone during June 9-12, 2019 (Figure 2-10; adapted from Johnson et al., 2019). Given the magnitude of the modeled impacts on Texas ozone and the fact that they occurred outside the climatologically favored region and season, we investigated the June event further. Using a combination of analyses, Johnson et al., (2019) found evidence suggesting a possible stratospheric intrusion on June 9-12 over the western US. To determine whether the magnitudes of the modelled stratospheric ozone impacts were affected by the vertical layer structure and/or choice of vertical coordinate system in WRF, we developed the following CAMx sensitivity runs:

1. eta vertical coordinate with 28 CAMx layers (same as 2019 NRTEEM Base configuration)
2. eta vertical coordinate with 32 CAMx layers
3. hybrid vertical coordinate with 28 CAMx layers (same as 2020 NRTEEM Base)
4. hybrid vertical coordinate with 32 CAMx layers (same as 2020 NRTEEM 32 Layer run)

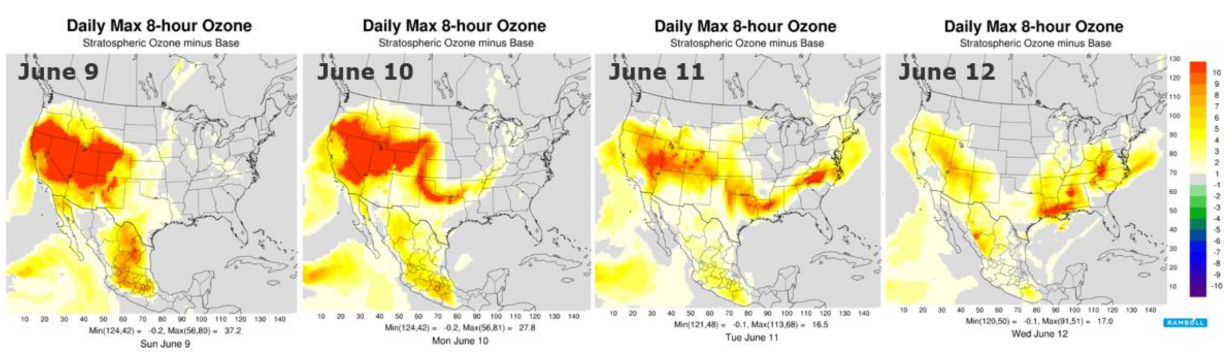

Figure 2-10. NRTEEM modeled stratospheric impacts on ground level MDA8 ozone within the 36 km grid June 9-12, 2019. Adapted from Johnson et al., (2019).

Figure 2-11 shows vertical profiles of ozone concentrations for ozonesonde observations (black dotted line) and CAMx runs over the Boulder, CO ozonesonde site on June 11, 2019. The eta 28-layer run (light blue line) has a high ozone bias below 10 km due to the thickness of model layers aloft (see Figure 2-5) that combine stratospheric (high ozone) and tropospheric (lower ozone) air. The hybrid 28-layer run (black line) shows improvement with smaller ozone biases below 10 km, but it still shows high biases that are an artifact introduced by the thick upper layers. Finally, the hybrid 32-layer run, which has better vertical resolution near the tropopause (red line) matches the observed profile very well below 10 km.

Figure 2-12 shows stratospheric ozone impacts in the surface layer for the eta 28-layer (left), hybrid 28-layer (middle) and hybrid 32-layer (right) runs. The eta 28-layer run shows the largest stratospheric ozone impacts. The hybrid 32-layer run has the smallest stratospheric ozone impacts.

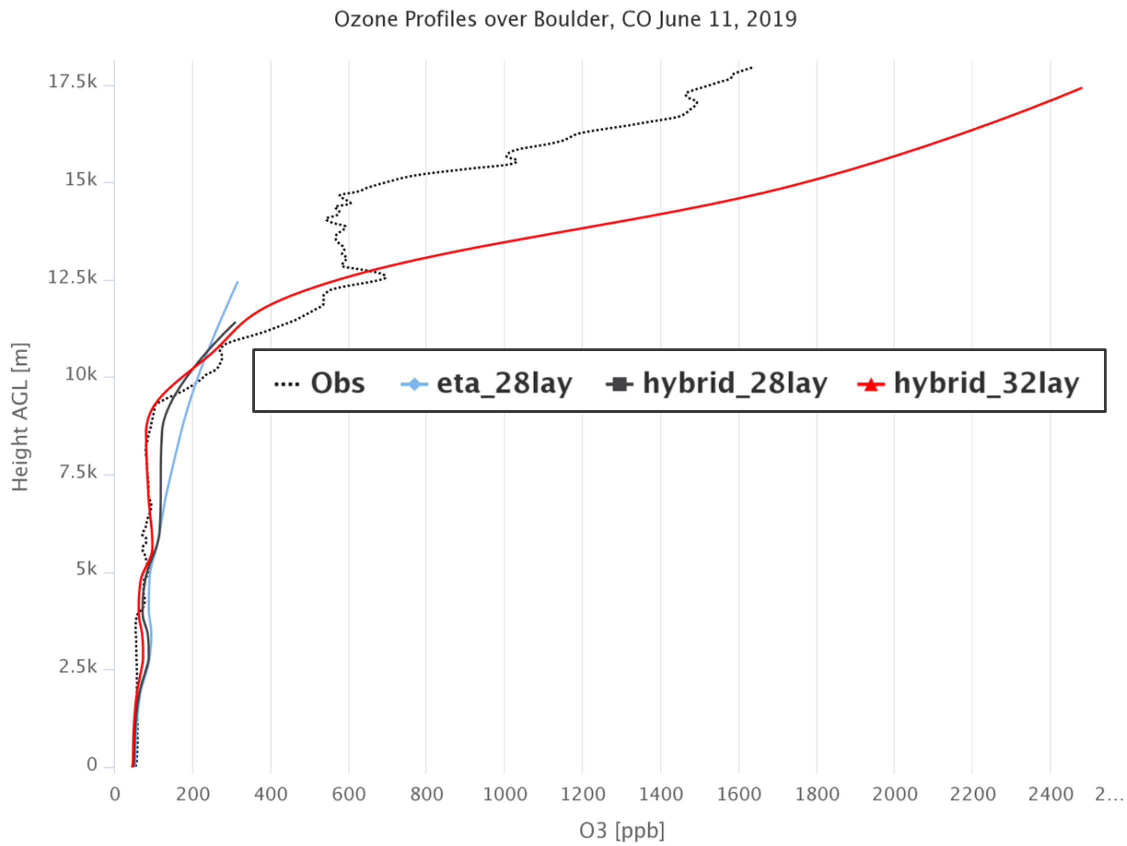

Figure 2-11. Vertical profile of ozone concentrations for ozonesonde observations (black dotted line), eta 28-layer run (light blue line), hybrid 28-layer run (black line) and hybrid 32-layer run (red line) over the Boulder, CO ozonesonde site on June 11, 2019.

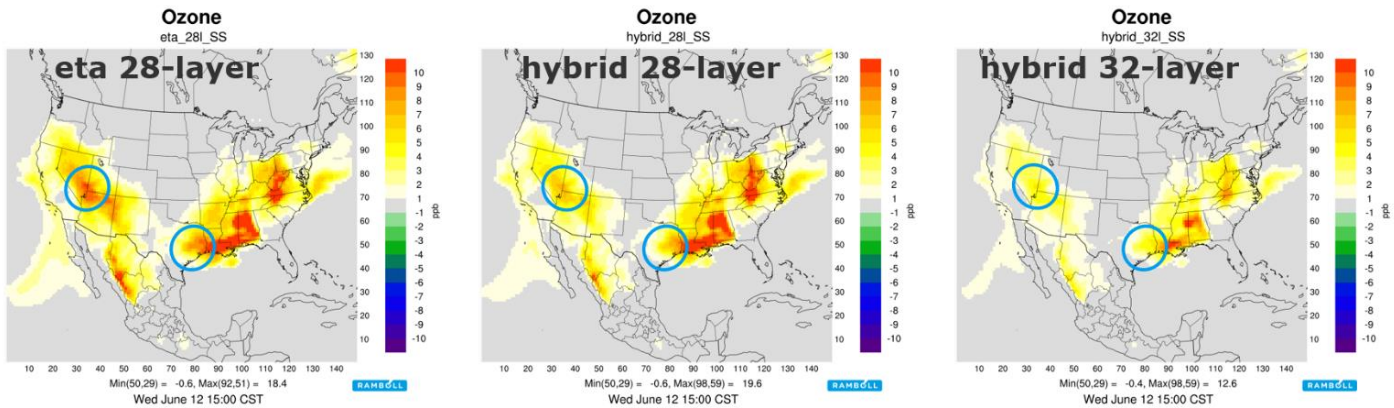

Figure 2-12. Stratospheric ozone impacts in the surface layer for the eta 28-layer (left), hybrid 28-layer (middle) and hybrid 32-layer (right) runs.

<u>March 28-29, 2020</u>

The results of vertical layer sensitivity tests for June 2019 episode suggested that continued evaluation during 2020 NRTEEM testing phase was warranted. During March 28-29, 2020, NRTEEM modeling indicated a widespread stratospheric impact at the surface across the western US, Midwest, Mexico and Texas.

Due to operational constraints, we were not able to run CAMx with 3-D outputs for comparison to ozonesonde observations during the testing phase. Instead, we present the stratospheric ozone impacts at the surface (Figure 2-13) for the Base (28 layers; top panels) and 32 Layer runs (bottom panels) for March 28 (left panels) and March 29 (right panels), 2020.The 32 Layer run shows lower stratospheric ozone impacts compared the Base run, especially on March 29. More investigation is needed to determine if a stratospheric intrusion occurred in reality and if so, what ozone concentrations were observed at the surface. However, given the very large ozone impacts in the Base run, we expect that the model is overestimating transport of stratospheric ozone to the surface in that run. The 32 Layer model better resolves the upper troposphere and lower stratosphere, which should decrease the amount of stratospheric ozone brought into the troposphere by using thicker layers near the tropopause in the 28 Layer run.

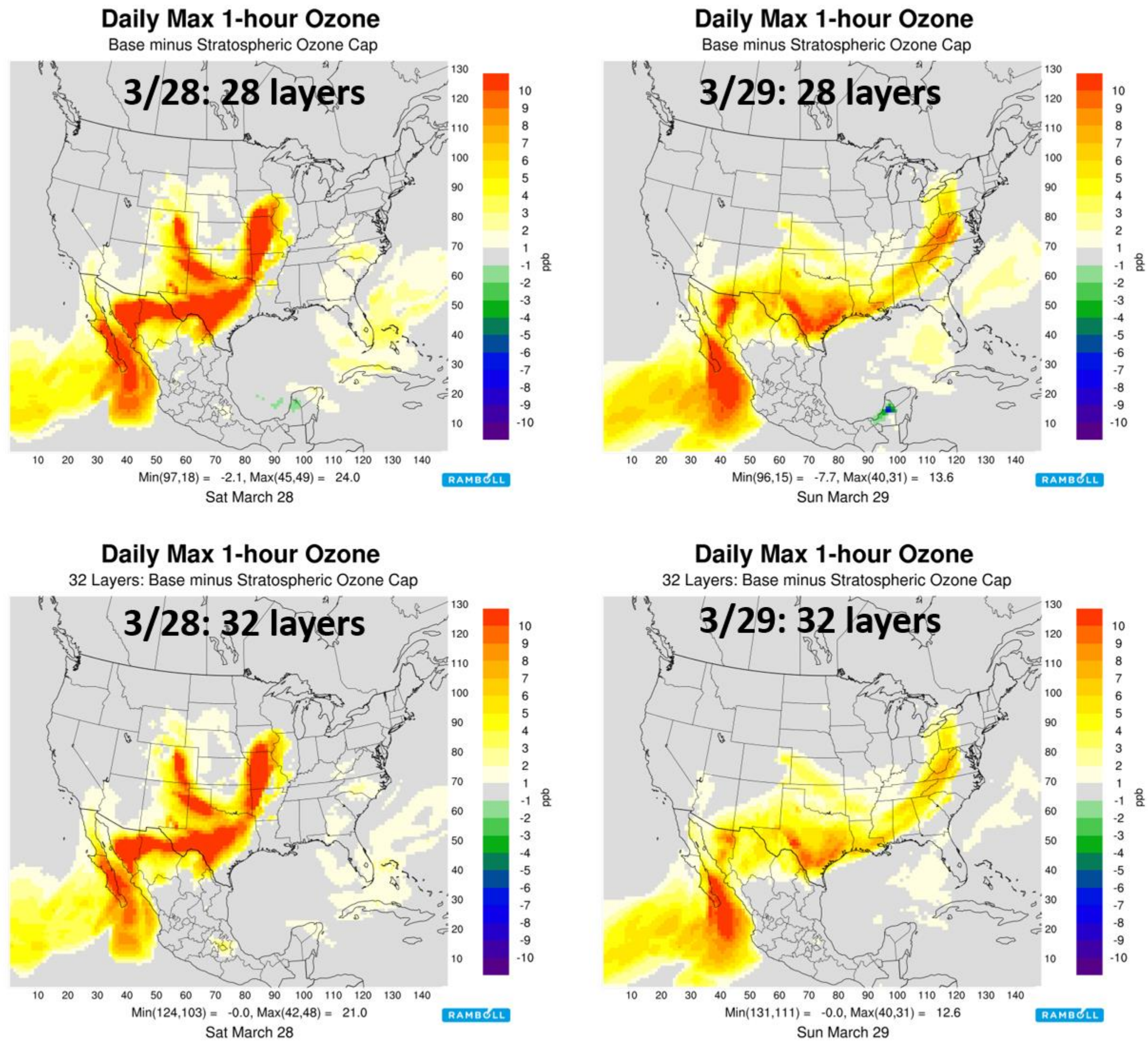

Figure 2-13. Stratospheric ozone impacts in the surface layer for the Base/28-layer (top) and 32-layer runs (bottom) for March 28 (left) and March 29, (right) 2020.

2.7 Operational Phase Sensitivity Tests

Based on analysis of results from the sensitivity testing phase, we recommended the runs specified in Table 2-7 for operational modeling that ran from April 15-October 15, 2020. We recommended the Base run use the 32-layer vertical layer mapping to better resolve the upper troposphere and lower stratosphere. All other runs share the Base configuration, except as noted below. The No Fires run does not include FINN fire emissions. The No Mexico Anthropogenic Emissions does not include Mexico anthropogenic emissions. The Stratospheric Ozone Cap run caps ozone top conditions (TCs) and ozone boundary conditions (BCs) above 370 mb at 60 ppb. Finally, the Fire Tagging run includes fire tagging using the 10 km group threshold. We decided to separate the fire tagging capability from the Base run as an operational consideration so that the Base and sensitivity run results (first 4 runs in Table 2-7) could be posted to the website in near-real time.

Table 2-7. List of CAMx simulations performed for NRTEEM operational modeling phase, April 15-October 15, 2020.

Number	Run	Description
1	Base	Includes NRT FINN fire emissions without fire tagging No capping Top Conditions/Boundary Conditions (TCs/BCs) Hybrid 32-layer vertical layer mapping
2	No Fires	Same as Base, but exclude FINN fire emissions
3	No Mexico Anthropogenic Emissions	Same as Base, but exclude Mexico anthropogenic emissions
4	Stratospheric Ozone Cap	Cap ozone TCs at 60 ppb; cap ozone for BC layers aloft at 60 ppb
5	Fire Tagging	Same as Base, but include fire tagging at 10 km threshold

3.0 MODEL EVALUATION

This section presents quantitative and qualitative evaluations of WRF meteorological and CAMx ozone performance. The objective is to determine if the 2020 NRTEEM model performs well enough to be useful as a tool for evaluating impacts from potential exceptional events.

In the sections below, we first provide results from the regional analysis of the base configuration, focusing on quantitative evaluation of the meteorological fields and ozone. Next, we introduce target plots as a new tool for summarizing ozone model performance. Then we provide an evaluation of the daily maximum 8-hour average (MDA8) ozone local increment (LI) analysis in Dallas, Houston and San Antonio. Finally, we present case studies that examine potential exceptional events as modeled by the NRTEEM system.

3.1 WRF Meteorological Model Performance Evaluation

We evaluate WRF 2-m temperature, 2-m humidity and 10-m wind speed and direction using the Integrated Surface Data (ISD) data set ds3505.0, archived at the National Climatic Data Center (NCDC). Meteorological data from the TCEQ’s CAMS are not used because some locations are known to have nearby obstructions that bias wind measurements from certain sectors (Johnson et al., 2015) and a systematic evaluation of which CAMS could be used for meteorological model performance evaluation is not currently available. For this report, we examine performance at ds3505.0 monitoring locations in Dallas-Fort Worth (DFW), Houston-Galveston-Brazoria (HGB), San Antonio (SA) and El Paso (EP) (see Figure 3-1).

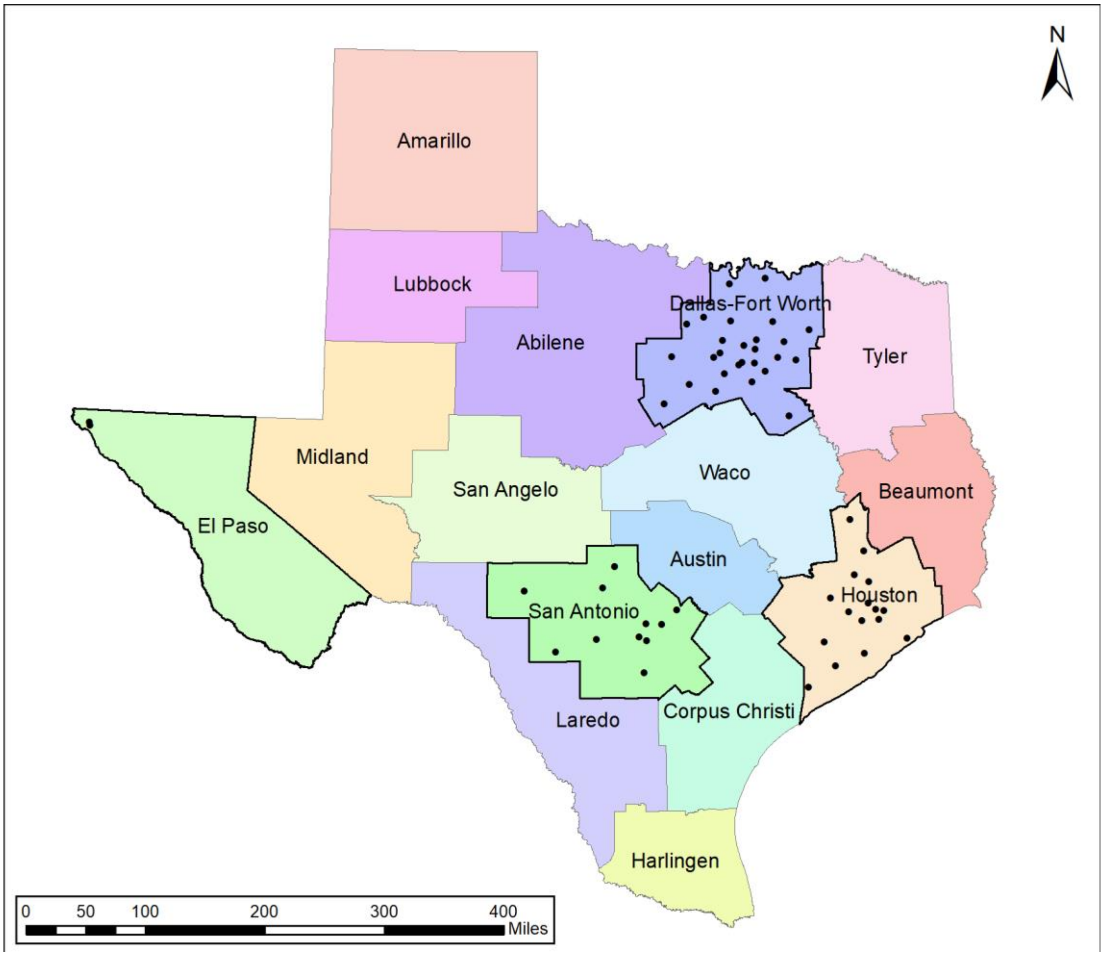

Figure 3-1. Map of ds3505.0 meteorological monitoring stations used in the WRF meteorological model performance evaluation.

Emery et al. (2001) derived and proposed a set of daily performance "benchmarks" for typical meteorological model performance. These standards were based upon the evaluation of about 30 MM5 and RAMS meteorological simulations of limited duration (multi-day episodes) in support of air quality modeling applications. These were primarily ozone model applications for cities in the eastern and Midwestern U.S. and Texas that were primarily simple (flat) terrain and simple (stationary high pressure causing stagnation) meteorological conditions. More recently these benchmarks have been used in meteorological modeling studies that include areas with complex terrain (McNally, 2009; ENVIRON and Alpine, 2012).

The purpose of the benchmarks is to help characterize how good or poor the results are relative to other model applications run for the U.S. In this section, the meteorological variables are compared to the benchmarks as an initial indication of the WRF performance. These benchmarks include model bias and error in temperature, wind direction and water vapor mixing ratio as well as the wind speed bias and Root Mean Squared Error (RMSE). The benchmarks for each parameter are as follows:

- Temperature Bias: less than or equal to ±0.5 °K; alternative of ≤±2.0 °K for complex conditions.
- Temperature Error: less than or equal to 2.0 °K; alternative of ≤2.5 °K for complex conditions.
- Mixing Ratio Bias: less than or equal to ±0.8 g/kg; alternative of ±1.0 g/kg for complex conditions.

- Mixing Ratio Error: less than or equal to 2.0 g/kg.
- Wind Direction Bias: less than or equal to ±10 degrees.
- Wind Direction Error: less than or equal to 30 degrees; alternative of 50 degrees for complex conditions.
- Wind Speed Bias: less than or equal to ±0.5 m/s; alternative of ±1.5 m/s for complex conditions.
  - Wind Speed RMSE: less than or equal to 2 m/s; alternative of 2.5 m/s for complex conditions.

The equations for bias and error are given below, with the equation for the Root Mean Squared Error (RMSE) similar only being the square of the differences between the model (M) and observation (O) and a square root is taken of the entire quantity.

$$\text{Bias} = \frac{1}{n}\sum_{i=1}^{n}(M_i - O_i)$$

$$\text{Error} = \frac{1}{n}\sum_{i=1}^{n}|M_i - O_i|$$

The April 15 – October 15, 2020 average statistics for wind speed, wind direction, temperature and humidity for all ds3505.0 stations within Dallas are displayed graphically in Figure 3-2 using "soccer plot" displays. Soccer plots graph monthly average bias versus monthly average error. For wind speed, error is replaced with RMSE. The model results are plotted along with the simple (plotted in black) and complex benchmark results (red), which form a box shaped like a soccer goal. Acceptable model performance is indicated when symbols are inside the benchmark outline (i.e., the model scores a goal in the soccer plot analogy).

The DFW plot (Figure 3-2) shows three months (April, July and October) outside the complex benchmark for wind direction and another month (August) within the complex benchmark but outside the simple benchmark. Wind speed performance is better with only a single month (October) outside the simple benchmark. All months except July and September are within the simple benchmark for temperature, which shows positive biases (warm) across the entire April 15-October 15, 2020 modeling period. All months achieve the humidity simple conditions benchmark which show a consistent negative (dry) bias across the modeling period.

We present soccer plot diagrams for HGB, San Antonio and El Paso in Figure 3-3, Figure 3-4 and Figure 3-5, respectively. We find generally good performance for HGB with points falling within or close to the simple benchmark goals. We find the same consistent dry bias at Houston as seen in the DFW plot. San Antonio shows similar performance features as in the HGB plots, but shows a mix of positive (wet) and negative (dry) biases for humidity. The El Paso soccer plots show the lowest performance scores of the four regions. In El Paso the wind direction complex benchmarks for both error and bias are exceeded. Errors in winds may be related to the complex terrain of the El Paso area, which may not be well-represented at WRF's 4 km grid resolution. In addition, there is a consistent wet bias evident in the humidity plot. The poor performance in El Paso may be impacted by overactive summertime convection associated with the North American Monsoon, which is a known and persistent issue in WRF in modeling the Southwestern US[3]. Overall, performance looks worse than that observed for 2019 NRTEEM.

[3] https://www.wrapair2.org/SNMOS.aspx

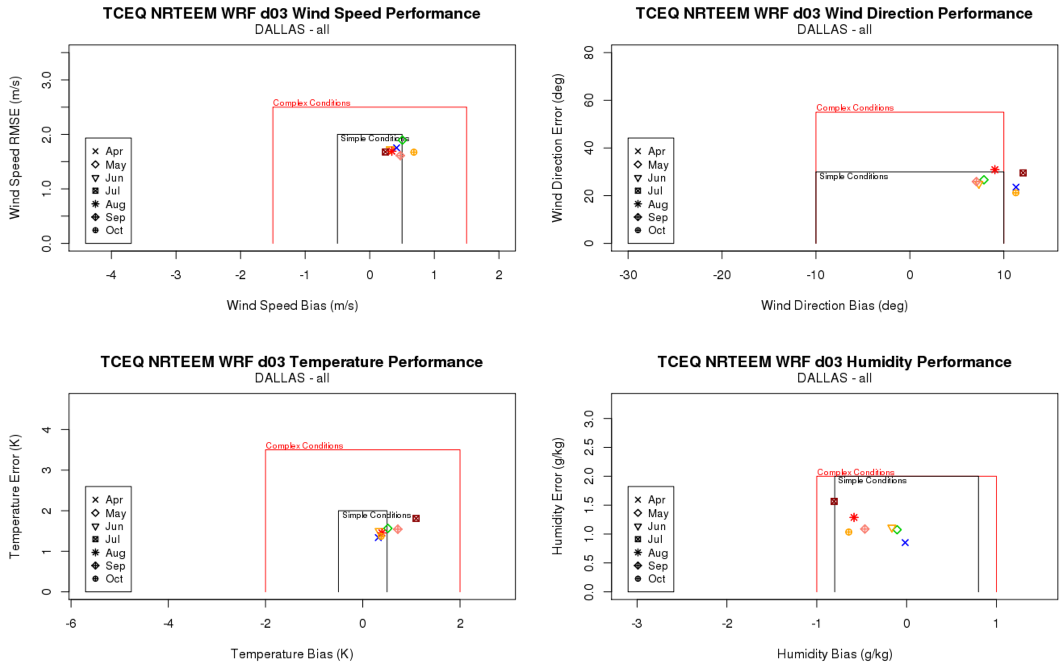

Figure 3-2. Soccer plots for wind speed (top left), wind direction (top right), temperature (bottom left) and humidity (bottom right) for all Dallas ds3505.0 monitoring stations covering April 15 – October 15, 2020.

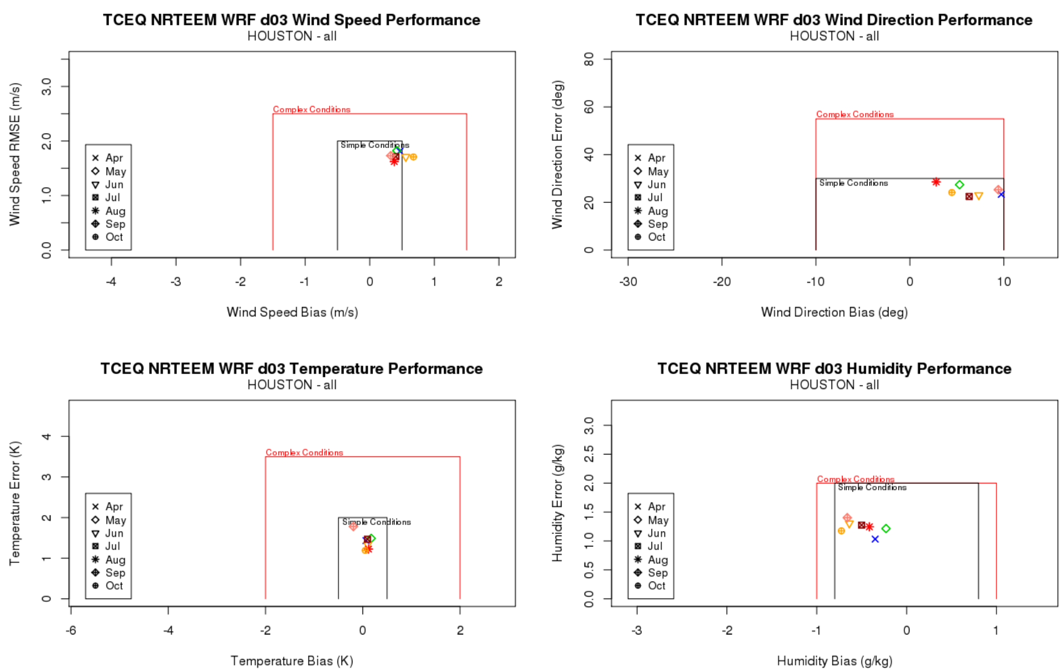

Figure 3-3. Soccer plots for wind speed (top left), wind direction (top right), temperature (bottom left) and humidity (bottom right) for all HGB ds3505.0 monitoring stations covering April 15 – October 15, 2020.

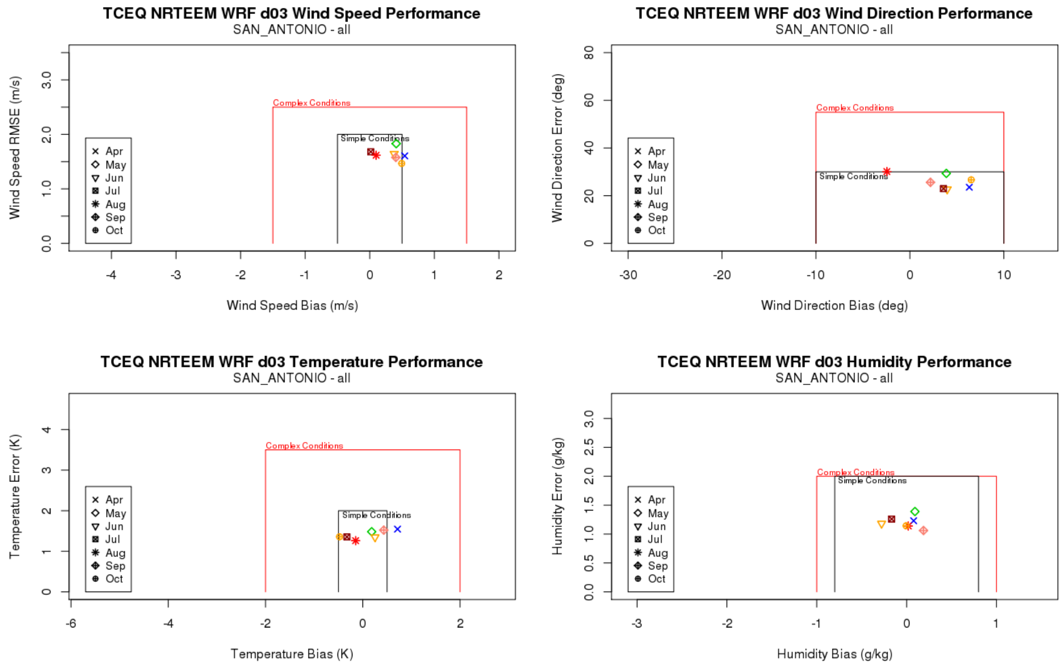

Figure 3-4. Soccer plots for wind speed (top left), wind direction (top right), temperature (bottom left) and humidity (bottom right) for all San Antonio ds3505.0 monitoring stations covering April 15 – October 15, 2020.

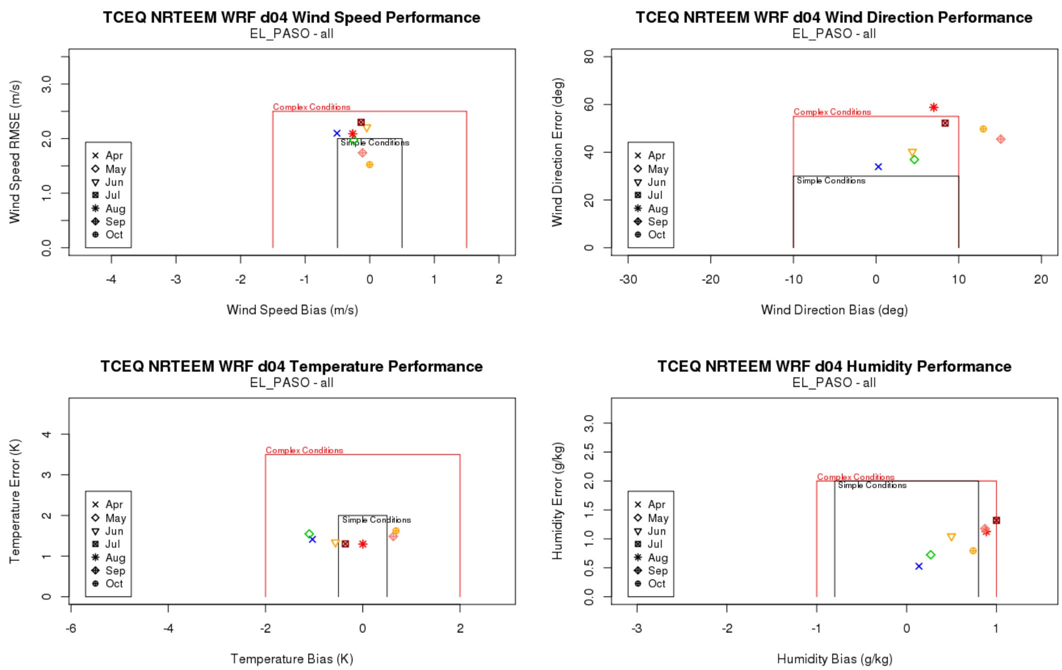

Figure 3-5. Soccer plots for wind speed (top left), wind direction (top right), temperature (bottom left) and humidity (bottom right) for all El Paso ds3505.0 monitoring stations covering April 15 – October 15, 2020.

3.2 Operational Evaluation

We present the number of observed occurrences of MDA8 ozone above 70 ppb for the Dallas-Fort Worth, Houston-Galveston-Brazoria, El Paso and San Antonio regions in Figure 3-6. The plot suggests that Dallas and Houston both had fewer high ozone days in 2020 than the previous three years, though Houston shows a sharper decline from 2019 (158 occurrences) to 2020 (91) compared to Dallas (2019: 58; 2020: 53). In contrast, there were slight increases in high ozone days from 2019 to 2020 for El Paso (2019: 25; 2020: 33) and San Antonio (2019: 8; 2020: 10).

Shutdowns and other COVID-related changes in activity do not appear to have an obvious impact on the number of observed occurrences of high ozone days. The emission inventory used in the NRTEEM modeling makes assumptions about typical levels of activity for each emissions source. During the COVID outbreak, activity levels likely changed within and outside in Texas, potentially reducing the correspondence between actual and modeled emissions. COVID impacts therefore introduce uncertainty in the emissions inventory used for NRTEEM, and the impacts of COVID on model performance are not well understood. Estimating the COVID-related impacts to the model is beyond the scope of this project. Our goal in the model performance evaluation in the following section is to determine if the 2020 NRTEEM model is a reasonable tool for evaluating impacts from potential exceptional events during 2020, given the uncertainties.

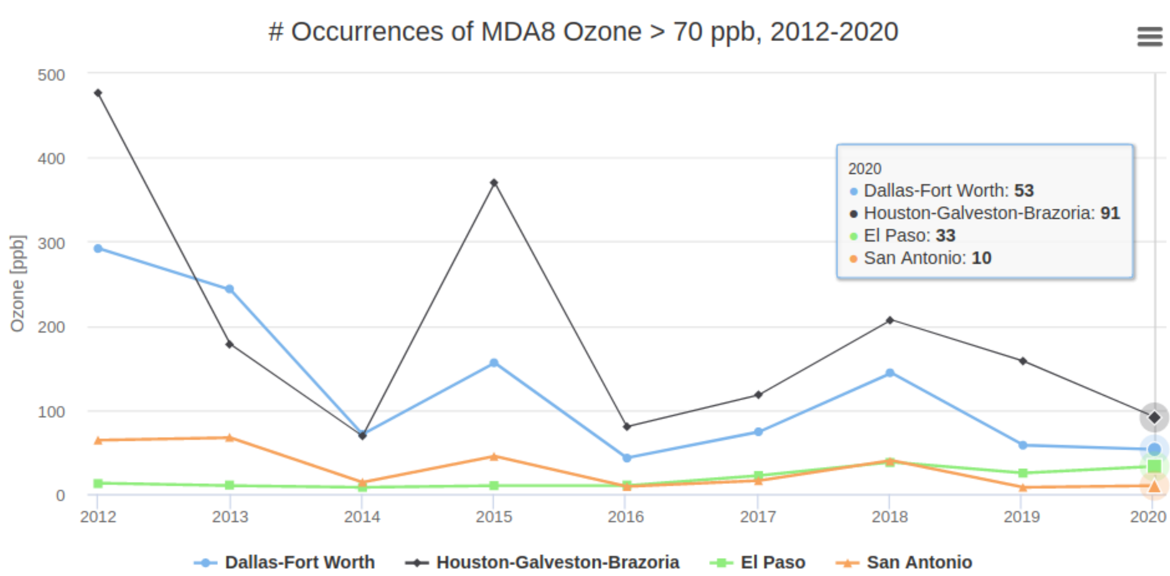

Figure 3-6. Number of occurrences of MDA8 ozone concentrations above 70 ppb during the for the years 2012-2020 for the Dallas-Fort Worth, Houston-Galveston-Brazoria, El Paso and San Antonio metropolitan regions.

3.3 Model Performance EvaluationCAMx Model Performance Evaluation

3.3.1 Statistics

The CAMx NRTEEM website has been set up to compute model performance statistics for each CAMx run when observed data are available. Statistical metrics are computed for individual CAMS monitoring sites, major urban areas and the entire CAMS network.

The statistical metrics computed for CAMS monitoring locations are:

- Normalized Mean Bias (NMB)

$$NMB = \frac{\sum_{i=1}^{n}(M_i - O_i)}{\sum_{i=1}^{n} O_i}$$

where M_i and O_i are the model and observed values (O_i, M_i) in a data pair and n is the number of observed/modeled data pairs.

- Normalized Mean Error (NME)
    -

$$NME = \frac{\sum_{i=1}^{n}|M_i - O_i|}{\sum_{i=1}^{n} O_i}$$

- Correlation coefficient (r)

$$r = \frac{\sum_{i=1}^{n} M_i O_i - \frac{(\sum_{i=1}^{n} M_i)(\sum_{i=1}^{n} O_i)}{n}}{\sqrt{\left[\left(\sum_{i=1}^{n} M_i^2 - \frac{(\sum_{i=1}^{n} M_i)^2}{n}\right)\left(\sum_{i=1}^{n} O_i^2 - \frac{(\sum_{i=1}^{n} O_i)^2}{n}\right)\right]}}$$

Statistical metrics were computed for:

- Hourly ozone, NO, NOx and CO
    - Hourly temperature, wind speed, wind direction, total solar radiation

A 20 ppb threshold was applied to observed ozone concentrations; thresholds of 1 mph and 10 Watts/m^2 were employed for wind speed and solar radiation, respectively. We note that because wind direction is an angular measurement, we replace NMB and NME with mean bias (MB) and mean error (ME), respectively.

We evaluated ozone model performance for the base simulation for the April 15 through October 15, 2020 modeling period.

3.3.2 1-Hour Ozone Statistical Evaluation

We present 1-hour ozone statistics across all DFW CAMS for the base model in Figure 3-7. Similar plots for Houston, San Antonio and El Paso are shown in Figure 3-8, Figure 3-9 and Figure 3-13, respectively. Similar figures are available on the NRTEEM website with interactive selection of date, region/site and model simulation. We observe the poorest performance (high positive bias) when ozone is relatively low (1-hour peak ozone below about 50 ppb). The base model performs very well during several high ozone days/episodes, including June 11-13, and August 3-5, 2020.

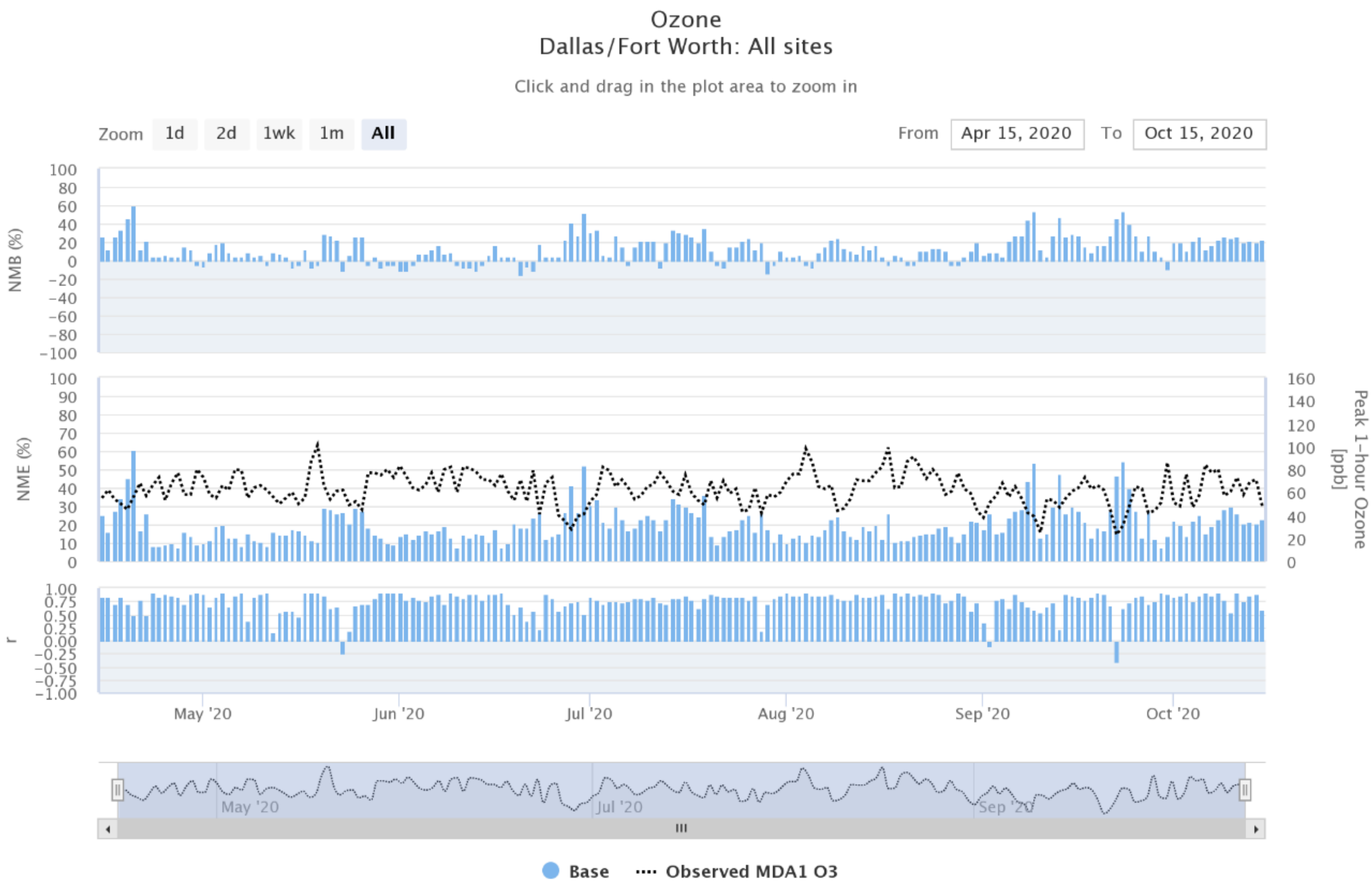

Figure 3-7. Dallas model performance statistics for ozone (20 ppb cutoff) by area for the base simulation for April 15-October 15, 2020.

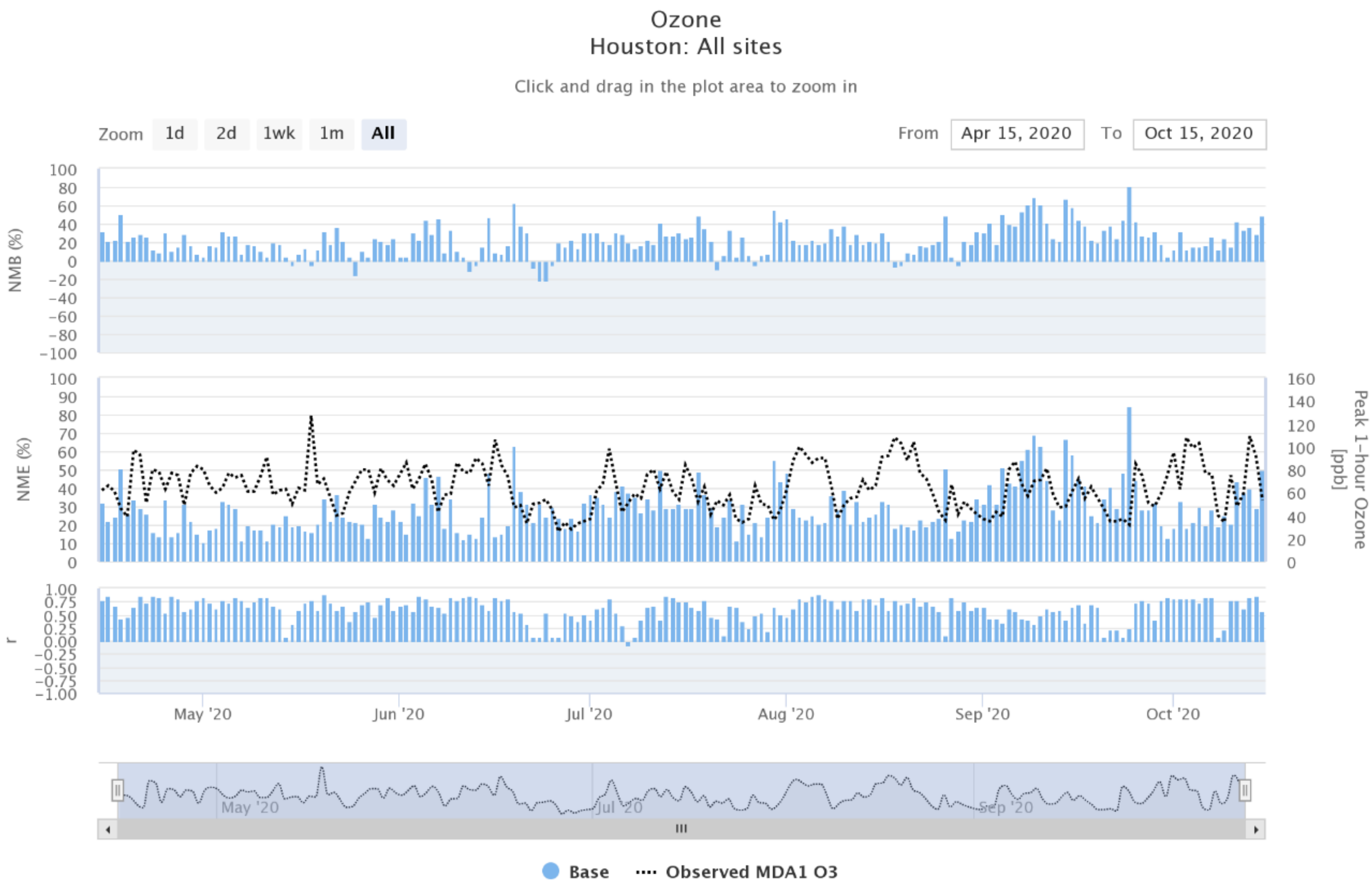

Figure 3-8. Houston model performance statistics for ozone (20 ppb cutoff) by area for the base simulation for April 15-October 15, 2020.

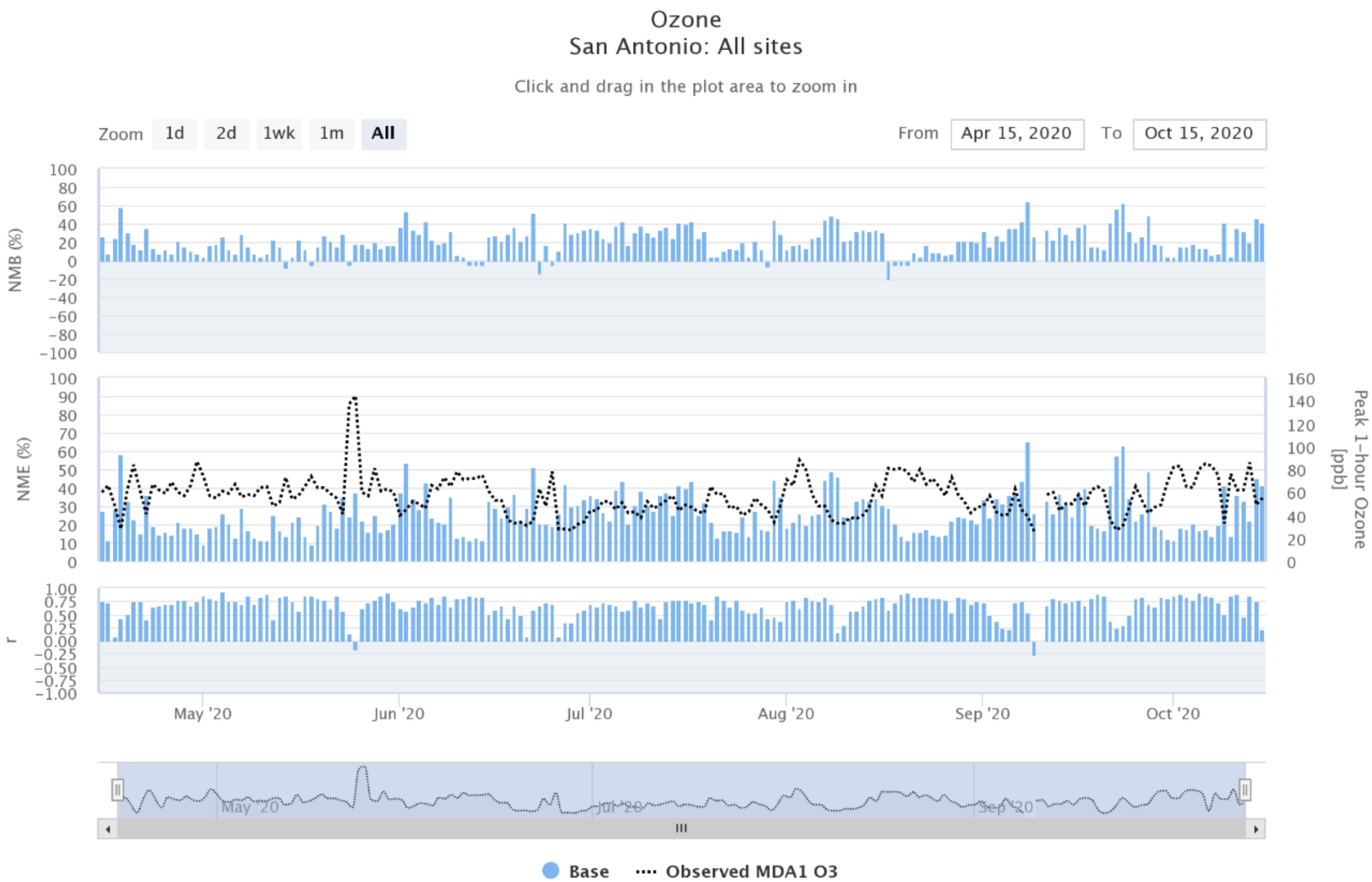

Figure 3-9. San Antonio model performance statistics for ozone (20 ppb cutoff) by area for the base simulation for April 15–October 15, 2020.

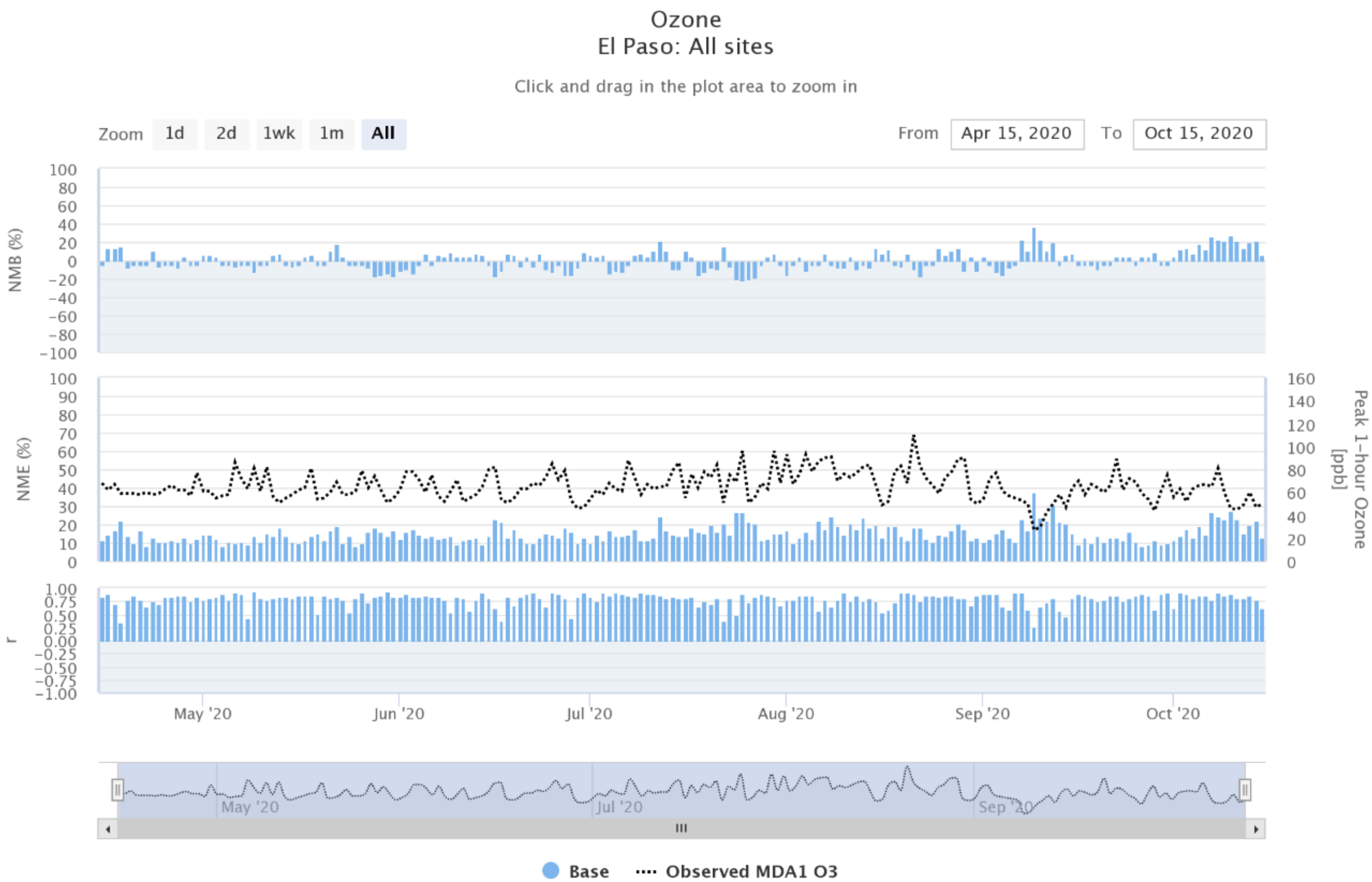

Figure 3-10. El Paso model performance statistics for ozone (20 ppb cutoff) by area for the base simulation for April 15–October 15, 2020.

3.3.3 Daily Maximum 8-hour Ozone Statistics

In Table 3-1, we present MDA8 ozone NMB and NME statistics for three sets of days: 1) all days (no threshold); 2) all days/monitors where observed MDA8 ozone exceeds 40 ppb; and 3) all days/monitors where observed MDA8 ozone exceeds 60 ppb. The table lists the Performance Goal and Criteria benchmarks as developed in Emery et al., (2017). Color coding for each region corresponds to the Performance Goals/Criteria for NMB and NME. Green shading represents performance metrics that are within the Performance Goal, blue shading is applied to performance metrics that meet the Performance Criteria and red shading means that the Criteria benchmark is exceeded. We also include r with no threshold applied. There are no Goal/Criteria benchmarks for r, so we do not apply any shading to these values.

Because the NRTEEM model is designed to evaluate potential exceptional event impacts, it is important the model perform well at higher ozone levels (60 ppb cutoff). However, NRTEEM should also be able to model background/lower ozone.

Overall, we observe good performance considering the uncertainty introduced by COVID and its presumed effects of the emissions inventory and therefore, model performance. With no cutoff, the model NMB is +15.8% and NME is 20.4% across all days and all Texas sites. Performance improves substantially at the 40 ppb (NMB: +5.4%; NME: 11.7%) and 60 ppb (NMB: -7.3%; NME: 10.3%) cutoffs. At the 60 ppb cutoff, NMB/NME stats are highest for the El Paso region, indicating less agreement with observed ozone in El Paso than in other areas of Texas. In addition, the correlation (r) is substantially lower (0.661) for El Paso than the next lowest region (Dallas: 0.787).

We present a similar table in Table 3-2 for the April 15-October 15, 2019 NRTEEM modeling period. Apart from El Paso, 2020 NRTEEM NMB/NME statistics are slightly higher (All Texas NMB: +15.8%; NME: 20.4%) than for 2019 NRTEEM (All Texas NMB: +12.4%; NME: 19.3%). Despite this fact, correlation is higher in 2020 (All Texas: 0.810) across all regions compared to 2019 (All Texas: 0.763). The 2020 model includes a new 4 km domain over El Paso, which may help improve model performance relative to 2019.

Table 3-1. Summary of April 15-October 15, 2020 MDA8 ozone bias (NMB) and error (NME) model performance statistics by region and comparison against ozone Performance Goals and Criteria.

Region	NMB (%)			NME (%)			r
	0 ppb cutoff	40 ppb cutoff	60 ppb cutoff	0 ppb cutoff	40 ppb cutoff	60 ppb cutoff	0 ppb cutoff
Performance Goal	≤±5%	≤±5%	≤±5%	≤15%	≤15%	≤15%	N/A
Performance Criteria	≤±15%	≤±15%	≤±15%	≤25%	≤25%	≤25%	N/A
All Texas	+15.8%	+5.4%	-7.3%	20.4%	11.7%	10.3%	0.810
Dallas	+8.7%	+2.6%	-8.4%	14.6%	10.2%	10.6%	0.787
Houston	+21.0%	+7.8%	-4.4%	24.9%	13.7%	9.7%	0.816
San Antonio	+19.0%	+6.7%	-7.9%	22.2%	11.7%	9.8%	0.834
El Paso	+0.5%	-0.2%	-9.6%	9.9%	9.4%	11.0%	0.661

Table 3-2. Summary of April 15-October 15, 2019 MDA8 ozone bias (NMB) and error (NME) model performance statistics by region and comparison against ozone Performance Goals and Criteria.

Region	NMB (%)			NME (%)			r
	0 ppb cutoff	40 ppb cutoff	60 ppb cutoff	0 ppb cutoff	40 ppb cutoff	60 ppb cutoff	0 ppb cutoff
Performance Goal	≤±5%	≤±5%	≤±5%	≤15%	≤15%	≤15%	N/A
Performance Criteria	≤±15%	≤±15%	≤±15%	≤25%	≤25%	≤25%	N/A
All Texas	+12.4%	+2.4%	-8.0%	19.3%	12.6%	12.3%	0.763
Dallas	+7.3%	+1.4%	-5.8%	14.1%	10.4%	10.6%	0.766
Houston	+17.9%	+5.3%	-6.9%	24.2%	15.2%	13.0%	0.766
San Antonio	+16.0%	+7.2%	-3.4%	19.0%	12.0%	9.4%	0.805
El Paso	-8.1%	-10.0%	-17.2%	13.0%	12.6%	17.6%	0.651

3.3.4 Target Plots

In this section, we present model assessment target plots as a new tool for evaluating model performance. Target plots provide a concise summary of model performance across a large number of sites. The advantage of using target plots rather than other performance metric displays such as soccer plots is that target plots incorporate measurement uncertainty in setting benchmarks for model performance.

The Forum for Air quality Modelling in Europe (FAIRMODE, Janssen et al., 2017) developed the model quality indicator (MQI, Thunis and Cuvelier, 2016) as a metric of model performance which depends on the measurement uncertainty. FAIRMODE defines the MQI as the ratio of the model bias and twice the measurement uncertainty.

$$MQI = \frac{RMSE}{2RMS_U}$$

where RMSE is defined as:

$$RMSE = \sqrt{\frac{1}{n}\sum_{i=1}^{n}(O_i - M_i)^2}$$

and RMS_U is the root mean square (RMS) of the measurement uncertainty as defined in Thunis et al. (2013) and Pernigotti et al. (2013).

To visualize the MQI, we utilize target plots adapted from Jolliff et al. (2009), Pederzoli et al. (2012) and Kushta et al. (2019), among others. We show an example target plot in Figure 3-11. The vertical axis represents the mean bias, normalized by the measurement uncertainty. The horizontal axis represents the central root mean square error:

$$CRMSE = \sqrt{\frac{1}{n}\sum_{i=1}^{n}\left[\left(M_i - \overline{M}\right) - \left(O_i - \overline{O}\right)\right]^2}$$

Negative x-axis values (left side of the target plot) indicate an unsystematic RSME ratio where model error is dominated by poor correlation. Positive x-axis values (right side of the target plot) indicate a systematic RMSE ratio dominated by high variability (standard deviation).

Triangle symbols on the plots in Figure 3-11 represent the MQI for a single monitor. Smaller MQI values (closer to the origin) indicate better model performance. All three triangles are in the upper right quadrant of the plot, indicating a positive bias (overestimation) and model error dominated by high variability (i.e. a model time series that has smaller or larger fluctuations than the observed times series).

The green triangle has an MQI less than 0.5 and indicates that the model result is within the range of observation uncertainty and therefore represents the good model performance. The yellow triangle is between 0.5 and 1.0 and indicates that the model errors are larger than the observation uncertainty, but the model may still be a better predictor of the actual concentrations than the observations[4]. Finally, the red triangle has an MQI greater than 1 and indicates a statistically significant difference between the model and observations. FAIRMODE specifies a Model Quality Objective (MQO) that 90% of stations have an MQI less than 1.

[4] https://fairmode.jrc.ec.europa.eu/document/fairmode/WG1/Guidance_MQO_Bench_vs2.1.pdf

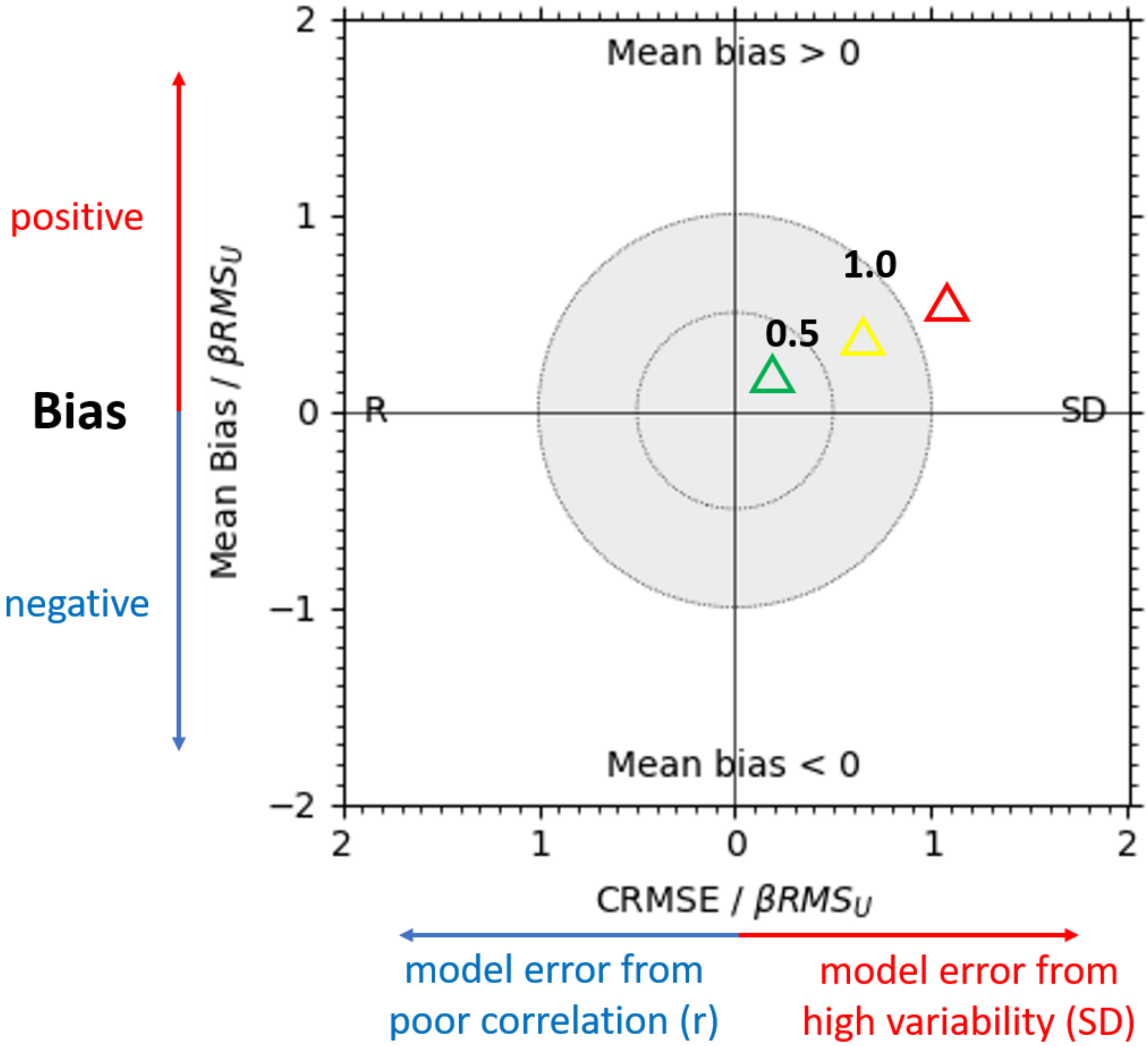

Figure 3-11. Example model assessment target plot. Each triangle represents a single station and the distance between the origin and the triangle corresponds to the MQI for that station.

In Figure 3-12, we present MDA8 ozone target plots for DFW (top left), HGB (top right), San Antonio (bottom left) and El Paso (bottom right) CAMS. To the right of each plot are the measurement uncertainty parameters developed specifically for MDA8 ozone by Peringotti et al. (2013), Thunis et al. (2013) and currently in use by FAIRMODE. Thunis et al. (2013) quantifies several sources of ozone measurement uncertainty including linear calibration, UV photometry and sampling losses. The measurement uncertainty parameters result from a linear fitting of these uncertainty estimates and they depend on a reference value (RV) for MDA8 ozone, defined as 120 ug/m^3, which we converted to 60 ppb. With similar instrumentation technology available in Europe, we assume that the ozone measurement uncertainties can be quantified similarly at CAMS in Texas. Therefore, we apply the same measurement uncertainty parameters as used in FAIRMODE.

We find good model performance across DFW (top left panel of Figure 3-12), with all CAMS within the 0.5 MQI value MQI_{90} = 0.464). Most sites show a small positive bias and model error at all sites is dominated by poor correlation (this also holds for HGB, San Antonio and El Paso). MQI is substantially higher for HGB CAMS (MQI_{90} = 0.757; top right panel of Figure 3-12). San Antonio (bottom left panel of Figure 3-12) performance lies between DFW and HGB (MQI_{90} = 0.648) with positive biases for all but one site (Camp Bullis C58). All 6 El Paso CAMS (bottom right panel of Figure 3-12) lie within the 0.5 MQI value and the MQI_{90} (0.338) is lowest among the 4 regions. In contrast with the other 3 regions, El Paso CAMS do not exhibit high positive biases, with all sites clustered tightly near the zero bias line. Despite the low MQI relative to the other 3 regions (MQI_{90} = 0.338), we find frequent large ozone underestimations at El Paso CAMS during periods of high observed ozone (as documented in Sec 3.3.6 and 3.4.3).

Overall, the MDA8 ozone target plots suggest acceptable performance across all sites in Dallas, Houston, San Antonio and El Paso (MQI < 1.0). Model error at all CAMS within Dallas and El Paso are within the range of the observation uncertainty (MQI < 0.5). Across all sites in all four regions, model error is dominated by poor correlation (negative x-axis values). A combination of poor correlation and high positive bias result in MQI between 0.5 and 1.0 for some CAMS in Houston and San Antonio.

As part of our evaluation of target plots, we attempted to use observed ozone cutoffs at 40 and 60 ppb to gain more information about performance during periods of high observed ozone. In the process of this evaluation, we found that the target plots were very sensitive to outliers. A large underestimation or overestimation on a single day could result in a substantial shift in the placement of a symbol on the plot. CAMS measurements for 2020 are preliminary and high ozone measurements may later be corrected or removed. Therefore, we decided against applying cutoffs in the target plots in this report. However, we suggest continuing the investigation of model performance that accounts for measurement uncertainty, which may include target plots.

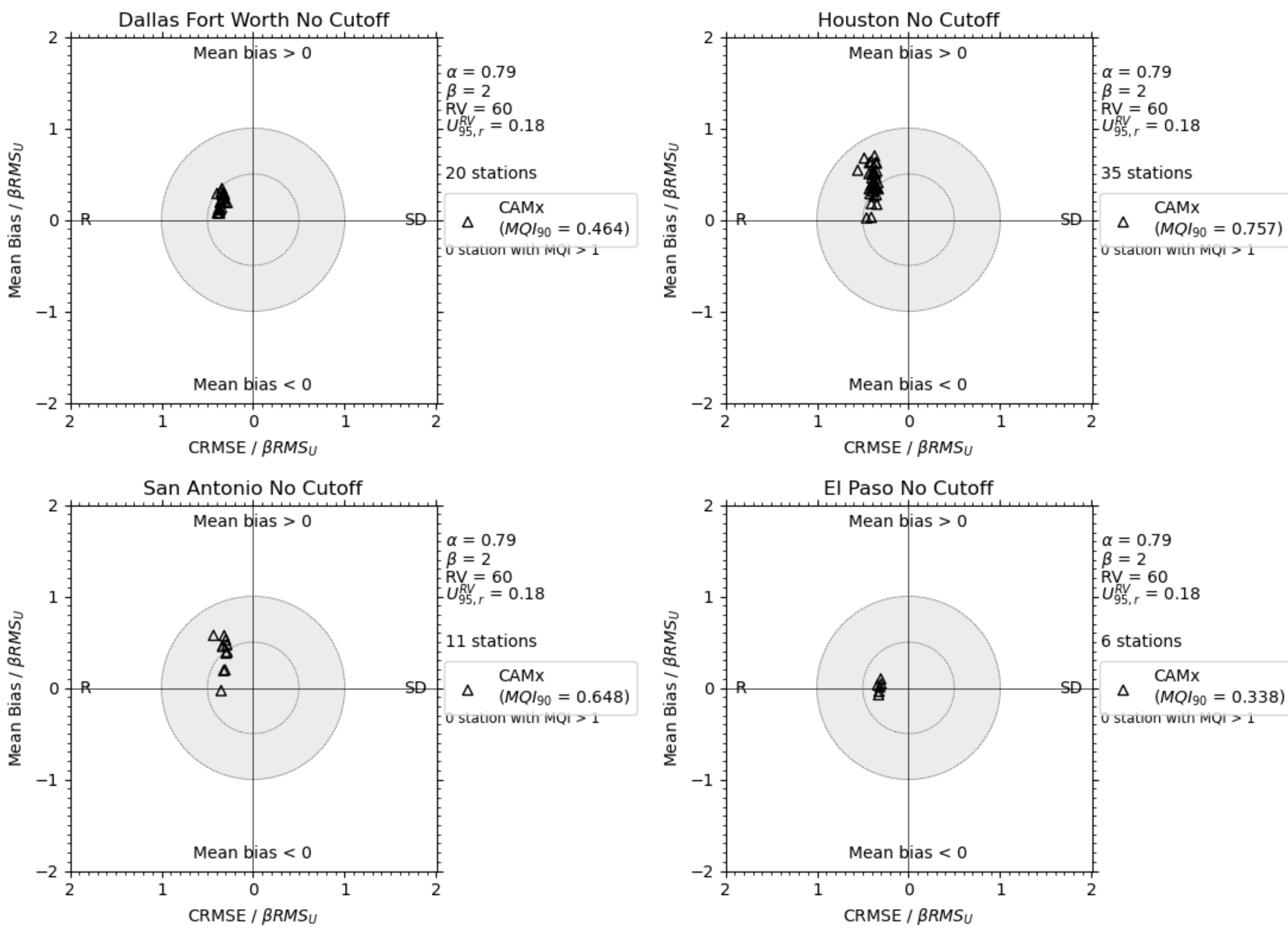

Figure 3-12. MDA8 ozone target plots for DFW (top left), HGB (top right), San Antonio (bottom left) and El Paso (bottom right) CAMS.

3.3.5 MDA8 Ozone Local Increment

In order to determine how well the base run estimates ozone production in a given metropolitan area, we calculate the MDA8 ozone local increment (LI) for observations and model simulations. The LI of ozone is sensitive to local ozone precursor emissions and the conduciveness of the atmosphere to ozone production on each day.

Figure 3-13 displays a map of all Dallas-Fort Worth CAMS and similar maps for Houston and San Antonio CAMS are provided in Figure 3-14 and Figure 3-15. We classify the monitors with green pushpins as potential background sites (meaning that when they are upwind of the urban area they are indicative of background) and calculate the median MDA8 ozone concentration across these monitors for each day. Then we find the difference between this background value and the maximum MDA8 ozone concentration across all monitors in the same region. We refer to this difference as the MDA8 ozone LI.

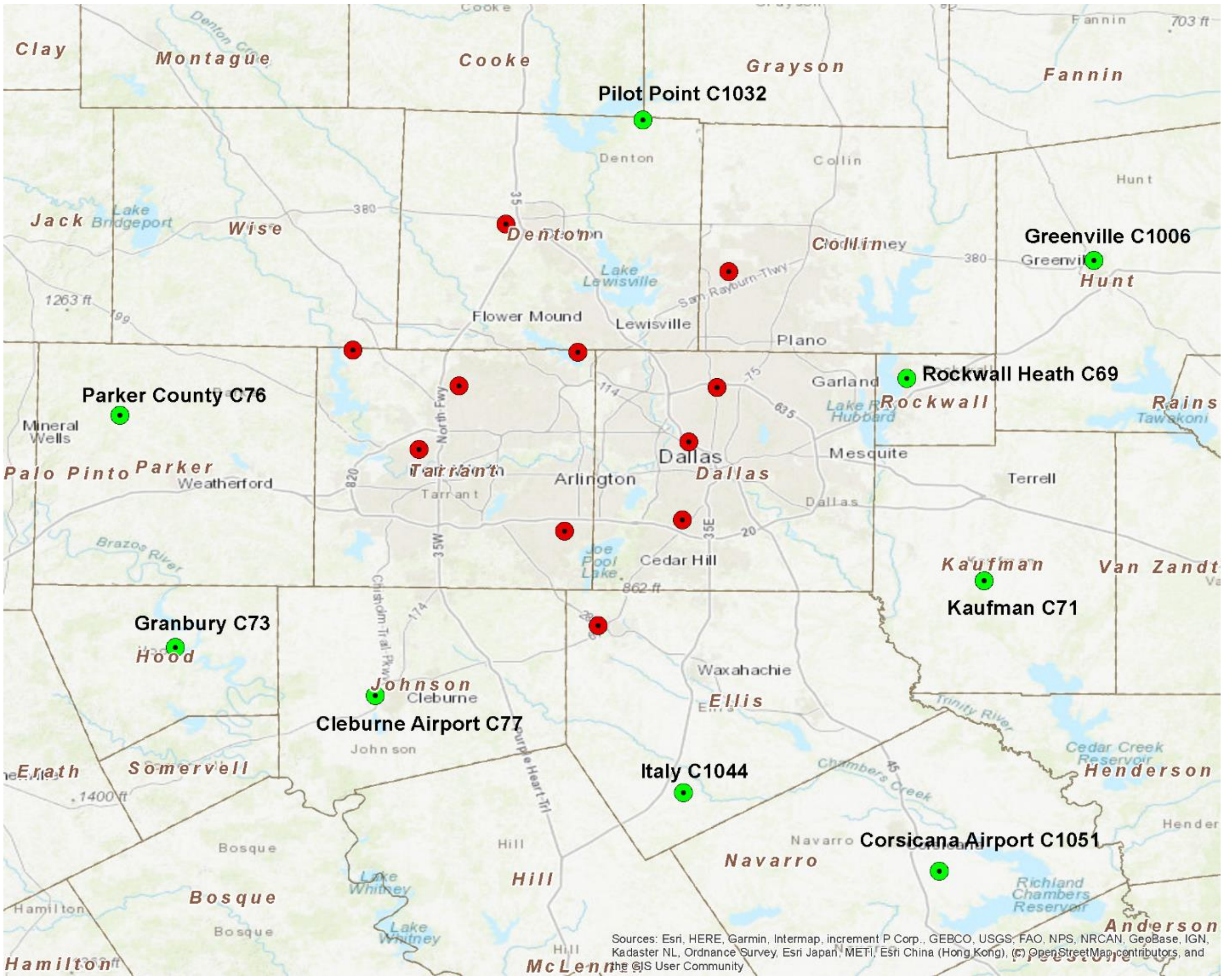

Figure 3-13. Map of Dallas-Fort Worth CAMS monitoring locations. The 10 potential background sites have green markers and are labelled.

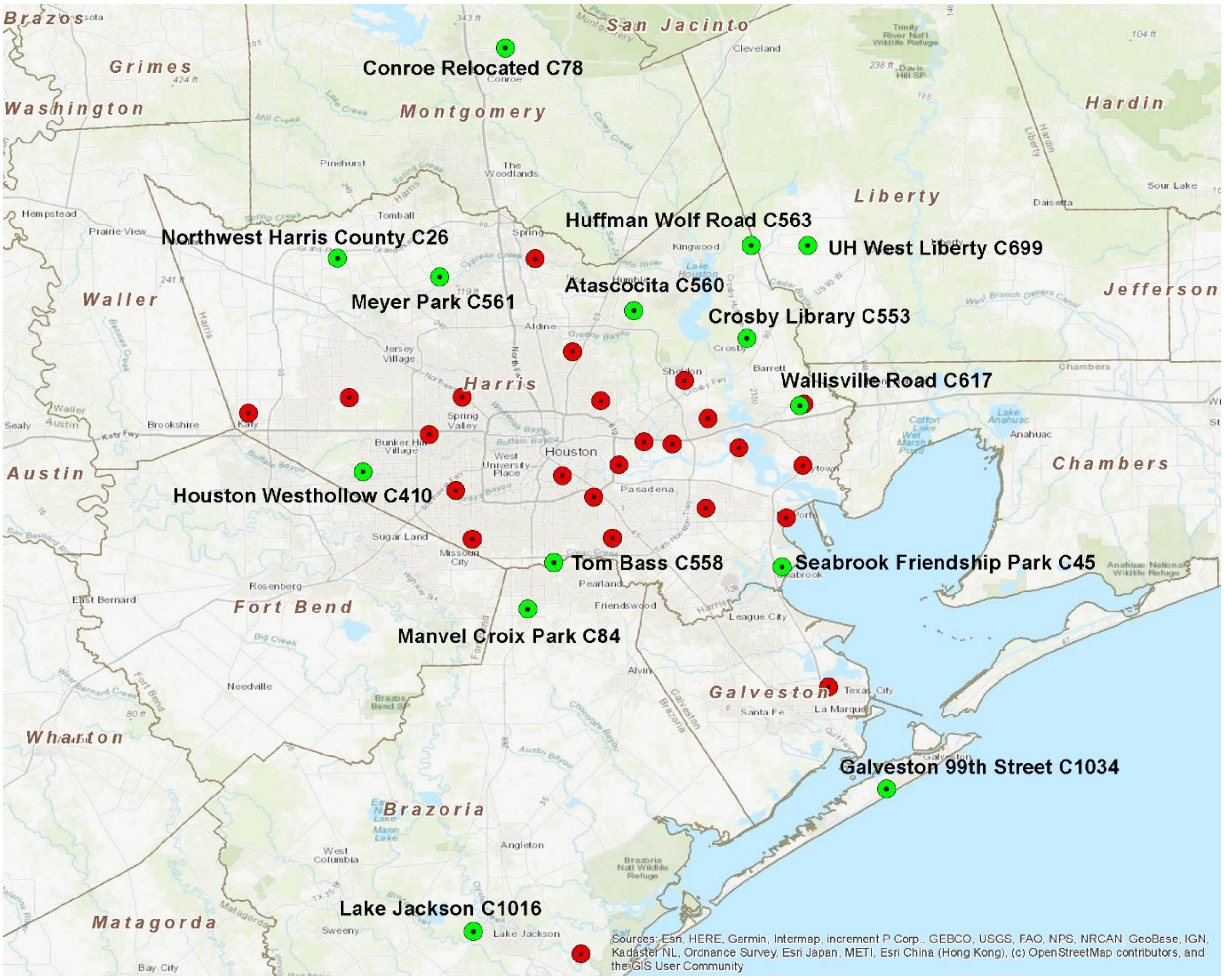

Figure 3-14. Map of Houston CAMS locations. The 12 potential background CAMS have green markers and are labelled.

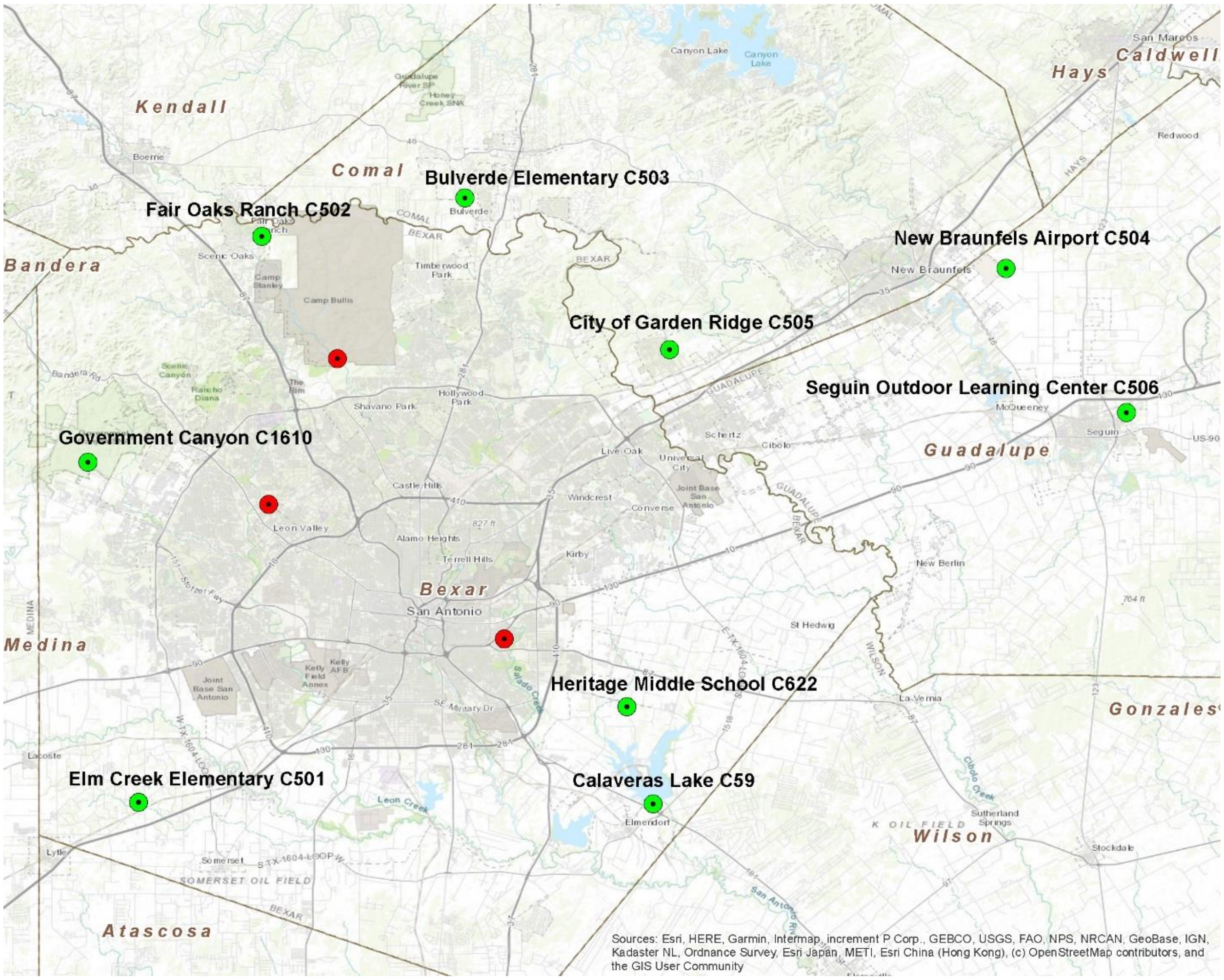

Figure 3-15. Map of San Antonio CAMS locations. The 16 potential background CAMS have green markers and are labeled.

In Figure 3-16, we present quantile-quantile (Q-Q) plots for Dallas (left), Houston (middle) and San Antonio (right) MDA8 ozone local increment for the base model. The top row shows results for April 15-October 15, 2020 while the bottom row shows the same time period for 2019.

We selected Q-Q plots as a way to understand if the model is capable of simulating the full range of observed MDA8 ozone LI. Q-Q plots can be considered a less stringent measure of model performance because the model and observations are not paired in time or space. However, the Q-Q plots provide more information about how well the model is able to simulate days when background ozone dominates (low LI) as well as days when local ozone production is high (high LI). This approach is especially appropriate for a short-term retrospective model such as NRTEEM, which relies on a future year emissions inventory.

For each plot, the x-axis shows the observed LI and the y-axis shows the base model LI. The Dallas plot shows better agreement than both Houston and San Antonio for 2020. All three plots for 2020 show a persistent underestimation that occurs throughout the full range of observed LI. The 2019 plots (bottom row of Figure 3-16) show substantially better agreement than the 2020 plots.

In Figure 3-17, we present similar Q-Q plots but instead of the showing the MDA LI, we show the median MDA8 at the background sites for each region. The 2020 plots (top row of Figure 3-17,) show a larger overestimation of the background MDA8 compared to 2019 (bottom row of Figure 3-17). COVID-related impacts on emissions and photochemistry is complex and uncertain. However, we expect background ozone concentrations to be lower in 2020 due to COVID impacts and the NRTEEM model cannot account for these impacts.

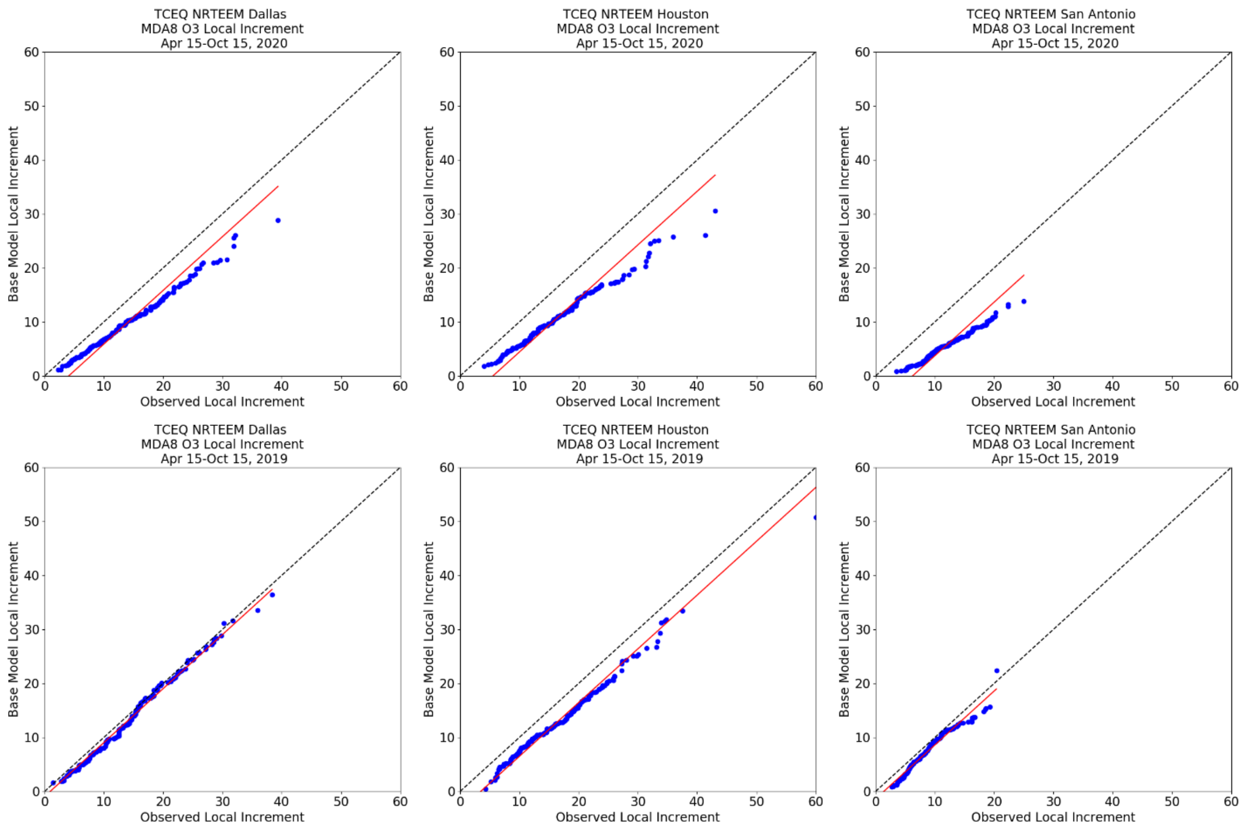

Figure 3-16. Quantile-quantile plots for Dallas (left), Houston (middle) and San Antonio (right) MDA8 ozone local increment for the base simulation for April 15-October 15, 2020 (top row) and April 15-October 15, 2019 (bottom row).

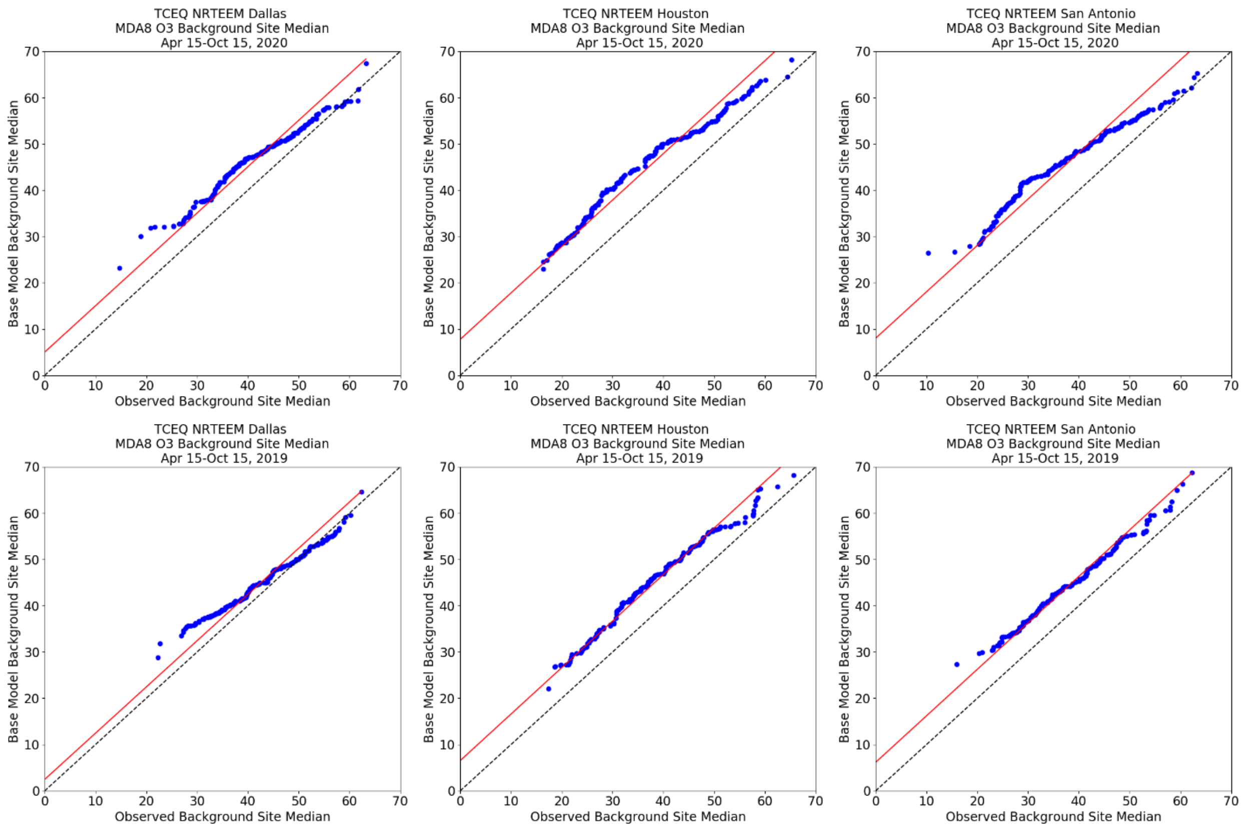

Figure 3-17. Quantile-quantile plots for Dallas (left), Houston (middle) and San Antonio (right) MDA8 ozone background site median for the base simulation for April 15-October 15, 2020 (top row) and April 15-October 15, 2019 (bottom row).

3.3.6 Case Study: August 1-8, 2020

Because 2020 NRTEEM introduced a 4 km domain over El Paso, we focus our case study on this region. Between August 1 and 8, 2020, there were 9 instances of an El Paso ozone recording an MDA8 values exceeding 70 ppb (see Figure 3-18).

Area	Monitoring Site	POC	August 2020																													
			1	2	3	4	5	6	7	8	9	10	11	12	13	14	15	16	17	18	19	20	21	22	23	24	25	26	27	28	29	30	31
El Paso-Juarez																																	
	El Paso UTEP C12/A125/X151/G125	2	81	60	68	60	54	62	56	85	59	NV	62	58	62	59	55	45	47	64	72	53	64	72	67	61	55	64	71	67	72	47	45
	Ascarate Park SE C37/A332/A172/X159	1	69	56	60	59	54	56	50	63	54	60	52	51	NV	71	44	41	41	61	65	53	77	69	59	53	47	57	56	64	67	41	35
	Chamizal C41/AH126	1	73	58	64	57	51	55	51	73	56	56	NV	57	57	65	49	42	40	61	NV	52	68	68	60	51	46	55	56	58	69	45	41
	Socorro Hueco C49/F312	1	74	63	65	74	59	58	67	55	56	69	58	52	48	74	43	44	45	71	67	60	102	73	61	57	52	57	54	63	68	47	44
	Skyline Park C72	1	69	58	59	74	54	62	54	73	57	62	53	64	65	60	52	43	46	61	71	58	79	66	62	59	54	59	63	67	58	49	46
	Ivanhoe C414/F514	1	67	58	58	71	64	59	54	61	57	64	53	55	54	68	45	42	42	58	73	60	82	67	62	56	51	56	55	68	61	45	43

Figure 3-18. TCEQ website graphic showing MDA8 ozone values for El Paso CAMS for August 2020.

To investigate how the base model simulation performed during the week in which this high ozone episode occurred, we present daily 1-hour ozone statistics (NMB, NME and correlation coefficient) charts for the El Paso region for August 1-9, 2020 in Figure 3-19. Numerical values for each statistic are shown for the day where observed MDA1 ozone was highest in El Paso, August 4. The base model shows underestimations on the days with highest observed ozone: August 1, 4 and 8, 2020. Table 3-3 shows MDA8 ozone NMB/NME statistics across all 6 El Paso CAMS on each of these 3 days. The Performance Criteria metric for NMB (≤±15%) is exceeded on both 8/1 (-17.4%) and 8/8 (-15.3%).

Table 3-3. MDA8 ozone bias (NMB) and error (NME) model performance statistics for El Paso CAMS and comparison against ozone Performance Goals and Criteria for August 1, 4 and 8, 2020.

Date	NMB(%)	NME (%)
Performance Goal	≤±5%	≤15%
Performance Criteria	≤±15%	≤25%
8/1	-17.4%	17.7%
8/4	-11.7%	12.6%
8/8	-15.3%	20.5%

In Figure 3-20, we present ozone time series (black dotted line: observations; blue line: base model) for August 1-9, 2020 at the El Paso Chamizal C41 monitor. The model does a reasonable job on August 1 (peak ozone underestimated by about 7 ppb at 2 PM CST). However, the model shows larger underestimates for midday peak ozone on August 6 and 8 of roughly 30 and 40 ppb, respectively. On both days, the model estimates ozone impacts from Mexico anthropogenic emissions in the 5-10 ppb range and these impacts may be underestimated in the model. In addition, large errors in wind direction on August 6 and 8 (see Figure 3-21) are likely contributing to the ozone underestimations. On both days, midday observations show winds from the southeast, putting the El Paso Chamizal C41 monitor directly downwind of Ciudad Juarez. It is likely that ozone produced in Ciudad Juarez is being transported to the Chamizal C41 monitor leading to the observed ozone spikes on these two days. However, the midday modeled winds on August 6 and 8 are from the northwest and west.

Figure 3-19. El Paso model performance statistics for ozone (20 ppb cutoff) by area for the base simulation for August 1-9, 2020. Statistics shown for the highest day of the week, August 4.

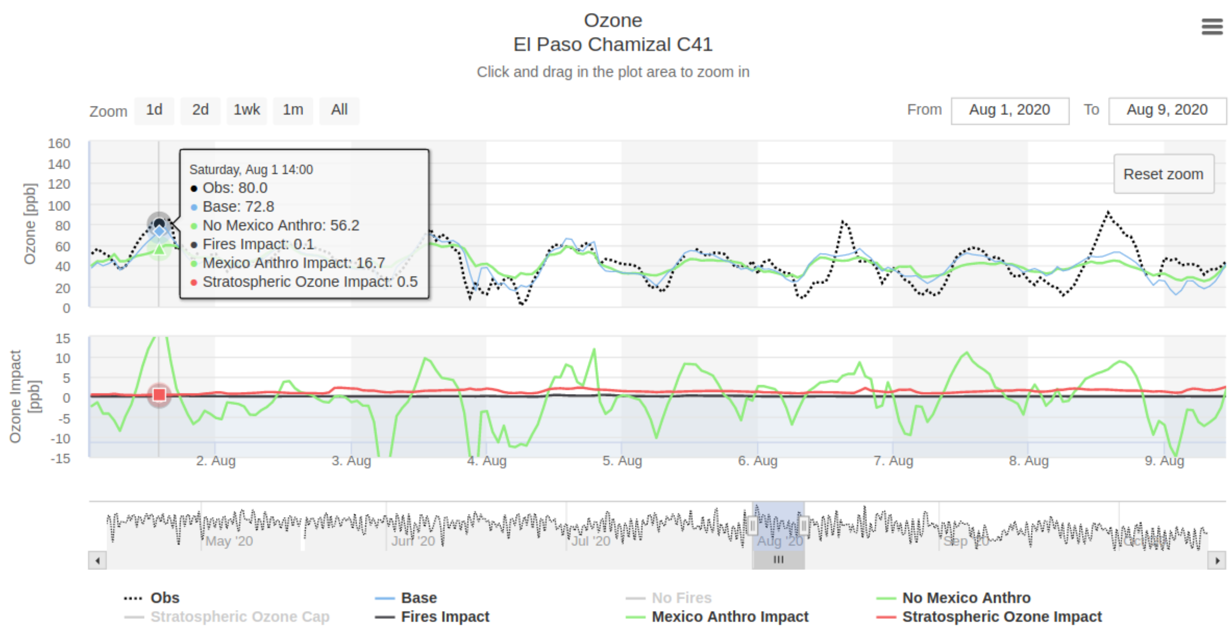

Figure 3-20. Observed (black dotted line), base model (blue) ozone time series for August 1-9, 2020 at the El Paso Chamizal C41 monitor.

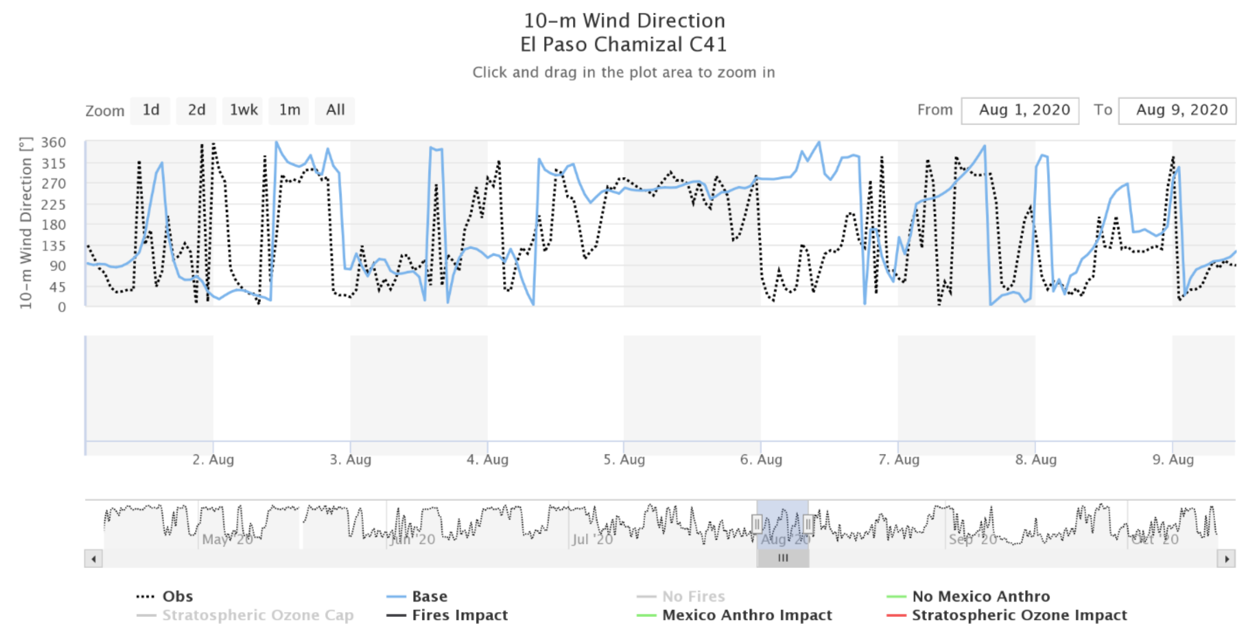

Figure 3-21. Observed (black dotted line), base model (blue) wind direction time series for August 1-9, 2020 at the El Paso Chamizal C41 monitor.

After extensive evaluation of model performance, we find that 2020 NRTEEM does not agree with observations as well as the 2019 model. COVID-related changes in activity may reduce the correspondence of actual emissions to modeled emissions and may explain some of this discrepancy. Despite this, we find the 2020 model performance acceptable for its intended purpose – to be used as a tool for TCEQ to quickly identify potential exceptional events.

3.4 High Ozone Day Summary and Event Case Studies

In this section, we review days on which observed MDA8 ozone exceeded 70 ppb and the NRTEEM modeled contribution from wildfires, Mexico anthropogenic emissions or stratospheric ozone equalled or exceeded 0.7 ppb (1% of the NAAQS). We then present three case studies that serve as examples of days when high ozone at Texas monitors was potentially influenced by fires, stratospheric ozone and transport from Mexico. The case studies outline application of the NRTEEM modeling to understanding causes of high ozone at Texas monitors and are intended to illustrate strengths in the NRTEEM system as well as areas where additional work is needed.

Because the 2020 ozone season is still in progress, it is premature to review specific individual high ozone days for their potential to be designated an exceptional event. EPA encourages air agencies to prepare demonstrations only for exceptional events with regulatory significance[5] and the regulatory significance of a particular event may not be known until the end of the 2020 ozone season. Also, the TCEQ is performing the review and validation of the monitoring data used in this section; therefore, this analysis is considered preliminary because observed values presented in this section are subject to change.

During the period of April 15-October 15, 2020, Houston, Dallas, Fort Worth, San Antonio, El Paso, Beaumont-Port Arthur and Austin area ozone monitors all recorded MDA8 values exceeding 70 ppb. Table 3-4 lists 44 days when a CAMS had MDA8 ozone > 70 ppb and NRTEEM modeled fire, stratosphere or Mexico anthropogenic EI impacts equalled or exceeded 0.7 ppb (1% of the NAAQS). These fire and stratosphere contributions may be relevant to attainment depending upon whether they are in the top four highest MDA8 observations for that CAMS at the end of the ozone season and whether the CAMS determines the attainment status for its area. The Mexico anthropogenic EI ozone contributions are potentially relevant to Section 179b demonstrations.

Table 3-4. CAMS observed MDA8 ozone and NRTEEM modeled impacts on MDA8 ozone for each day where observed MDA8 exceeded 70 ppb and NRTEEM modeled fire, stratosphere or Mexico anthropogenic EI impacts were equal to or greater than 0.7 ppb (1% of the NAAQS) for the April 15-October 15, 2020 period. Red shading indicates an impact on MDA8 ozone equal to or exceeding 0.7 ppb.

Date	Region	Site Name	MDA8 Ozone (ppb)		Impact on MDA8 Ozone (ppb)		
			Observed	NRTEEM	Fires	Mexico Anthro Emissions	Stratosphere
4/20	SA	Camp Bullis C58	72.38	69.44	0.04	1.20	5.78
4/20	HGB	Houston Westhollow C410	71.25	64.41	0.58	-1.51	0.94
4/23	HGB	Texas City 34th Street C620	75.43	66.87	0.45	-0.23	0.96
4/24	HGB	Conroe Relocated C78	72.63	66.98	0.72	0.21	1.91
4/30	SA	Camp Bullis C58	81.86	70.37	0.29	0.00	1.07
5/6	EP	El Paso UTEP C12	74.63	65.58	0.27	8.69	1.21

[5] https://www.epa.gov/sites/production/files/2018-10/documents/exceptional_events_rule_revisions_2060-as02_final.pdf

Date	Region	Site Name	MDA8 Ozone (ppb)		Impact on MDA8 Ozone (ppb)		
			Observed	NRTEEM	Fires	Mexico Anthro Emissions	Stratosphere
5/9	EP	El Paso UTEP C12	75.00	61.25	0.35	7.51	1.87
5/9	EP	El Paso Chamizal C41	72.13	61.17	0.34	6.76	1.87
5/9	EP	Socorro Hueco C49	73.25	64.38	0.36	10.99	1.90
5/11	HGB	Northwest Harris County C26	74.75	66.63	0.31	0.09	0.96
5/18	HGB	Texas City 34th Street C620	88.25	58.86	0.37	0.89	0.36
5/18	HGB	Galveston 99th Street C1034	76.13	54.50	0.34	0.86	0.35
5/18	HGB	Seabrook Friendship Park C45	75.75	64.45	0.39	0.71	0.33
5/18	Austin	Dripping Springs School C614	72.38	62.93	1.52	2.08	0.28
5/19	DFW	Dallas Hinton C401	75.25	67.04	1.20	2.24	0.25
5/19	DFW	Dallas North #2 C63	72.88	70.07	1.04	1.89	0.23
5/19	DFW	Eagle Mountain Lake C75	74.33	78.52	1.03	2.61	0.24
5/19	DFW	Fort Worth Northwest C13	83.13	71.97	1.24	2.81	0.28
5/19	DFW	Keller C17	74.75	77.94	1.05	2.31	0.24
5/19	DFW	Grapevine Fairway C70	86.63	77.96	0.95	1.78	0.22
5/29	DFW	Cleburne Airport C77	72.50	58.16	1.56	0.07	0.11
5/30	DFW	Eagle Mountain Lake C75	73.63	55.55	0.73	0.00	0.32
6/1	DFW	Grapevine Fairway C70	72.50	59.52	0.72	0.05	0.38
6/2	HGB	Northwest Harris County C26	71.00	60.57	0.62	0.91	0.54
6/2	HGB	Lang C408	73.25	55.45	0.76	1.05	0.57
6/10	HGB	Oyster Creek C1607	73.75	59.61	1.01	0.02	1.90
6/13	HGB	Texas City 34th Street C620	80.88	55.30	0.42	0.00	0.71
6/16	HGB	Mercer Arboretum C557	71.88	72.44	0.74	0.01	0.54
6/17	HGB	Huffman Wolf Road C563	72.88	63.10	1.29	0.01	0.32
6/17	HGB	Conroe Relocated C78	79.13	68.03	1.19	0.01	0.35
6/25	EP	El Paso UTEP C12	75.13	65.52	0.93	16.08	0.95
7/7	EP	El Paso UTEP C12	79.13	68.97	0.15	14.79	1.82
7/7	EP	El Paso Chamizal C41	73.25	65.52	0.14	11.43	1.88
7/14	EP	Socorro Hueco C49	71.75	60.30	0.51	10.98	1.01
7/25	EP	El Paso UTEP C12	83.38	47.83	0.15	17.54	0.93
7/25	EP	El Paso Chamizal C41	71.38	43.25	0.16	15.80	0.87
8/1	EP	El Paso UTEP C12	81.13	68.31	0.14	12.13	0.49
8/1	EP	El Paso Chamizal C41	73.75	65.26	0.15	9.53	0.50
8/1	EP	Socorro Hueco C49	74.63	54.01	0.16	1.81	0.56
8/4	DFW	Dallas Redbird Airport Executive C402	73.13	59.70	2.91	0.27	0.12
8/4	EP	Ivanhoe C414	71.88	58.75	0.23	4.63	2.14
8/4	EP	Socorro Hueco C49	74.13	56.89	0.21	5.43	2.30
8/4	EP	Skyline Park C72	74.00	59.60	0.34	4.98	2.08
8/4	HGB	Baytown Garth C1017	76.00	58.76	1.91	0.04	0.08
8/6	HGB	Conroe Relocated C78	77.63	70.69	0.82	0.06	0.12

Date	Region	Site Name	MDA8 Ozone (ppb)		Impact on MDA8 Ozone (ppb)		
			Observed	NRTEEM	Fires	Mexico Anthro Emissions	Stratosphere
8/8	EP	El Paso Chamizal C41	73.63	49.58	0.11	6.74	1.70
8/8	EP	Skyline Park C72	73.75	48.58	0.12	6.76	1.80
8/14	EP	Ascarate Park SE C37	71.00	65.36	0.08	18.97	1.38
8/14	EP	Socorro Hueco C49	74.25	63.16	0.09	17.53	1.45
8/16	DFW	Grapevine Fairway C70	77.67	60.07	0.23	1.29	0.35
8/18	HGB	Manvel Croix Park C84	98.75	75.75	1.13	0.04	0.03
8/18	HGB	Lake Jackson C1016	73.88	69.31	1.18	0.02	0.04
8/18	EP	Socorro Hueco C49	71.88	52.70	0.18	1.95	0.97
8/18	HGB	Houston Croquet C409	81.63	72.68	1.09	0.04	0.03
8/18	HGB	Houston Bayland Park C53	82.88	69.59	0.93	0.06	0.06
8/18	HGB	Houston Monroe C406	80.29	64.86	1.06	0.05	0.05
8/18	HGB	Houston Westhollow C410	74.38	64.00	0.80	0.08	0.10
8/18	HGB	Park Place C416	80.13	64.05	1.07	0.05	0.06
8/18	HGB	Tom Bass C558	87.25	70.44	1.12	0.03	0.04
8/18	HGB	UH Moody Tower C695	80.38	65.32	0.99	0.06	0.07
8/18	HGB	Clinton C403	72.17	59.16	1.01	0.05	0.07
8/18	HGB	Houston Deer Park #2 C35	81.13	58.45	0.80	0.05	0.08
8/19	EP	Ivanhoe C414	73.86	61.23	0.23	1.21	1.02
8/19	EP	El Paso UTEP C12	72.50	65.86	0.25	6.61	1.27
8/19	EP	Skyline Park C72	71.13	64.42	0.25	2.73	1.23
8/19	HGB	Texas City 34th Street C620	71.38	50.83	1.02	0.00	-0.01
8/20	HGB	Houston Bayland Park C53	73.63	72.72	1.05	0.00	-0.02
8/20	HGB	Tom Bass C558	71.13	57.94	1.08	0.00	-0.01
8/20	DFW	Eagle Mountain Lake C75	71.75	65.63	1.03	0.00	0.01
8/20	DFW	Fort Worth Northwest C13	75.13	73.96	0.96	0.01	0.01
8/21	EP	Ivanhoe C414	82.63	70.23	0.94	3.03	5.09
8/21	EP	Ascarate Park SE C37	77.13	66.24	1.00	-0.14	6.24
8/21	EP	Socorro Hueco C49	102.25	73.51	0.88	8.59	4.25
8/21	EP	Skyline Park C72	79.88	62.29	1.08	1.69	5.56
8/21	HGB	Wallisville Road C617	71.13	69.25	0.76	0.00	0.12
8/21	HGB	Lynchburg Ferry C1015	72.63	78.15	0.72	0.01	0.09
8/21	HGB	Baytown Garth C1017	71.88	69.25	0.76	0.00	0.12
8/21	HGB	Houston Deer Park #2 C35	74.00	73.94	0.71	0.01	0.08
8/22	EP	El Paso UTEP C12	72.25	63.26	0.69	6.34	2.29
8/22	EP	Socorro Hueco C49	73.00	57.04	0.75	4.11	2.46
8/24	DFW	Fort Worth Northwest C13	72.38	72.56	0.74	0.05	0.78
8/27	EP	El Paso UTEP C12	71.50	68.21	0.49	12.45	2.40
8/29	EP	El Paso UTEP C12	72.50	57.71	0.52	3.44	2.15
10/1	SA	Camp Bullis C58	72.63	60.30	0.64	1.21	0.34

Date	Region	Site Name	MDA8 Ozone (ppb)		Impact on MDA8 Ozone (ppb)		
			Observed	NRTEEM	Fires	Mexico Anthro Emissions	Stratosphere
10/1	HGB	Texas City 34th Street C620	74.88	57.31	1.74	0.00	0.27
10/3	HGB	Northwest Harris County C26	76.75	59.96	1.65	0.00	-0.04
10/3	HGB	Meyer Park C561	77.25	60.22	1.48	0.00	-0.03
10/4	HGB	Manvel Croix Park C84	80.75	64.91	2.38	0.04	-0.02
10/4	HGB	Tom Bass C558	77.75	63.08	2.42	0.05	-0.02
10/4	HGB	Houston Deer Park #2 C35	73.00	60.96	2.33	0.05	-0.01
10/5	HGB	Houston Bayland Park C53	81.13	63.39	1.34	0.06	-0.02
10/5	HGB	Park Place C416	72.25	57.23	1.39	0.05	-0.01
10/5	HGB	UH Moody Tower C695	79.25	57.00	1.39	0.05	-0.01
10/5	HGB	Houston East C1	72.00	53.02	1.36	0.05	0.00
10/5	HGB	Clinton C403	71.63	53.43	1.34	0.05	0.00
10/6	SA	Camp Bullis C58	77.86	69.52	1.35	0.76	0.06
10/6	HGB	Oyster Creek C1607	71.13	63.82	2.93	0.04	-0.03
10/6	DFW	Frisco C31	71.38	64.46	2.09	0.56	-0.02
10/6	DFW	Pilot Point C1032	71.13	68.09	1.99	0.70	-0.01
10/7	SA	San Antonio Northwest C23	71.25	69.91	1.68	1.19	0.02
10/7	SA	Camp Bullis C58	74.50	67.47	1.57	1.19	0.05
10/8	DFW	Denton Airport South C56	71.50	73.67	5.46	0.57	0.03
10/13	HGB	Houston Croquet C409	82.88	81.95	0.36	1.23	0.32
10/13	HGB	Park Place C416	77.13	74.50	0.72	1.48	0.35
10/14	HGB	Conroe Relocated C78	73.00	80.26	0.54	0.89	0.27
Total # of Occurrences ≥ 70 ppb					**65**	**53**	**38**
DFW					16	8	1
HGB					39	8	6
EP					6	31	29
SA					3	5	2
Austin					1	1	0

On high ozone days, there were 65 instances of a monitor with fire impacts on the MDA8 ≥ 0.7 ppb, 53 instances of impacts exceeding this threshold from Mexico anthropogenic emissions and 38 instances of stratospheric ozone impacts exceeding the threshold (Table 3-4). 29 of 38 stratospheric ozone impacts ≥ 0.7 ppb on 2020 days with MDA8 ozone ≥ 70 ppb occurred at El Paso area monitors. 31 of 53 occurrences of Mexico Anthropogenic emission impacts to MDA8 ozone ≥ 70 ppb occurred at El Paso area monitors.

A major difference between the NRTEEM modeling of 2019 and 2020 is the number of days with stratospheric ozone impacts. During the March 1–July 15, 2019 modeling period, there were 103 instances of monitors with stratospheric MDA8 ozone impacts ≥ 0.7 ppb. During the longer 2020 modeling period April 15-October 15, there were 38 instances. Stratospheric ozone impacts were larger overall in the 2019 NRTEEM modeling. In Figure 3-22, we compare the magnitude of stratospheric ozone contributions to the MDA8 in 2019 and 2020 for all days and monitors (left panel) and for monitors that had days with MDA8 ≥ 70 ppb.

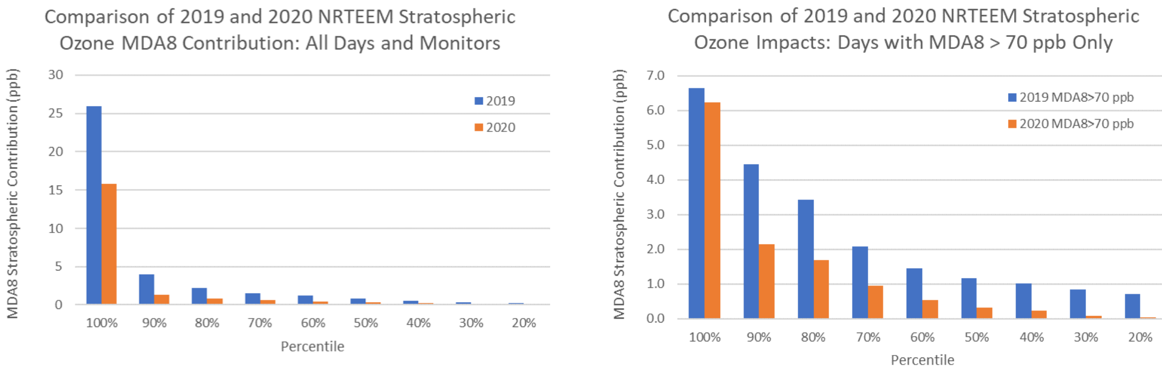

Figure 3-22. Comparison of distribution of stratospheric ozone contributions to the MDA8 for all Texas CAMS during 2019 (blue) and 2020 (orange). Values for percentiles less than 20 are not reported due to their small (<0.1 ppb magnitude).

2020 values of the stratospheric contribution are lower than those in 2019 across all quantiles of the distribution regardless of whether all days are considered, or only days with MDA8 ≥ 70 ppb. Figure 3-23 and Figure 3-24 show the 2019 and 2020 breakdown by Texas region of days with stratospheric ozone impacts ≥ 0.7 ppb and MDA8 ozone ≥ 70 ppb. In 2019, there was a greater number of days that met these two criteria, and, of these days, the largest fraction occurred in the Houston area. In 2020, there were far fewer days with stratospheric ozone impacts ≥ 0.7 ppb and these days were concentrated in the El Paso region. The 2020 distribution of stratospheric ozone impacts is more consistent with the conceptual model of stratospheric ozone intrusions having a greater influence on high elevation areas like El Paso than on low elevation areas like Houston[6]. While it is not clear how much of this variation between the years is driven by differences in weather, the fact that stratospheric contributions were smaller in 2020 at monitors across Texas suggests that change in the model layer structure contributed to the smaller 2020 stratospheric ozone impacts.

[6] https://www.epa.gov/sites/production/files/2018-11/documents/exceptional_events_soi_guidance_11-8-2018.pdf

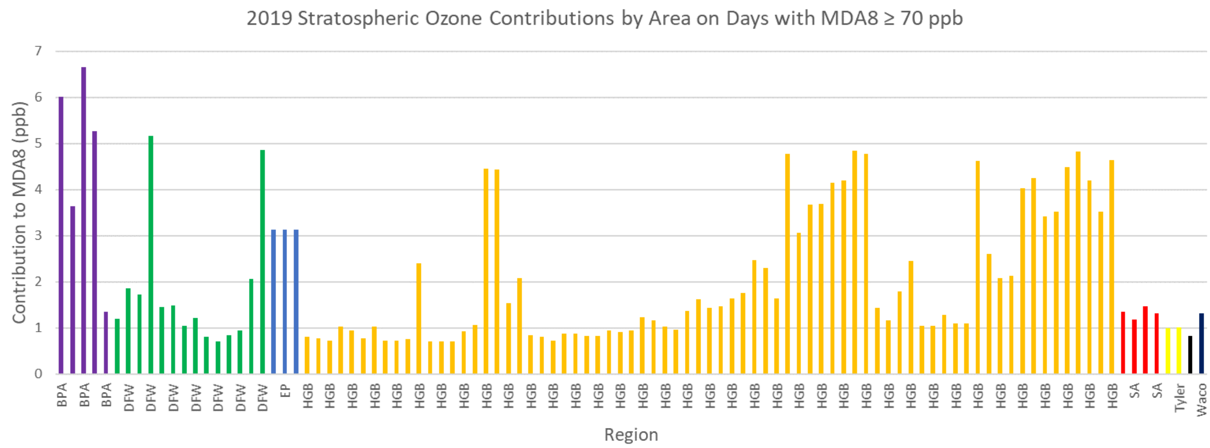

Figure 3-23. Breakdown by Texas region of 2019 days with stratospheric ozone impacts ≥ 0.7 ppb on 2020 days with MDA8 ozone ≥ 70 ppb. The bars show the stratospheric ozone contribution for each day and are color coded by area with HGB orange, El Paso blue, etc.

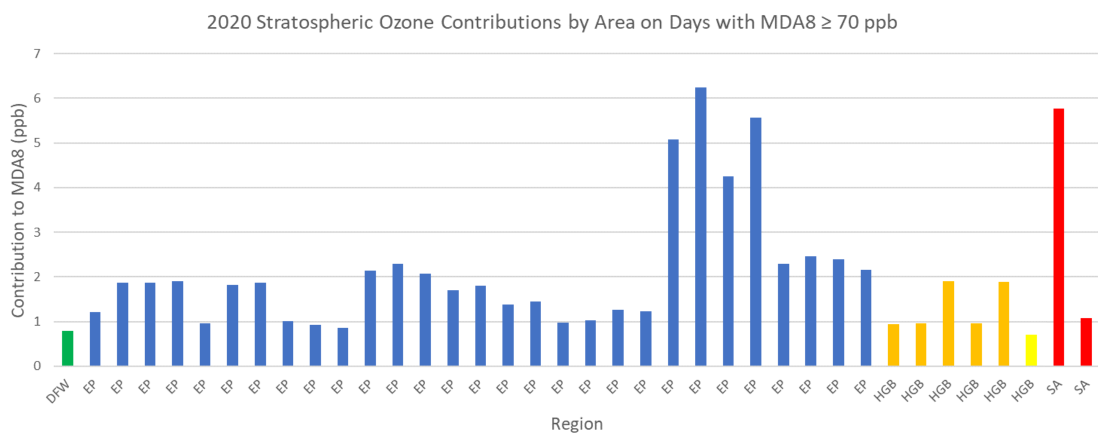

Figure 3-24. Breakdown by Texas region of 2020 days with stratospheric ozone impacts ≥ 0.7 ppb on 2020 days with MDA8 ozone ≥ 70 ppb. The bars show the stratospheric ozone contribution for each day and are color coded by area with HGB orange, El Paso blue, etc.

In Sections 3.4.1, 3.4.2 and 3.4.3, we present case studies for fire, stratosphere and Mexico transport impacts. We focus on days and monitors which had modeled MDA8 ozone impacts that were among the largest of each type during April 15-October 15, 2020.

3.4.1 Fire Impacts

On October 8, 2020, Denton Airport South CAMS 56 in the Dallas-Fort Worth recorded an MDA8 ozone value of 71 ppb. The NRTEEM modeled wildfire contribution to the MDA8 at CAMS 56 was 5.5 ppb (Table 3-4), which was the highest wildfire contribution to any Texas CAMS in 2020 and was the fourth highest MDA8 value of 2020 for CAMS 56[7]. CAMS 56 recorded the highest MDA8 ozone of any monitor in the DFW area on October 8.

[7] https://www.tceq.texas.gov/cgi-bin/compliance/monops/8hr_4highest.pl

The TCEQ's Daily Air Quality Forecast Update for October 8 predicted, "*Light to moderate amounts of smoke from wildfires in Colorado and Wyoming may continue lingering over the Texas Panhandle through the Permian Basin while expanding into Far West Texas and the Rio Grande Valley, though much of the smoke may remain aloft. Meanwhile, the light to moderate amounts of smoke from seasonal fires across portions of East Texas and the Southeast U.S. may linger over the eastern two-thirds of the state as well*."

The NRTEEM MDA8 ozone map for October 8 (left panel of Figure 3-25) shows a broad swath of wildfire impacts across Texas and surrounding states. In Figure 3-26, we present ozone time series for August 5-8 at CAMS 58 (black dotted line: observations; blue line: base model; No Fires: black). The base model generally simulated ozone well during this period. The model underestimated peak 1-hour ozone on August 8 by 7 ppb and showed a maximum 1-hour average ozone impact from wildfires of 6 ppb.

To explore potential source-receptor relationships between wildfires and ozone at CAMS 58 on October 8, we developed back trajectories using NOAA's Hybrid Single-Particle Lagrangian Integrated Trajectory model (HYSPLIT). We used online tools on NOAA ARL's Real-time Environmental Applications and Display sYstem (READY) website (Rolph, 2017) to develop back trajectories with three-dimensional gridded weather data provided by the North American Model (NAM). The NAM has spatial resolution 12 km. Back trajectories originating above CAMS 58 have curved paths which indicate shifting winds in the period leading up to August 8. From October 5-6, air originating in the Colorado-Nebraska-Kansas region travelled southeast toward the DFW area. By October 7, the wind shifted so that the trajectories began turning clockwise and by October 8 winds in the DFW area were from the southeast as Hurricane Delta drew near.

The yellow arrow in Figure 3-27 shows the location of wildfires near the Wyoming-Colorado border on October 5. A large plume of smoke is visible extending east and southeast from these large fires. These plumes are visible on October 5 in the NRTEEM PM fine smoke tracer as well as in the Deep Blue Aerosol Optical Depth (AOD) product displayed in the Earth Observing System Data and Information System (EOSDIS) Worldview viewer (Figure 3-28). There is reasonably good correspondence between the NRTEEM smoke tracer and the AOD. This indicates that the NRTEEM modeling system has produced a fire plume that generally agrees with satellite retrievals that indicate smoke plume locations. The HYSPLIT back trajectories indicate the potential for this smoke-affected air mass over the central plains states to have influenced air in DFW on October 8.

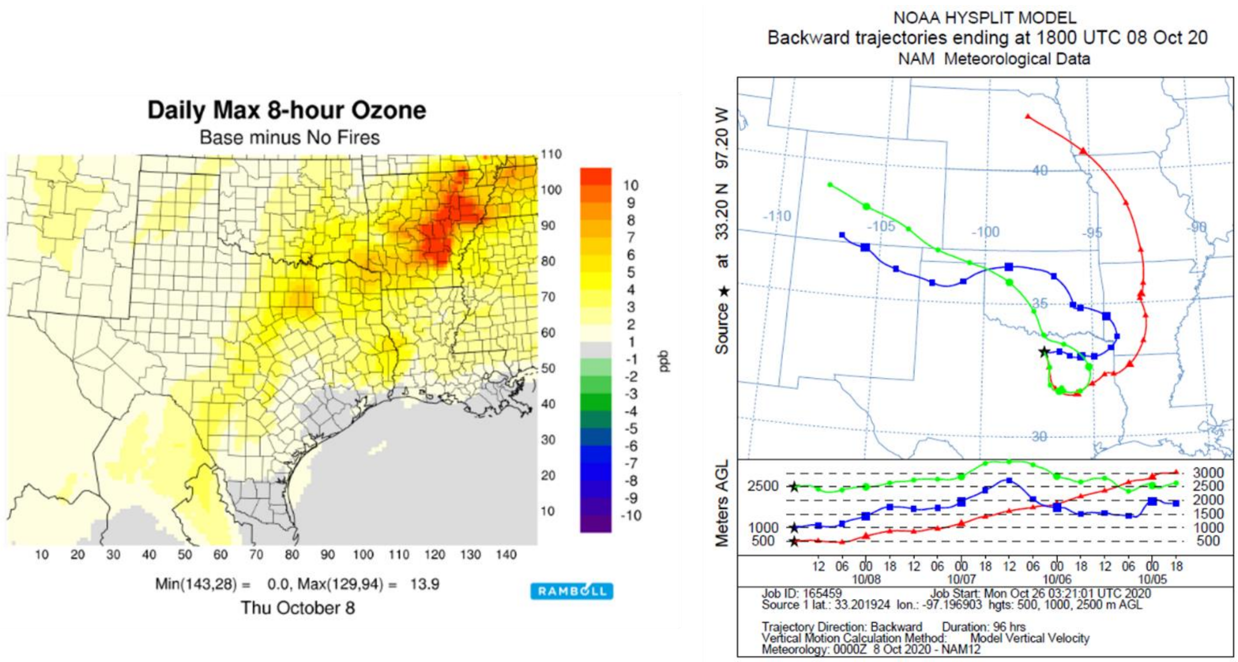

Figure 3-25. Left panel: NRTEEM modeled fire impacts on MDA8 ozone within the 12 km grid. Right panel: HYSPLIT back trajectories ending at CAMS 56 at the time of peak 1-hour ozone. Back trajectories ending at 500 m (red), 1,000 m (blue) and 2,500 m (green) above CAMS 56 are shown.

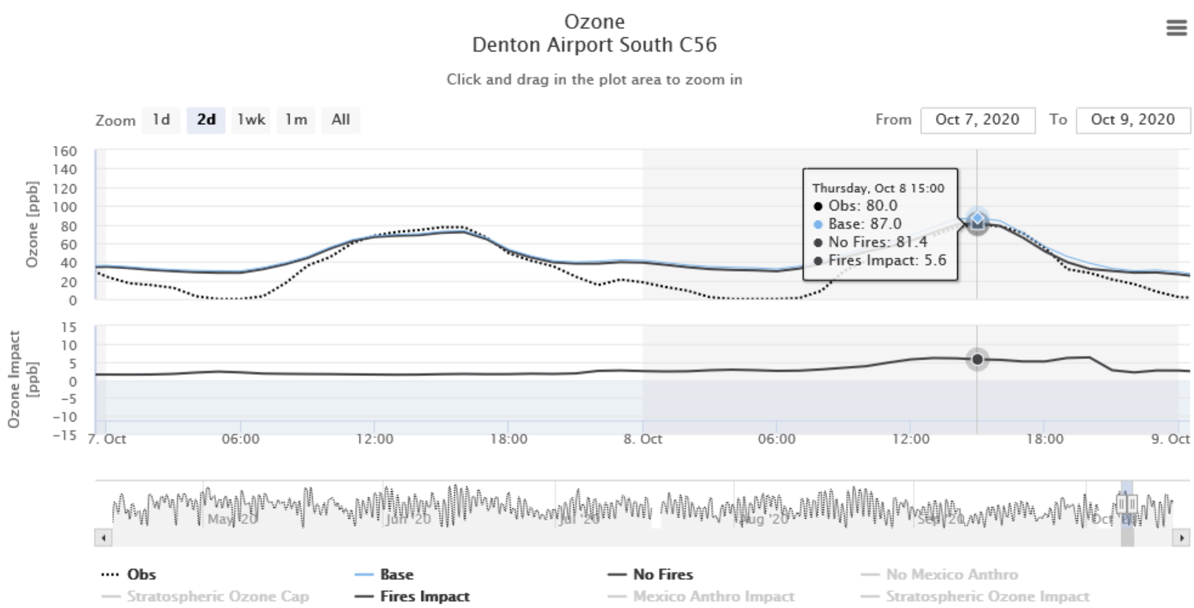

Figure 3-26. Observed (black dotted line), base model (blue) and No Fires sensitivity run differences from base model (black) ozone time series for October 7-8, 2020 at Denton Airport South CAMS 56.

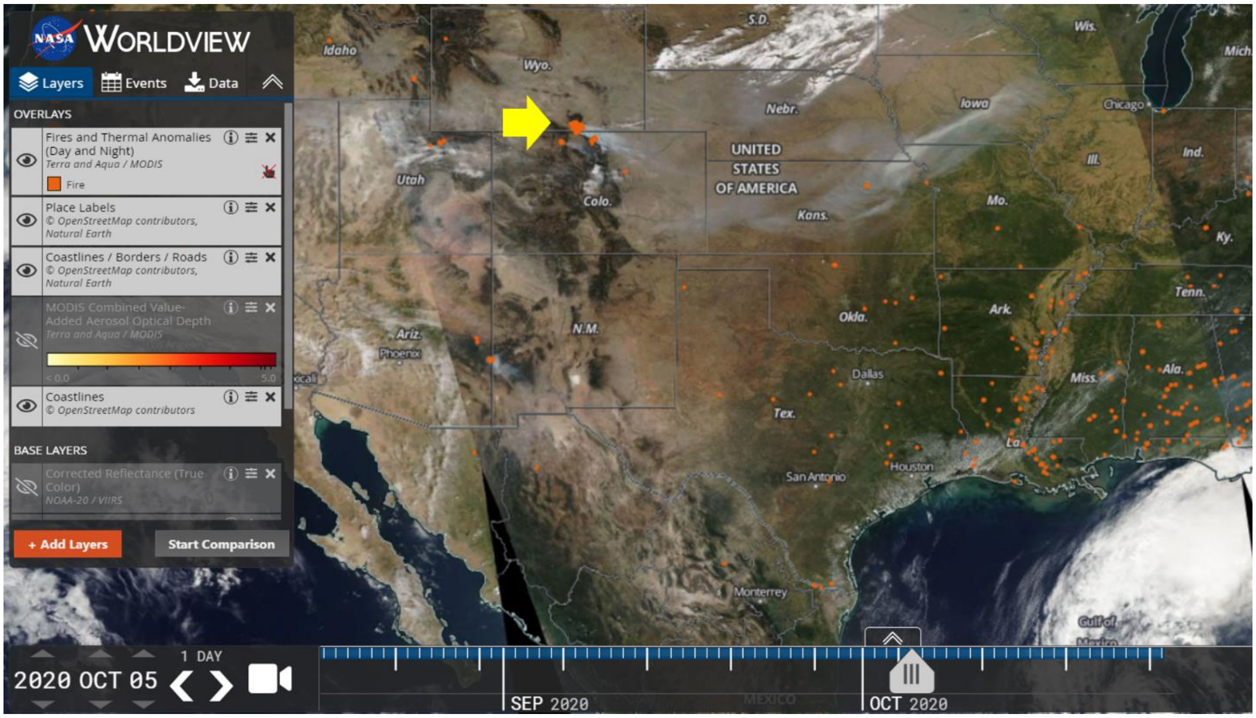

Figure 3-27. NASA EOSDIS Worldview plots of wildfires (orange icons) along the Colorado border (yellow arrow). Smoke plumes extend to the east and southeast of these wildfires. The outer bands of Hurricane Delta are visible in the Gulf of Mexico.

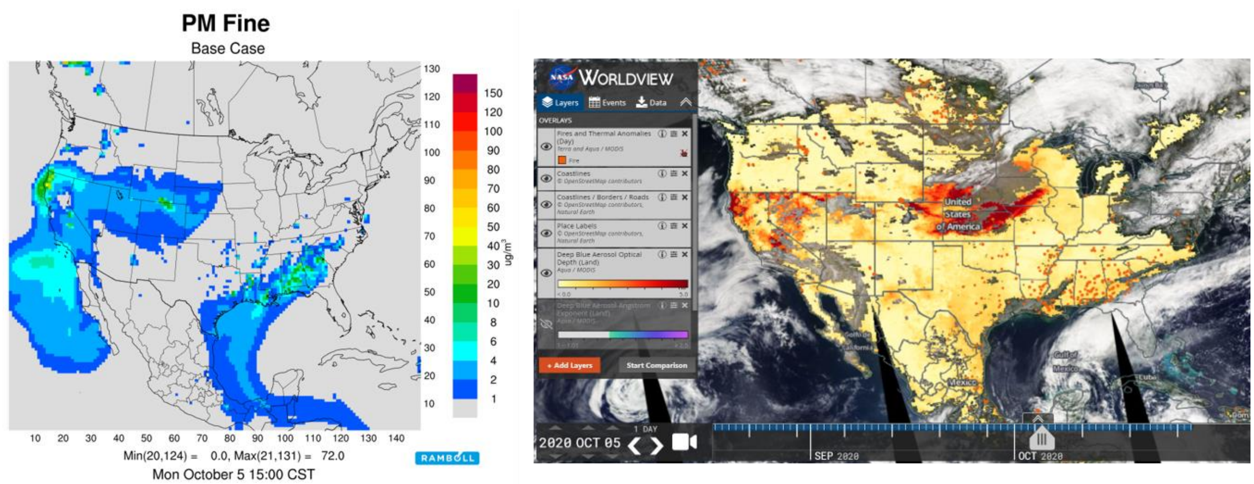

Figure 3-28. Left panel: NRTEEM modeled 1-hour average PM Fine within the 36 km grid at 3 pm CST on October 5. Right panel: NASA EOSDIS Worldview plots of wildfires (orange icons) and Deep Blue Aerosol Optical Depth.

By October 7, wildfire activity in the Mississippi Valley intensified. In Figure 3-29, wildfires are visible along the Mississippi Valley into East Texas. Smoke from Wyoming fires is visible in the DFW area and over the Texas Panhandle. Clouds from Hurricane Delta prevented retrieval of thermal anomalies from fires and AOD over East Texas. On October 7, NRTEEM shows smoke and ozone impacts from a large number of small fires in the Mississippi Valley and East Texas (Figure 3-30). Between October 7 and October 8, the NRTEEM PM fine and fire ozone impact animations show southeasterly winds over East Texas bringing the fire-affected air toward the DFW area. By October 8, there is a large, diffuse area of enhanced PM fine and ozone impacts from the fires over the DFW area, other parts of North Texas and Oklahoma and Arkansas. By 3 pm, Hurricane Delta was moving inland and an area of clear air was present along the Texas coastline.

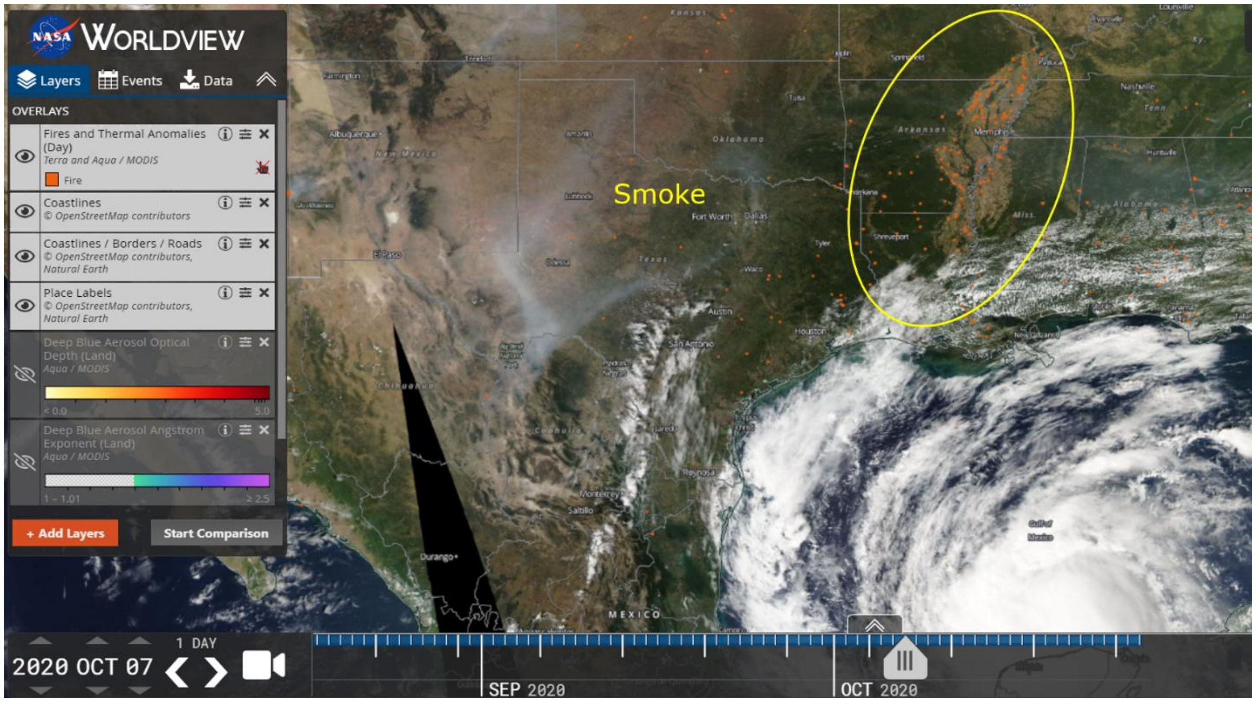

Figure 3-29. NASA EOSDIS Worldview plots of wildfires (orange icons) along the Mississippi Valley (yellow oval). Smoke transported south from the Wyoming/Colorado wildfires is visible over the Texas Panhandle and the DFW area. Hurricane Delta is visible in the Gulf of Mexico and southeast Texas.

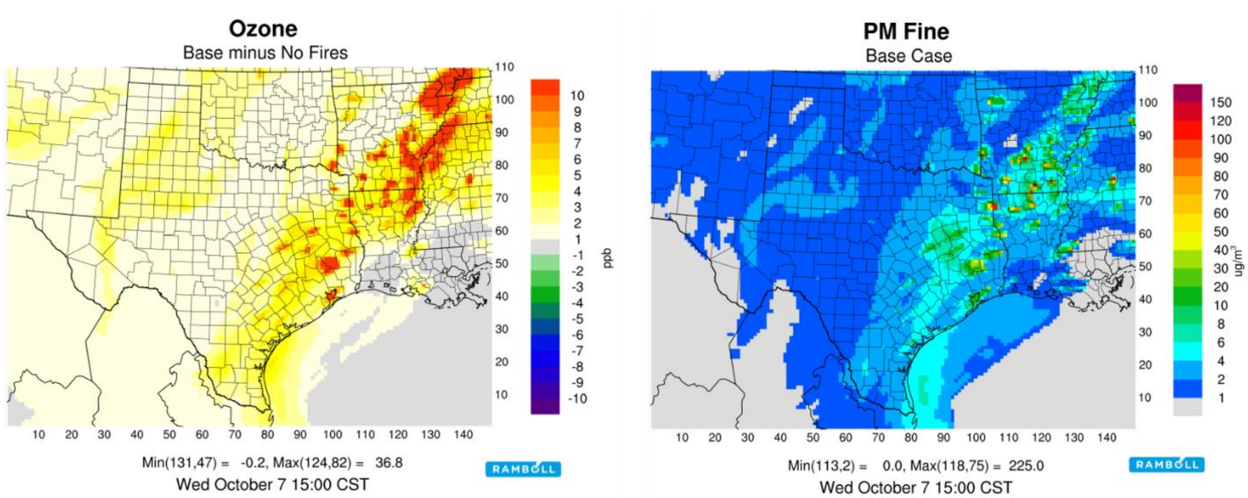

Figure 3-30. Left panel: NRTEEM modeled fire impacts on MDA8 ozone within the 12 km grid at 3 pm CST on October 7. Right panel: NRTEEM modeled 1-hour average PM Fine within the 36 km grid at 3 pm CST on October 7.

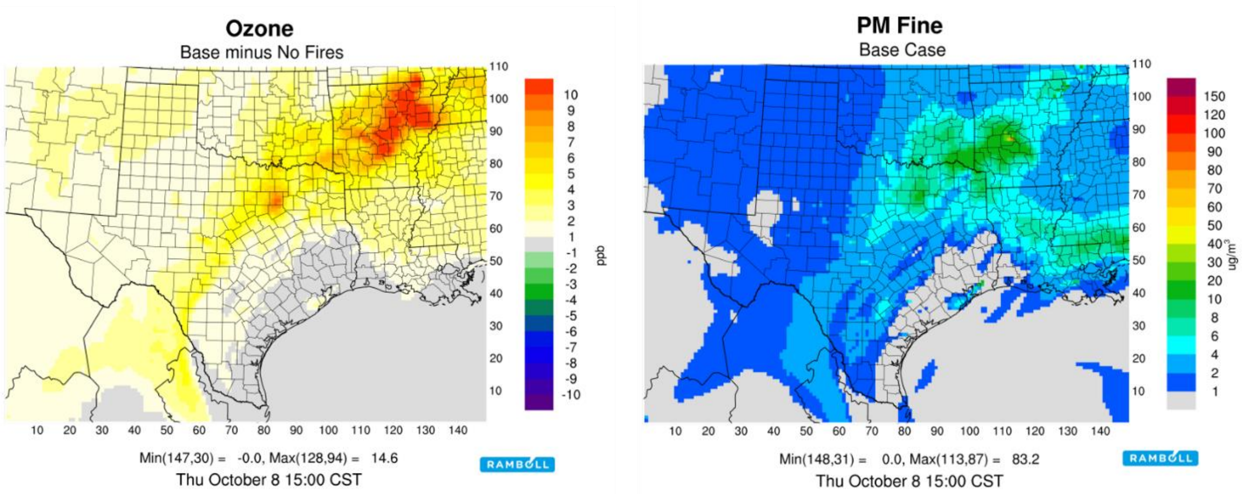

Figure 3-31. Left panel: NRTEEM modeled fire impacts on MDA8 ozone within the 12 km grid at 3 pm CST on October 8. Right panel: NRTEEM modeled 1-hour average PM Fine within the 36 km grid at 3 pm CST on October 8.

In order to establish a clear, causal relationship between fires and ozone at a monitor, it is necessary to show that fire emissions had an impact at the monitor. While satellite imagery can be used to diagnose the presence of smoke within the column of atmosphere between the earth's surface and the satellite sensor, it does not indicate whether smoke was present at ground level. Biomass burning markers such as levoglucosan and/or enhanced values of ground-level $PM_{2.5}$ can be used to establish this type of impact. CAMS 56 monitors hourly ground-level $PM_{2.5}$ and the hourly $PM_{2.5}$ time series is shown along with hourly ozone for CAMS 56 in Figure 3-32. Also shown are $PM_{2.5}$ time series for other DFW area $PM_{2.5}$ monitors. Values missing from hourly ozone and $PM_{2.5}$ measurements Figure 3-32 were flagged by TCEQ as QAS[8].

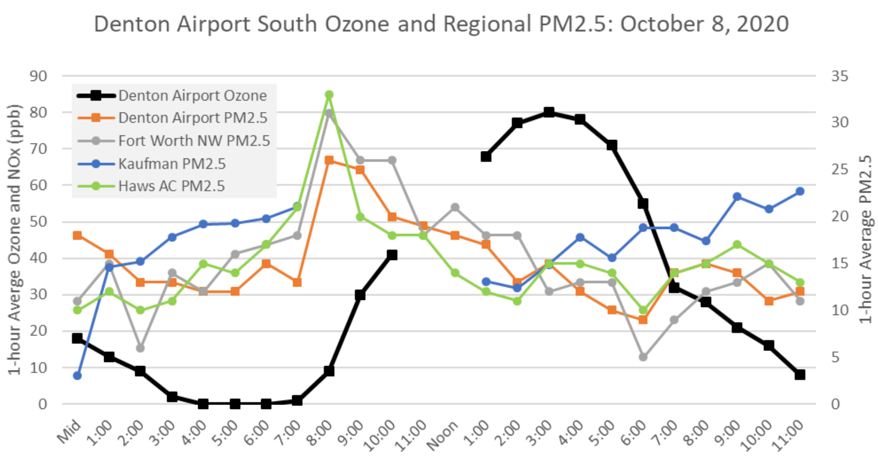

Figure 3-32. Time series of hourly observed ozone and $PM_{2.5}$ from Denton Airport South CAMS 56 on October 8, 2020. Also shown are time series of hourly observed $PM_{2.5}$ from DFW area monitors. Time series data from the TCEQ TAMIS website[9].

[8] Quality control audit in progress

[9] https://www.tceq.texas.gov/cgi-bin/compliance/monops/daily_summary.pl?cams=0085

Enhanced values of PM2.5 suggest that the fire plumes affected ground level air quality on October 8 in the DFW area. It is also possible that local (non-fire) emissions sources affected CAMS 56, given that CAMS 56 had the highest MDA8 value in the DFW area. The lack of correlation between the CAMS 56 PM2.5 and ozone time series suggest that the wildfires contributed to the background ozone entering DFW but did not impact CAMS 56 alone as a narrow, discrete plume.

During 2020, Ramboll developed the capability to track fires and evaluate their emissions-to-distance ratio, Q/D, which is a metric used by the EPA to determine the Tier required for an exceptional event demonstration. The threshold for a Tier II analysis is ≥ 100 (tpd/km). Figure 3-33 shows the Q/D ratio for all fire groups on October 5 and October 7. On October 5, the Wyoming fires had a Q/D ratio of 2.5, which is the largest value of any fire in the domain on that day. By October 7, fire activity in the Mississippi Valley and East Texas intensified and a group of fires with Q/D in the 1-2 tpd/km range are visible, None of these fire groups that potentially influenced CAMS 56 meets the EPA threshold for a Tier II analysis.

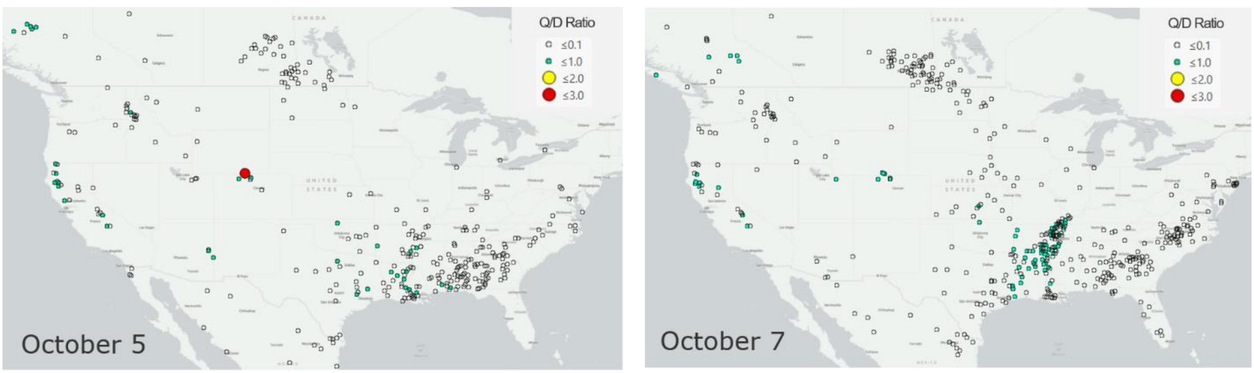

Figure 3-33. Q/D ratios for fire groups on October 5 (left panel) and October 7 (right panel).

The current NRTEEM fire group tracking capability allows a fire to be tracked for one day only. During this episode, it was difficult to determine from satellite imagery whether smoke from the Mississippi Valley fires influenced ozone at CAMS 56 because clouds from Hurricane Delta prevented retrieval of the AOD along the HYSPLIT transport path between those fires and CAMS 56 on October 7 and October 8. Expanding the existing fire group tracking across multiple days will allow identification of fires that contributed to ozone at a particular monitor. This is important because EPA requires that ozone impacts be attributed to specific wildfires during exceptional event demonstrations and multi-day tracking of wildfires will allow identification of wildfires for photochemical modeling with source apportionment that isolates the contribution of those fires to the affected monitor.

In summary, on October 8, wildfires near the Colorado/Wyoming border and agricultural fires in East Texas, the Mississippi Valley, Louisiana and Arkansas produced plumes that brought particulates and ozone to the DFW area. NRTEEM-modeled MDA8 ozone wildfire impacts were largest at Denton Airport South CAMS 56. October 8 produced the fourth highest value of the MDA8 ozone monitored at CAMS 56 in 2020 and the largest wildfire impact on any Texas monitor on days with MDA8 ≥ 70 ppb. Although peak 1-hour ozone was overestimated at CAMS 56, the NRTEEM smoke plume simulation is consistent with satellite smoke and AOD retrieval products and supports a source-receptor relationship between the fires and monitors in Wyoming. It was not possible to evaluate consistency of modeled smoke tracer and satellite AOD products for wildfires to the east and southeast of the DFW area due to the presence of clouds from Hurricane Delta. We recommend developing a multi-day tracking capability to enable identification of source fire groups in order to tag them for source apportionment analysis to support future exceptional event demonstrations.

3.4.2 Stratospheric Ozone Impacts

The NRTEEM system accounts for stratospheric ozone impacts through evaluation of ozone in air entering the domain through top of the model and through lateral boundaries near model top. Air entering through the lateral boundaries above ~325 mb is included in the stratospheric contribution because the tropopause can be lower than the NRTEEM model top depending upon latitude and season. The NRTEEM base model caps the lateral and top boundary conditions for ozone at 60 ppb. To quantify the stratospheric ozone contribution, we perform a Stratospheric Ozone simulation identical to the base model except that the lateral and top boundary conditions for ozone are not capped. We then subtract the base model ozone concentrations from the Stratospheric Ozone simulation in order to calculate the impact of ozone of stratospheric origin.

The second largest stratospheric ozone contribution for any Texas CAMS in 2020 as of October 15 occurred on April 20 at Camp Bullis (CAMS 58) in the San Antonio area. On April 20, CAMS 58 had observed MDA8 ozone 72 ppb and its NRTEEM-modeled stratospheric ozone contribution to the MDA8 ozone was 5.6 ppb (Table 3-4). The peak 1-hour stratospheric ozone contribution was 7.2 ppb (Figure 3-34). The model simulated hourly ozone reasonably well on April 20 with a base run NMB of 13%.

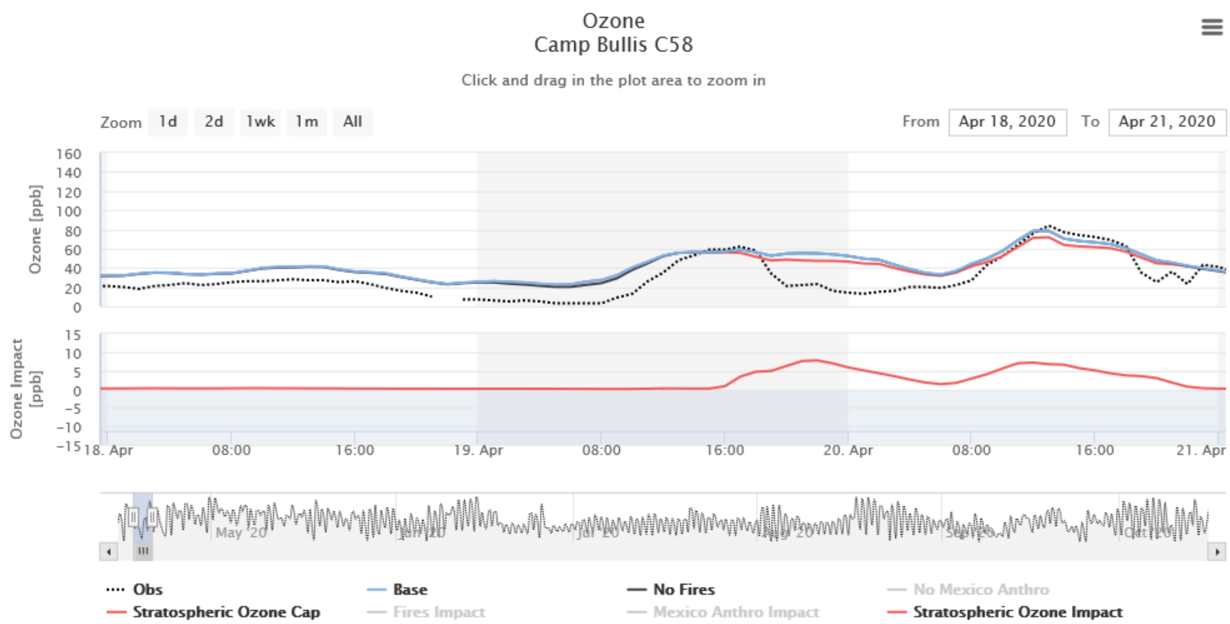

Figure 3-34. Time series of observed (black) and modeled (blue) 1-hour average ozone and stratospheric ozone contribution (red, lower time series) for CAMS 58.

Stratospheric ozone intrusions occur most frequently along the mid-latitude storm tracks and over regions of high terrain such as the Rocky Mountains (e.g. Skerlak et al., 2014; Sprenger and Wernli, 2003). The impact of stratospheric ozone intrusions on surface ozone is typically greatest in the spring months of March, April and May (e.g. Jaffe et al., 2018). The NRTEEM modeling indicates a regional-scale, multi-day stratospheric impact on the southwestern US and Texas surface ozone during April 18-20 (Figure 3-35 and Figure 3-36). Given the magnitude of the modeled impacts on ground-level ozone in East Texas and the fact that the impacts occurred outside the climatologically favored region, we investigated the April event further.

We developed back trajectories using the HYSPLIT model with three-dimensional gridded weather data provided by the 12 km NAM. Back trajectories originating above CAMS 58 at 1,000 m -3,000 m extend back from San Antonio across the southwest. The HYSPLIT back trajectories show that on April 18-19, air travelling toward CAMS 58 passed over the Nevada, Arizona and New Mexico. The back trajectories indicate that air that was above 6,000 m on April 17-19 eventually descended below 1,000 m on April 20 in the vicinity of CAMS 58. This is well within the typical mixed layer depth for the San Antonio area.

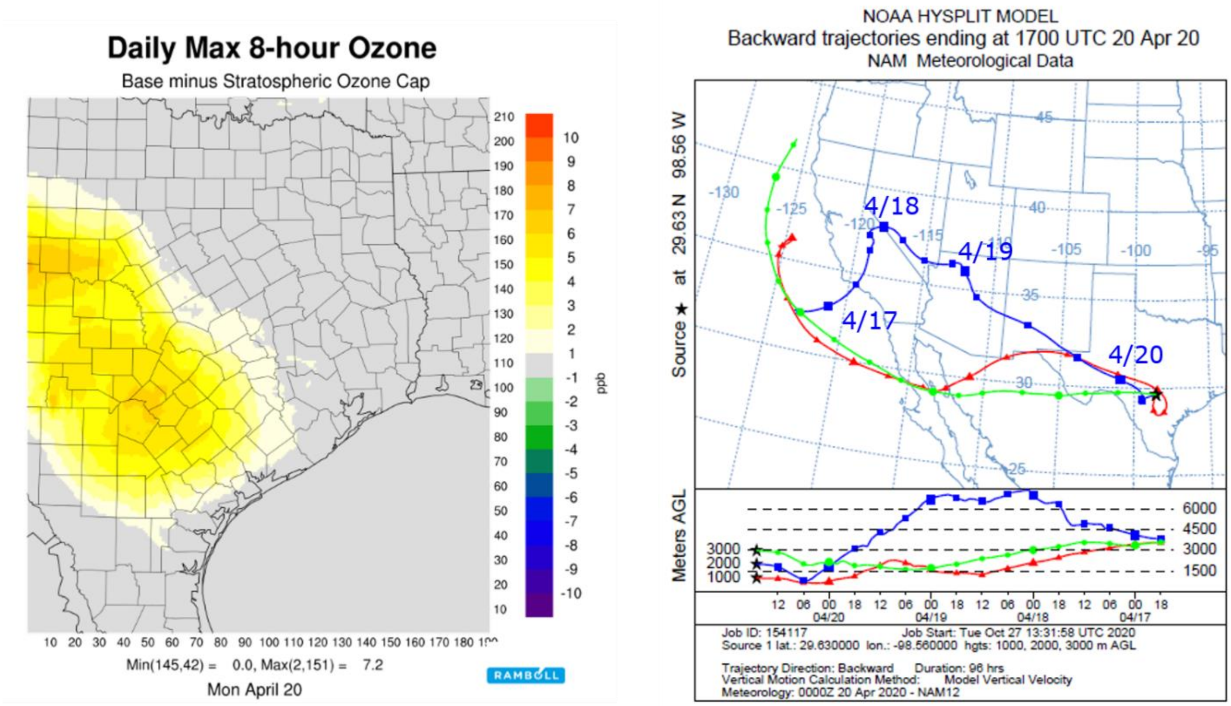

Figure 3-35. Left panel: NRTEEM modeled stratospheric impacts on MDA8 ozone within the 4 km grid on June 12. Right Panel: HYSPLIT back trajectories ending at CAMS 58 at the time of peak 1-hour ozone. Back trajectories ending at 1000 m (red), 2,000 m (blue) and 3,000 m (green) above CAMS 56 are shown.

NOAA's Climate Prediction Center[10] describes conditions associated with stratospheric intrusions: "Stratospheric Intrusions are identified by very low tropopause heights, low heights of the 2 potential vorticity unit (PVU) surface, very low relative and specific humidity concentrations, and high concentrations of ozone. Stratospheric Intrusions commonly follow strong cold fronts and can extend across multiple states…Along with the dry air, Stratospheric Intrusions bring high amounts of ozone into the tropospheric column and possibly near the surface." Stratospheric air is typically low in carbon monoxide (CO). EPA recommends evaluating whether areas of enhanced total column ozone and low total column CO are collocated, which may indicate the presence of a stratospheric intrusion[11].

The upper panels of Figure 3-36 show that NRTEEM modeled an area of stratospheric ozone impacts in the southwestern US extending eastward to the Texas coast by April 20. The middle panels of Figure 3-36 show NOAA's 250 mb analysis of isotachs, divergence (blue shading) and streamlines for April

[10] https://www.cpc.ncep.noaa.gov/products/stratosphere/strat_int/

[11] https://www.epa.gov/sites/production/files/2018-11/documents/soi_forecasting_tools_november_2018.pdf

18-20. The 250 mb field shows the presence of an upper level trough over the western US on April 18 in the vicinity of the April 18 HYSPLIT back trajectories shown in Figure 3-35. The lower panel of Figure 3-36 shows that the tropopause pressure was relatively high (i.e. tropopause heights were relatively low) in the region where the 250 mb trough was present on April 18-19 compared to the April 20 long-term mean tropopause pressure field (Figure 3-37).

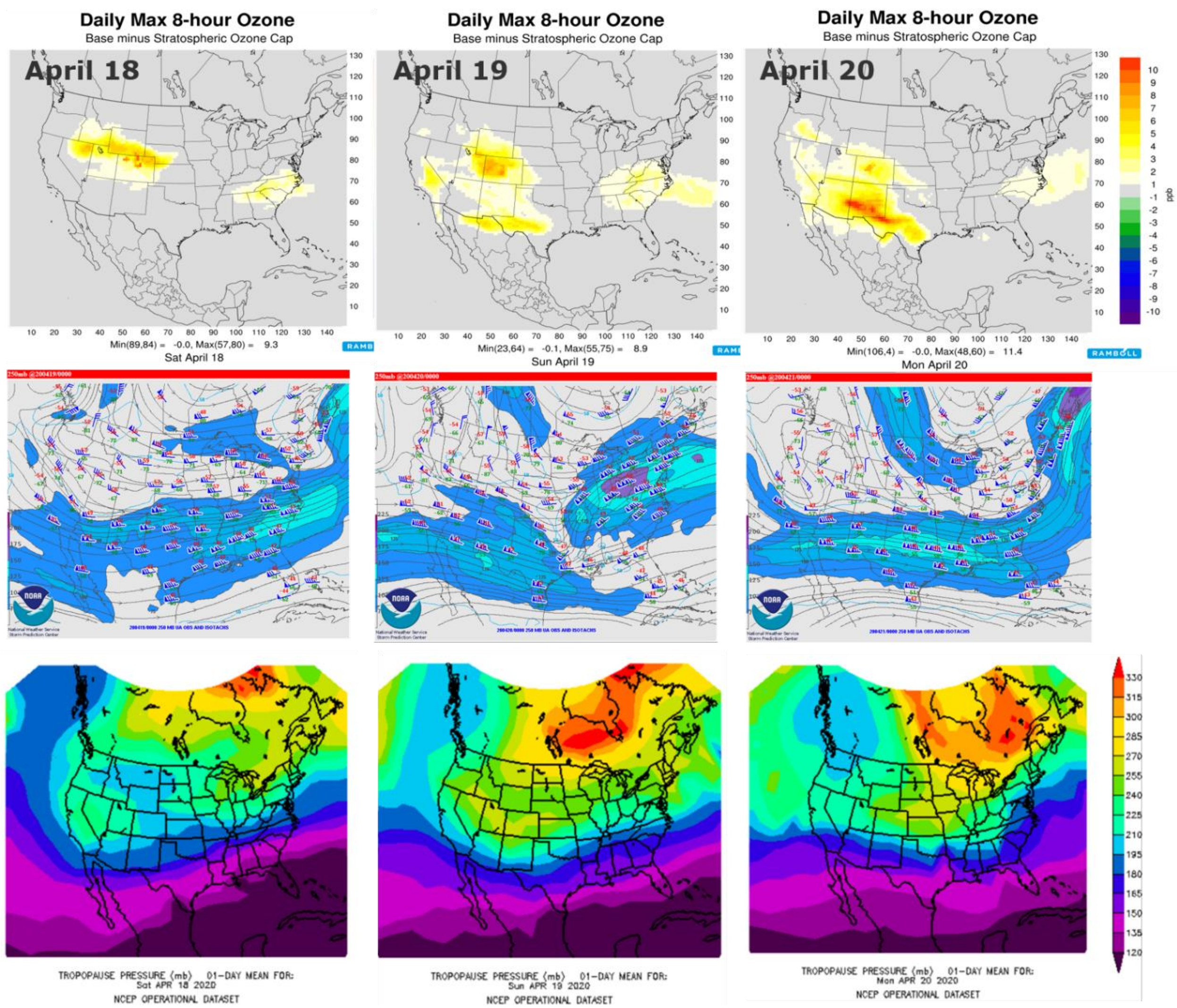

Figure 3-36. Upper panels: NRTEEM modeled stratospheric impacts on ground level MDA8 ozone within the 36 km grid April 18-20, 2020. Middle panels: 250 mb streamlines, isotachs, and divergence (blue shading) for April 18-20, 2020. Lower panels: NCEP Reanalysis tropopause pressure contours for April 18-20, 2020.

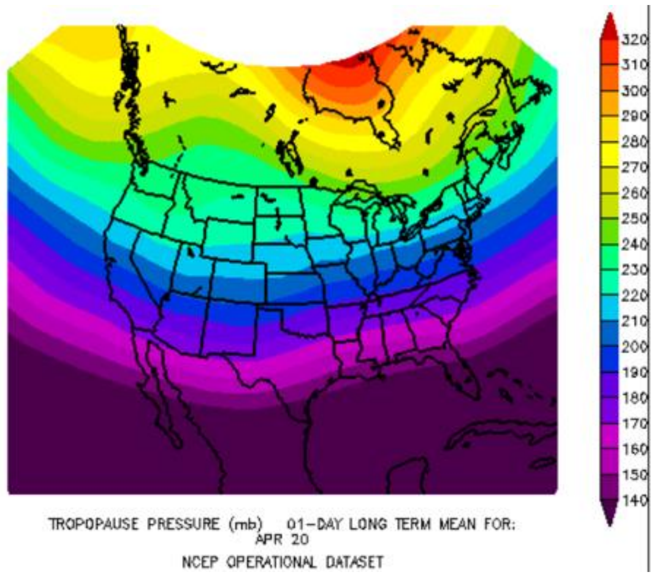

Figure 3-37. NCEP Reanalysis long-term mean tropopause pressure contours for April 20.

Figure 3-38 shows a NASA Real Time Air Quality Monitoring System (RAQMS) longitudinal ozone cross sections along the 30°N latitude line, which lies about 40 km east of CAMS 58. The cross section shows a filament of high ozone air extending down from the stratosphere toward the surface and suggests a possible influence on lower tropospheric ozone near the latitude of San Antonio by April 20. Figure 3-39 shows a similar longitudinal cross section for the WACCM stratospheric ozone tracer, O3S. As in the RAQMS cross section, the WACCM modeling shows that stratospheric air extended downward into the troposphere and moved eastward with time, reaching the longitude of San Antonio by April 20. Figure 3-40 shows maps of WACCM O3S at 992.5 hPa for April 18-20 and illustrates the eastward movement of the area of enhanced O3S tracer across Texas and into the San Antonio area.

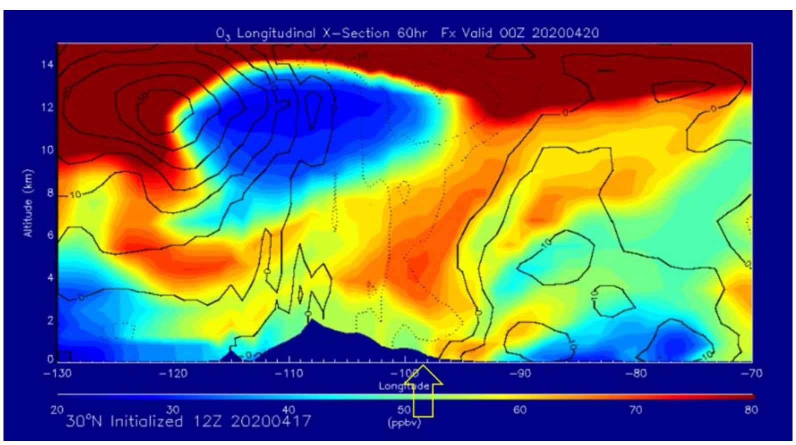

Figure 3-38. RAQMS longitudinal ozone cross section along 30°N for April 20 at 0 UTC. The 30°N latitude line is approximately 40 km north of CAMS 58. The yellow arrow shows the approximate longitude of CAMS 58.

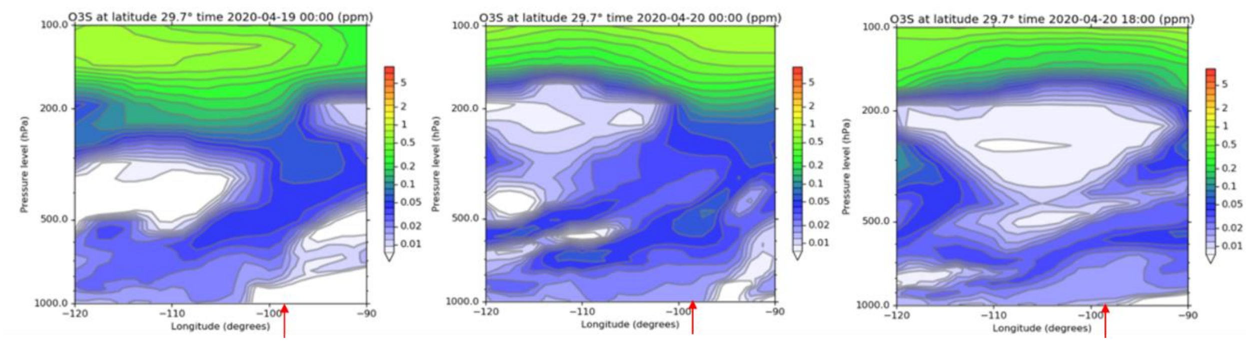

Figure 3-39. Longitudinal ozone cross sections of the WACCM stratospheric ozone tracer (in ppm) along 29.7°N for April 19 at 0 UTC (left), April 20 at 0 UTC (center) and April 20 at 18 UTC (center). The red arrow shows the approximate longitude of CAMS 56.

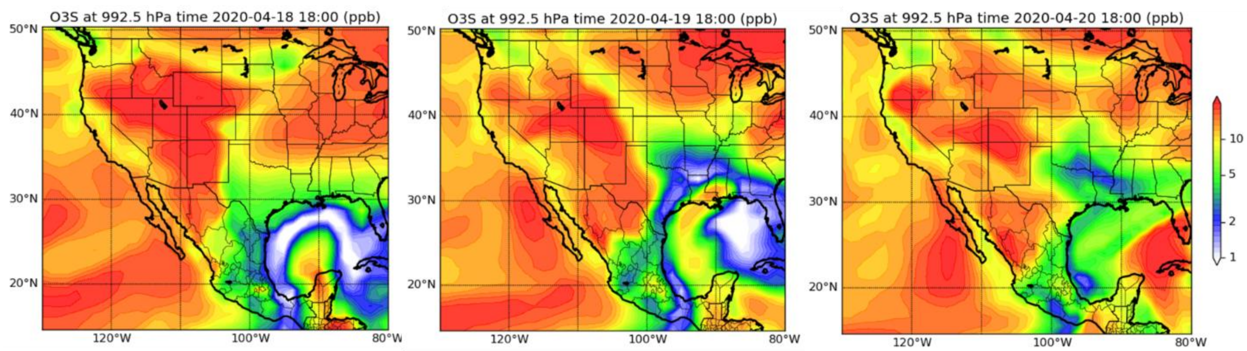

Figure 3-40. WACCM stratospheric ozone tracer (O3S) plots at 992.5 hPa for April 18 (left), April 19 (center) and April 20 (right). Units are ppb.

The AIRS total column CO was not available for this period. Ramboll reviewed the Suomi NPP/OMPS total ozone column product for April 18-20, but no enhanced areas of total ozone were present in the western US (not shown). We reviewed upper air soundings to determine whether dry air consistent with a stratospheric ozone intrusion was present along the HYSPLIT back trajectories shown in Figure 3-35.

Figure 3-41 is a skew-T diagram that plots temperature, dew point and wind data from the radiosonde sounding above Santa Teresa, NM at 12 UTC on April 19. The skew-T plot indicates the presence of a deep layer of dry air extending from about 3,000-6,500 m in the vicinity of the back trajectory. The dry layer is diagnosed through inspection of the dew point depression, which is the distance between the temperature (red line) and the dew point (black dotted line). During April 19, air with low relative humidity was present near ground level in the west Texas (Figure 3-42) indicating the presence of very dry air near the surface.

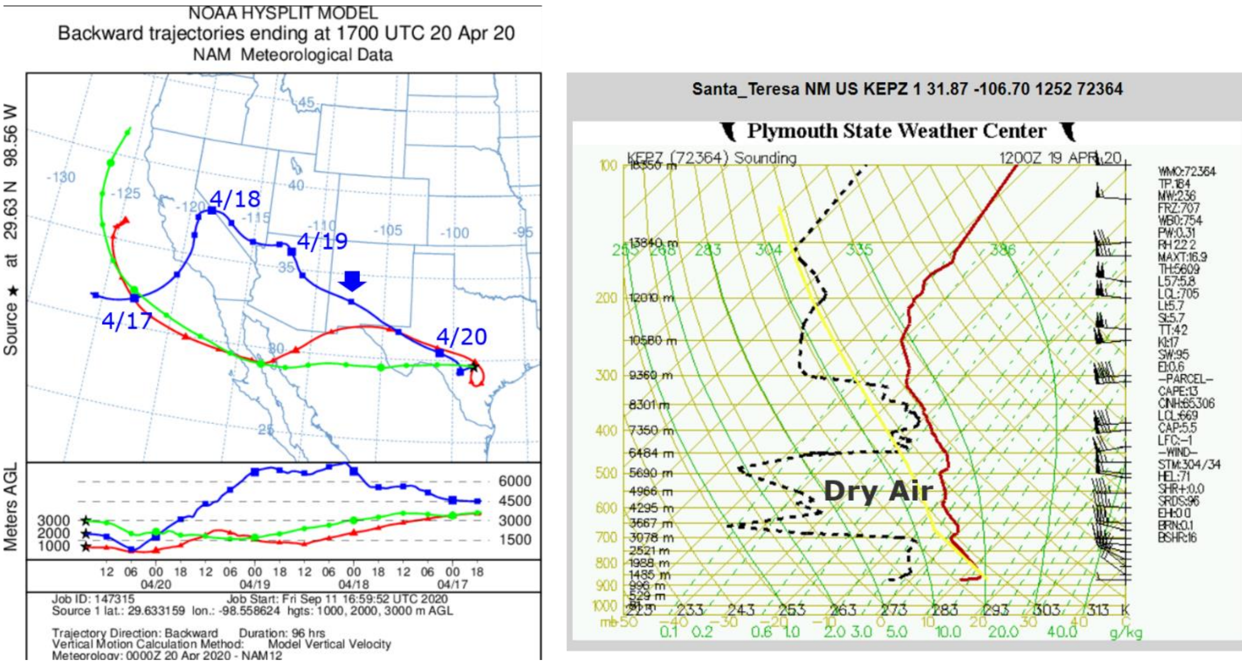

Figure 3-41. Left panel as in Figure 3-35. Right panel: skew T diagram for Santa Teresa, NM at 12:00 UTC on April 19 showing a dry layer of air in the mid-troposphere in the vicinity of the back trajectory. The red solid line is the temperature sounding and the black dashed line is the dew point. The blue arrow in the HYSPLIT plot shows the trajectory point for 12:00 UTC on April 19. Santa Teresa, NM is southeast of this point near the TX-NM border.

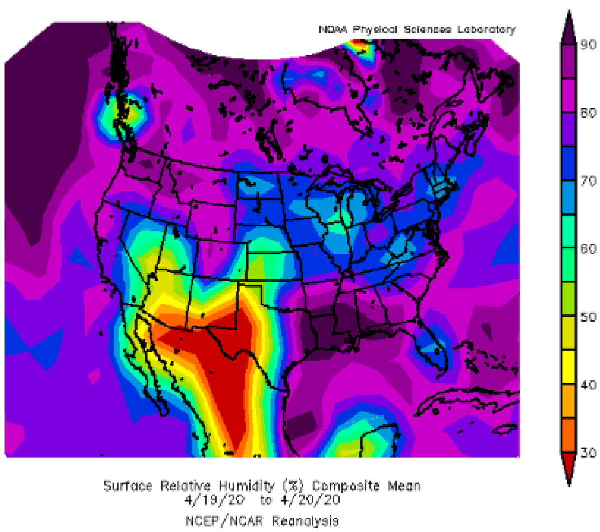

Figure 3-42. NCEP Reanalysis contour plot of average surface relative humidity for April 19-20. Plot developed using NCEP online tools[12].

Another possible mechanism for bringing ozone-rich stratospheric air to ground-level is deep convection. Strong downdrafts that accompany vigorous mixing within deep convective clouds can

[12] https://psl.noaa.gov/data/composites/day/

bring stratospheric air downward. Animations of true color imagery on NOAA's AerosolWatch site indicate that there were no clouds consistent with deep convection in the San Antonio region on April 20 (not shown).

The products described above are consistent in suggesting a possible stratospheric intrusion on June 9-12 over the western US. The lack of a substantial signal in the total column ozone suggests it was not a very strong intrusion, but the weight of evidence from the other data products suggest that the location and magnitude of NRTEEM-modeled stratospheric impacts at the surface in San Antonio is reasonable.

NRTEEM simulated a contribution > 0.7 ppb from stratospheric ozone at monitors across a broad region of southeast Texas on April 20. The highest modeled stratospheric impact occurred in San Antonio at the Camp Bullis CAMS 58, but impacts were modeled to occur across south central Texas. HYSPLIT back trajectories and meteorological and satellite analysis products suggest the air arriving in San Antonio on April 20 may have been influenced by a stratospheric ozone intrusion associated with an upper level disturbance crossing the southwestern US several days earlier. Further investigation would be required to develop an analysis that demonstrates stratospheric influence on San Antonio ozone on April 20. For example, analysis of the height of the 2 PVU surface and the potential vorticity of the 320 K surface could provide evidence that a tropopause folding event occurred over the US during April 18-19.

3.4.3 Impacts from Mexican Anthropogenic Emissions

Next, we examine impacts from Mexican anthropogenic emissions at Texas monitors on days when MDA8 ozone exceeded 70 ppb during April 15-July 15, 2019. The largest ozone impacts in Texas from Mexican anthropogenic emissions tend to occur under a southerly wind regime, when ozone is typically low to moderate (Johnson et al., 2017). There is considerable uncertainty in the Mexico emissions inventory (Shah et al., 2018). While some emissions sources/sectors could be biased high, the inventory could also be missing significant sources. 2020 NRTEEM modeling results are also affected by uncertainty in emissions due to the influence of COVID-19 on emissions source activity levels.

The largest modeled ozone impacts from Mexico anthropogenic emissions on days when monitored MDA8 ozone exceeded 70 ppb occurred in El Paso. During August 2020, El Paso saw several high ozone episodes. For all El Paso monitors, some or all of the 4 highest MDA8 days during 2020 occurred in August (Figure 3-43). On these August days, El Paso monitors frequently saw contributions of 5 ppb or more from Mexico anthropogenic emissions (Table 3-4). In this section, we review August 21, 2020 as an example of a high ozone day in El Paso with large impacts from ozone transport from Mexico. August 21 was the highest MDA8 ozone day in 2020 for the Ascarate Park, Socorro Hueco, Skyline Park and Ivanhoe CAMS.

El Paso-Juarez													
El Paso UTEP C12/A125/X151/G125	2	08/08/2020	1100	85	07/25/2020	1100	83	08/01/2020	1000	81	07/07/2020	1000	79
Ascarate Park SE C37/A332/A172/X159	1	08/21/2020	1100	77	08/14/2020	1100	71	05/09/2020	1100	70	08/22/2020	1000	69
Chamizal C41/AH126	1	08/08/2020	1000	73	08/01/2020	0800	73	07/07/2020	1000	73	05/09/2020	1100	72
Socorro Hueco C49/F312	1	08/21/2020	1100	102	08/14/2020	1100	74	08/04/2020	1100	74	08/01/2020	0800	74
Skyline Park C72	1	08/21/2020	1000	79	08/04/2020	1100	74	08/08/2020	1100	73	08/19/2020	1000	71
Ivanhoe C414/F514	1	08/21/2020	1100	82	08/19/2020	0900	73	08/04/2020	1100	71	09/03/2020	1100	68

Figure 3-43. Dates and MDA8 ozone values for the four highest MDA8 ozone days of 2020 as of October 27, 2020 for El Paso area CAMS. Figure from TCEQ website[13].

Figure 3-44 shows spatial plots of MDA8 ozone and the contribution to MDA8 ozone from Mexico anthropogenic emissions on the El Paso 4 km grid. Mexico anthropogenic emission impacts are largest in Mexico and near the Texas-Mexico border with a region of impacts exceeding 10 ppb extending north from Mexico into Texas. The largest Mexico anthropogenic emission contributions in the El Paso area on August 21 occurred at Socorro Hueco CAMS 49 and Ivanhoe CAMS 414, which were modeled to have impacts of approximately 8.6 ppb and 3.0 ppb, respectively (Table 3-5). A region of small ≤ (±1 ppb) MDA8 ozone impacts is visible near the intersection of the New Mexico, Texas and Mexico borders. Ascarate Park CAMS 37 had a small negative MDA8 ozone contribution from Mexico emissions, and the two other CAMS in the vicinity of the negative MDA8 impacts, El Paso UTEP and Chamizal, had small positive contributions and did not exceed 70 ppb on August 21[14].

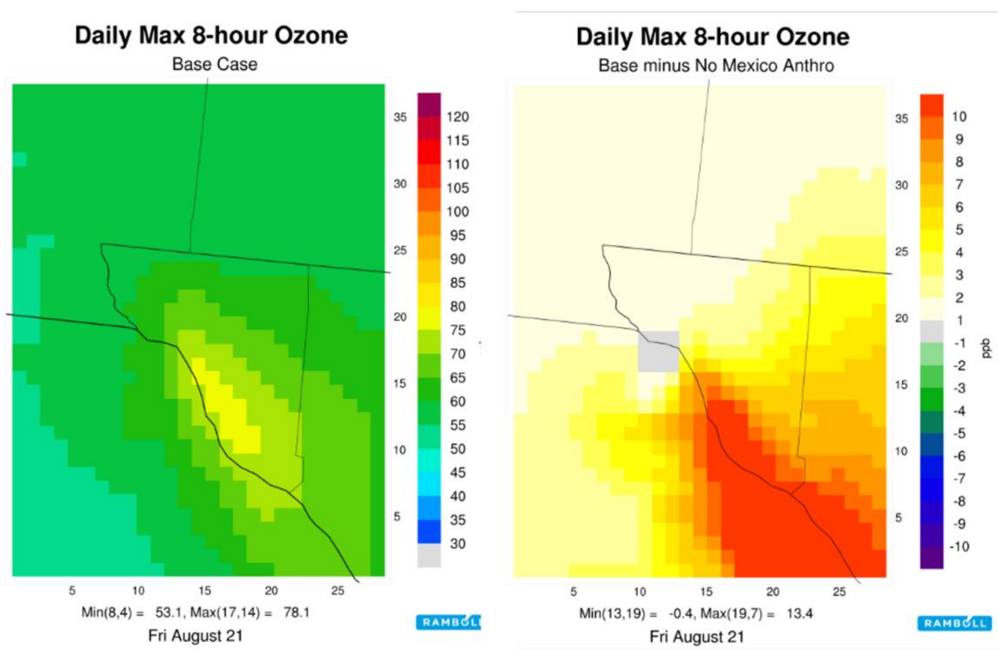

Figure 3-44. NRTEEM modeled MDA8 ozone within the 4 km El Paso grid on August 21 (left) and modeled impacts from Mexico anthropogenic emissions on MDA8 ozone (right).

[13] https://www.tceq.texas.gov/cgi-bin/compliance/monops/8hr_4highest.pl
[14] https://www.tceq.texas.gov/cgi-bin/compliance/monops/8hr_monthly.pl

Table 3-5. Impacts from Mexico anthropogenic emissions on MDA8 ozone for El Paso area CAMS with MDA8 ozone > 70 ppb on August 21, 2020.

Date	Site Name	MDA8 Ozone (ppb)		Impact on MDA8 Ozone (ppb)		
		Observed	NRTEEM	Fires	Mexico Anthro Emissions	Stratosphere
8/21	Ivanhoe C414	82.63	70.23	0.94	3.03	5.09
8/21	Ascarate Park SE C37	77.13	66.24	1.00	-0.14	6.24
8/21	Socorro Hueco C49	102.25	73.51	0.88	8.59	4.25
8/21	Skyline Park C72	79.88	62.29	1.08	1.69	5.56

The NRTEEM modeling system underestimated peak 1-hour ozone at all El Paso CAMS on August 21. (Figure 3-45 and Figure 3-46). The low bias was especially pronounced at Socorro Hueco CAMS 49, where peak 1-hour ozone was underestimated by approximately 30 ppb. Peak ozone was better simulated at the UTEP and Chamizal monitors, which had lower peak values (MDA8 <70 ppb) on August 21 (not shown). The time series of the modeled wind speed at Socorro Hueco shows a high bias throughout most of the day on August 21 (Figure 3-47). The modeled wind direction was steady and from the west from midnight through 4 pm on August 21. The observed wind direction, however, was more variable. Figure 3-48 indicates there were several wind shifts at Socorro Hueco over the course of the day that WRF did not capture. Wind shifts occurred at other El Paso area CAMS but were not simulated by WRF, which modeled steady westerly winds at El Paso monitors (not shown). Simulated winds that are stronger and steadier than the observed lighter shifting winds may have contributed to the underestimate of peak hourly ozone on August 21 at Socorro Hueco CAMS 49. Light, shifting winds would enhance local ozone in El Paso by recirculating ozone and precursors, whereas stronger steady winds would ventilate the area, reducing ozone.

In addition to the challenges of modeling El Paso's complex terrain and meteorology, the emission inventory for Ciudad Juarez introduces substantial uncertainty in modeling of El Paso. Further analysis would be needed to understand the sources of the model's underestimate of peak 1-hour ozone at these monitors and to understand whether the simulation of Mexico anthropogenic impacts played a role in the underestimate.

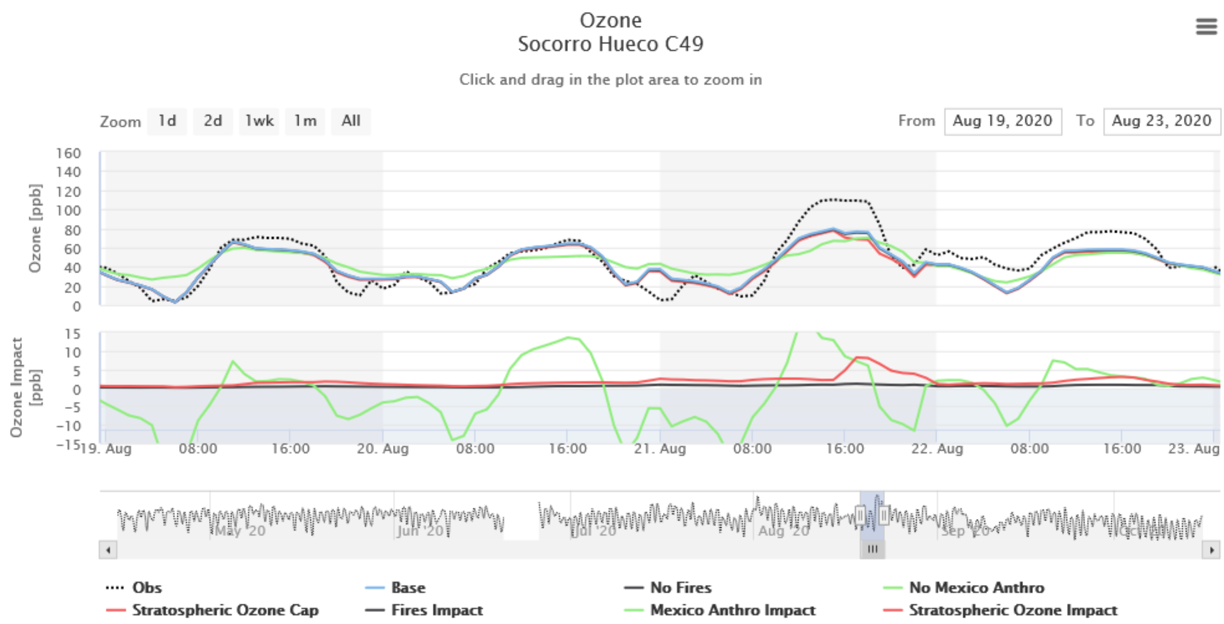

Figure 3-45. Upper panel: observed (black dotted line), base model (blue), No Mexico Anthro sensitivity run differences from base model (green) ozone time series for August 19-22 at Socorro Hueco (CAMS 49). Lower panel: Mexico anthropogenic impacts are shown in green and stratospheric ozone impacts are shown in red.

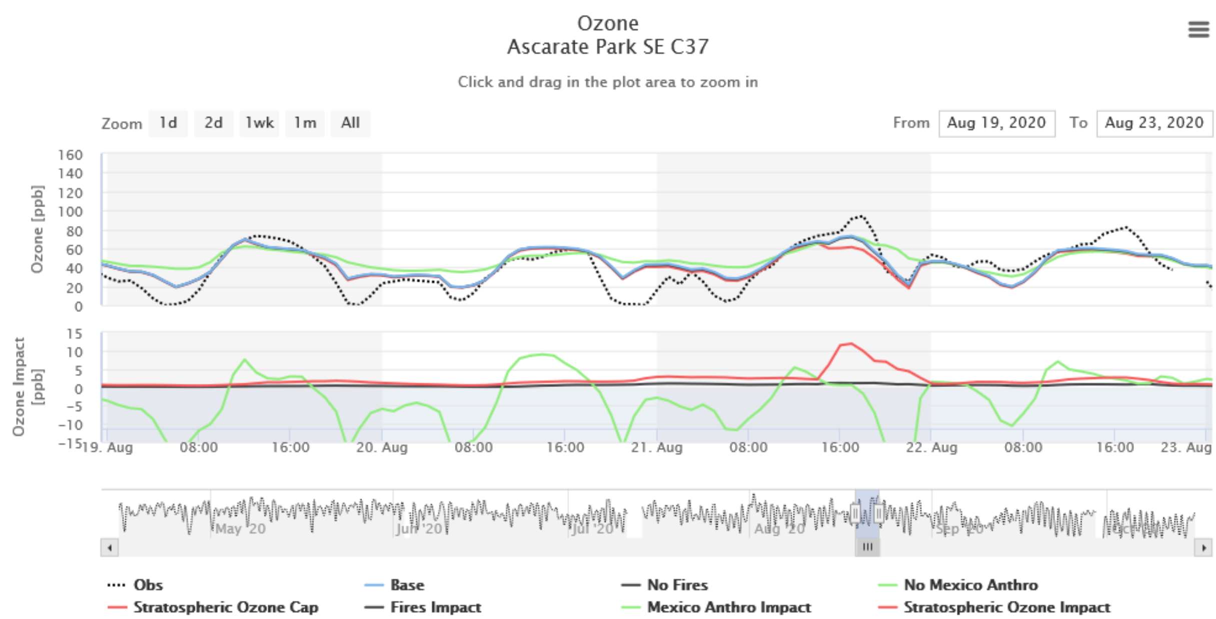

Figure 3-46. As in Figure 3-45 for Ascarate Park CAMS 37.

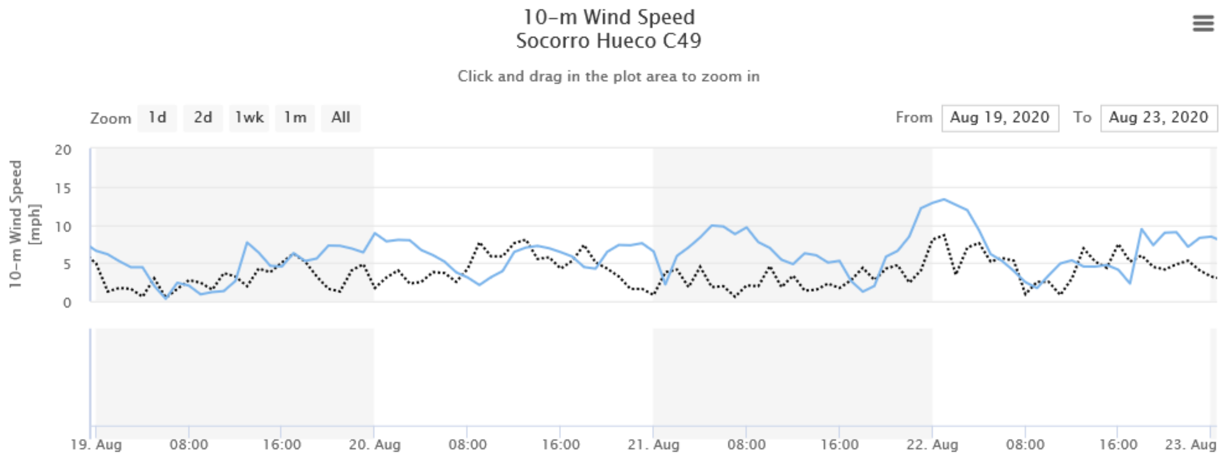

Figure 3-47. Wind speed at 10 meters above ground level for the Socorro Hueco CAMS 49 monitor for August 19-22, 2020.

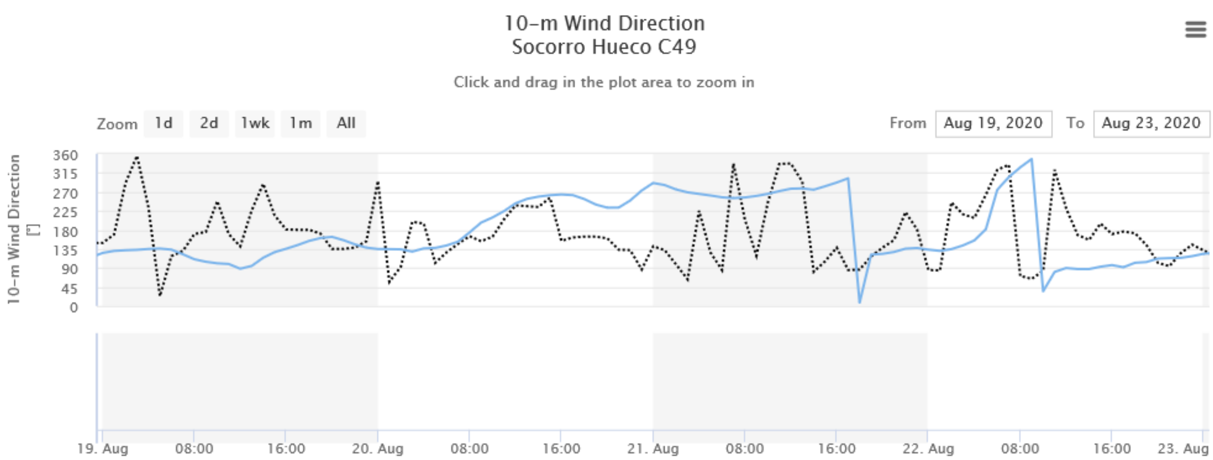

Figure 3-48. Wind direction at 10 meters above ground level for the Socorro Hueco CAMS 49 monitor for August 19-22, 2020.

Throughout 2020, NRTEEM modeling shows strong evidence of ozone impacts sources of background ozone in El Paso. In 2020, El Paso had frequent modeled impacts from stratospheric ozone as well as from international ozone transport from Mexico. Impacts from wildfires were generally small in 2020 but occurred intermittently throughout the ozone season.

3.5 Overall Assessment

3.5.1 Main Findings

Evaluation of WRF meteorological statistical metrics revealed that El Paso had more months outside the simple and complex benchmarks than the DFW, HGB and San Antonio regions. Errors in winds may be related to the complex terrain of the El Paso area, which may not be well-represented at WRF's 4 km grid resolution. In addition, there is a consistent wet bias evident in the humidity plot. The poor performance in both winds and humidity in El Paso may be impacted by overactive summertime convection associated with the North American Monsoon.

MDA8 ozone NMB and NME statistics suggest that overall, 2020 NRTEEM model results to not agree with observations as well as the 2019 model across all regions except El Paso, which may have benefitted from the new El Paso 4 km CAMx domain in the 2020 model. Similar to 2019, we find performance improves substantially when higher observed ozone cutoffs are used.

Next, we developed target plots to provide a concise summary of model performance across sites. The advantage of using target plots rather than other performance metric displays such as soccer plots is that target plots incorporate measurement uncertainty in setting benchmarks for model performance. While the plots indicate acceptable performance (MQI<1.0), more work is needed to make these products a more useful tool for diagnosing model performance issues.

Then we examined the local increment (LI) to MDA8 ozone to measure the CAMx model's ability to estimate ozone production from emissions in a given metropolitan area. Agreement with observed LI was substantially worse in DFW, HGB and San Antonio than with 2019 NRTEEM, mainly due to larger overestimations of background MDA8 compared to the 2019 model. We expect background ozone concentrations may be lower in 2020 due to COVID impacts and the NRTEEM model cannot account for these impacts.

Finally, we presented a case study for the El Paso region during August 1-8, 2020, a period of high observed ozone. Large underestimates of midday peak ozone appear to be influenced by wind errors in the model. In addition, the emission inventory for Ciudad Juarez introduces substantial uncertainty in modeling of El Paso.

3.5.2 Exceptional Event Impact Summary

The NRTEEM system implements and refines the photochemical grid model system used by the TCEQ for SIP modeling by modeling exceptional event impacts and international transport from Mexico in a NRT mode. The system demonstrates usefulness by identifying potential days when exceptional events and international transport may play an important role in ozone exceedances.

NRTEEM includes three sensitivity simulations to identify potential exceptional events and impacts from international transport from Mexico. During April 15-October 15, we found 44 days when the observed MDA8 ozone exceeded 70 ppb and NRTEEM modeled impacts to MDA8 ozone from fires, stratospheric ozone or Mexico anthropogenic emissions equalled or exceeded 0.7 ppb (1% of the NAAQS). Fire and stratosphere ozone contributions may be relevant to attainment for an area depending upon whether they are in the top four highest MDA8 observations at the end of the ozone season and whether the monitor ends up determining the attainment status for an area.

We have presented three case studies that serve as examples of days when high ozone at Texas monitors was potentially influenced by fires, stratospheric ozone and transport from Mexico. The case studies outlined application of the NRTEEM modeling results to understanding causes of high ozone at a monitor and are intended to illustrate strengths in the NRTEEM modeling system as well as areas where additional work is needed.

The NRTEEM modeling system successfully simulated impacts on Texas air quality from distant Wyoming wildfires and from fires burning in East Texas and the Mississippi Valley in October 2020. Although peak 1-hour ozone was underestimated at CAMS 56, the NRTEEM smoke plume simulation matched satellite smoke and AOD retrieval products well and supports a source-receptor relationship between the fires and DFW monitors. The NRTEEM model also simulated an episode of transport from Mexico in which anthropogenic emissions in Mexico produced an ozone impact on monitors in El Paso.

NRTEEM modeled stratospheric impacts were generally smaller in 2020 than in 2019. This may be partly due to weather influences, but another likely cause is the change in the 2020 NRTEEM vertical coordinate system and vertical layer structure. The need for these changes was indicated by the magnitude of the 2019 modeled stratospheric contributions and the fact that they often occurred outside the season and geography where stratospheric ozone intrusions are expected. Sensitivity testing in March 2020 showed that the increased resolution of the model near the tropopause and the new vertical coordinate can improve the simulation of ozone in the lower stratosphere and upper troposphere. During the 2020 NRTEEM modeling, stratospheric ozone contributions were smaller overall than in 2019. In 2019, the largest fraction of stratospheric ozone impacts ≥ 0.7 ppb on days with MDA8 ozone ≥ 70 ppb occurred in the Houston area. In 2020, there were far fewer days with stratospheric ozone impacts ≥ 0.7 ppb on high ozone days and these days were concentrated in the El Paso area. The 2020 geographic distribution of stratospheric ozone impacts is more consistent with the conceptual model of stratospheric ozone intrusions having a greater influence on high elevation areas like El Paso than on low elevation areas like Houston[15].

Even with the overall reduction in the magnitude of stratospheric contributions in 2020, stratospheric air continued to have an occasional influence on ground level ozone in Texas on the order of 5 ppb. Analysis of NRTEEM-diagnosed stratospheric intrusion events in 2019 and 2020 suggests that NRTEEM is able to indicate the influence of these events on surface ozone and can be used to identify events where a diagnostic exceptional event analysis is warranted.

[15] https://www.epa.gov/sites/production/files/2018-11/documents/exceptional_events_soi_guidance_11-8-2018.pdf

4.0 RECOMMENDATIONS FOR IMPROVEMENTS TO MODELING SYSTEM IN 2021

We provide the following recommendations to improve the usefulness of the modeling system:

- Develop a method to identify fires responsible for potential exceptional events by tracking tracers associated with fire emissions across multiple days. These fires can later be tagged for source apportionment analysis to quantify ozone impacts at specific locations.
- Provide Q/D plots through the NRTEEM website for fires above a defined Q/D threshold
- Investigate methods to improve persistent negative biases found on the highest observed ozone days
- Investigate alternate methods of model performance evaluation that incorporate measurement uncertainty
- Investigate alternate sources of near real-time fire emissions if available
- Use the latest available versions of WRF and CAMx model code
- Use an updated emissions inventory from TCEQ if available
- Work with TCEQ to refine the Mexico emission inventory used in the NRTEEM modeling
- Other improvements proposed by TCEQ

In addition, we recommend that TCEQ investigate using WRF’s hybrid vertical coordinate system along with increased vertical resolution in the upper troposphere/lower stratosphere for their SIP modeling efforts.

5.0 REFERENCES

Emery, C., E. Tai, G. Yarwood, and R. Morris, 2011. Investigation into approaches to reduce excessive vertical transport over complex terrain in a regional photochemical grid model. Atmospheric Environment. 45. 7341-7351. 10.1016/j.atmosenv.2011.07.052.

Ek, M., Bill Lapenta, Geoff DiMego, Hendrik Tolman, John Derber, Yuejian Zhu, Vijay Tallapragada, Mark Iredell, Shrinivas Moorthi, Suru Saha. 2014. The NOAA Operational Numerical Guidance System. 29th Session of the World Weather/Climate Research Programme (WWRP/WCRP) Working Group on Numerical Experimentation (WGNE-29) Bureau of Meteorology, Melbourne, Australia, 10-14 March 2014.

Emery, C., E. Tai, and G. Yarwood, 2001. "Enhanced Meteorological Modeling and Performance Evaluation for Two Texas Ozone Episodes." Prepared for the Texas Natural Resource Conservation Commission, prepared by ENVIRON.

Emery, C., Z. Liu, A. G. Russell, M. T. Odman, G. Yarwood and N. Kumar, 2017. Recommendations on statistics and benchmarks to assess photochemical model performance, Journal of the Air & Waste Management Association, 67:5, 582-598, DOI: 10.1080/10962247.2016.1265027.

ENVIRON and Alpine. 2012. Western Regional Air Partnership (WRAP) West-wide Jump-start Air Quality Modeling Study (WestJumpAQMS) – WRF Application/Evaluation. ENVIRON International Corporation, Novato, California. Alpine Geophysics, LLC. University of North Carolina. February 29. (http://www.wrapair2.org/pdf/WestJumpAQMS_2008_Annual_WRF_Final_Report_February29_2012.pdf).

Guenther, A., Karl, T., Harley, P.,Wiedinmyer, C., Palmer, Geron, C. 2006. Estimates of global terrestrial isoprene emissions using MEGAN (Model of Emissions of Gases and Aerosols from Nature), Atmos. Chem Phys., 6, 3181-3210.

Jaffe, D. A., Cooper, O. R., Fiore, A. M., Henderson, B. H., Tonnesen, G. S., Russell, A. G., ... & Moore, T. (2018). Scientific assessment of background ozone over the US: Implications for air quality management. Elementa (Washington, DC), 6(1), 56.

Janssen, S., Guerreiro, C., Viaene, P., Georgieva, E., and Thunis, P. 2017. Guidance Document on Modelling Quality Objectives and Benchmarking, Version 2.1, Forum for air quality modelling in Europe, available at: http://fairmode.jrc.ec.europa.eu/document/fairmode/WG1/Guidance_MQO_Bench_vs2.1.pdf (last access: October 23 2020).

Johnson, J., E. Tai, P. Karamchandani, G. Wilson, and G. Yarwood. 2013. TCEQ Ozone Forecasting System. Prepared for Mark Estes, TCEQ. November.

Johnson, J., G. Wilson, D.J. Rasmussen, G. Yarwood. 2015. "Daily Near Real-Time Ozone Modeling for Texas." Prepared for Texas Commission on Environmental Quality, Austin, TX. January.

Johnson, J., G. Wilson, D.J. Rasmussen, G. Yarwood. 2016a. "Daily Near Real-Time Ozone Modeling for Texas." Prepared for Texas Commission on Environmental Quality, Austin, TX. January.

Johnson, J., G. Wilson, A. Wentland, W. -C. Hsieh, and G. Yarwood. 2016b. "Daily Near Real-Time Ozone Modeling for Texas." Prepared for Texas Commission on Environmental Quality (TCEQ), TX. December.

Johnson, J., G. Wilson, M. Jimenez, T. Shah, R. Beardsley and G. Yarwood. 2017. "Fire Impact Modeling with CAMx." Prepared for Texas Commission on Environmental Quality (TCEQ), TX. July.

Johnson, J., G. Wilson, J. Bandoro, K. Richman, L. Huang, R. Beardsley and G. Yarwood, 2018. Near-Real Time Exceptional Event Modeling. Prepared for Mark Estes, TCEQ. August 2018.

Johnson, J., G. Wilson, S. Kemball-Cook, K. Tanner, Y. Shi, J. Guo, R. Beardsley and G. Yarwood. 2019. Near Real-Time Exceptional Event Modeling. Prepared for Mark Estes, TCEQ. August.

Jolliff J.K., Stow C.A., McGillicuddy D.J. Jr, Doney S.C., Allen J.I., Rose K.A., Wallhead P. 2009. Skill assessment for coupled biological/physical models of marine systems. J Mar Syst 76:4–15.

Kota, S. H., G. Schade, M. Estes, D. Boyer, Q. Ying. 2015. Evaluation of MEGAN predicted biogenic isoprene emissions at urban locations in Southeast Texas, Atmos. Environ., 110, 54-64. doi:10.1016/j.atmosenv.2015.03.027.

Kushta, J., Georgiou, G.K., Proestos, Y. et al. Evaluation of EU air quality standards through modeling and the FAIRMODE benchmarking methodology. Air Qual Atmos Health 12, 73–86 (2019). https://doi.org/10.1007/s11869-018-0631-z.

McDonald-Buller, E., Y. Kimura, C. Wiedinmyer, C. Emery, Z. Liu and G. Yarwood. 2015. Targeted Improvements in the Fire INventory from NCAR (FINN) Model for Texas Air Quality Planning. Prepared for David Sullivan, Texas Air Quality Research Program and The University of Texas at Austin. August.

McNally, D. E., 2009. "12km MM5 Performance Goals." Presentation to the Ad-Hoc Meteorology Group. 25-June. (http://www.epa.gov/scram001/adhoc/mcnally2009.pdf).

Park, S., J.B. Klemp, and J. Kim, 2019: Hybrid Mass Coordinate in WRF-ARW and Its Impact on Upper-Level Turbulence Forecasting. Mon. Wea. Rev., 147, 971–985, https://doi.org/10.1175/MWR-D-18-0334.1.

Pederzoli A., Thunis P., Georgieva E., Borge R., Carruthers D., Pernigotti D. 2012. Performance criteria for the benchmarking of air quality model regulatory applications: the 'target' approach. Int J Environ Pollut 50:175–189. https://doi.org/10.1504/IJEP.2012.051191.

Pernigotti, D., Gerboles, M., Belis, C. A., and Thunis, P. 2013. Model quality objectives based on measurement uncertainty, Part II: NO2 and PM10, Atmos. Environ., 79, 869–878.

Ramboll. 2020. The User's Guide to the Comprehensive Air Quality Model with Extensions Version 7.00. Available at http://www.camx.com (accessed October 23, 2020).

Rolph, G., Stein, A., and Stunder, B. 2017. Real-time Environmental Applications and Display sYstem: READY. Environmental Modelling & Software, 95, 210-228, https://doi.org/10.1016/j.envsoft.2017.06.025

Shah, T., L. Parker, J. Grant and Greg Yarwood. 2018. "Modeling Inventories for Mexico and Caribbean Countries to Support Quantitative Analysis of International Transport Impacts on Ozone Design Values and Regional Haze." Prepared for Texas Commission on Environmental Quality (TCEQ), TX. June.

Skamarock, W. C., J. B. Klemp, J. Dudhia, D. O. Gill, Z. Liu, J. Berner, W. Wang, J. G. Powers, M. G. Duda, D. M. Barker and X-Y. Huang. 2019. A Description of the Advanced Research WRF Model Version 4 (No. NCAR/TN-556+STR). doi:10.5065/1dfh-6p97 (https://opensky.ucar.edu/islandora/object/technotes%3A576/datastream/PDF/download/citation.pdf)

Škerlak, B., Sprenger, M., & Wernli, H. (2014). A global climatology of stratosphere-troposphere exchange using the ERA-Interim data set from 1979 to 2011. Atmospheric Chemistry and Physics, 14(2), 913-937.

Sprenger, M., & Wernli, H. (2003). A northern hemispheric climatology of cross-tropopause exchange for the ERA15 time period (1979–1993). Journal of Geophysical Research: Atmospheres, 108(D12).

Thunis P., Pernigotti D., and Gerboles M. (2013). Model quality objectives based on measurement uncertainty. Part I: ozone. Atmos Environ 79:861–868.

Thunis, P. and Cuvelier, C.: DELTA Version 5.4 Concepts/User's Guide/Diagrams, available at: http://fairmode.jrc.ec.europa.eu/document/fairmode/WG1/DELTA_UserGuide_V5_4.pdf, last access: October 23, 2020.

Wiedinmyer, C., Akagi, S. K., Yokelson, R. J., Emmons, L. K., Al-Saadi, J. A., Orlando, J. J., and Soja, A. J.: The Fire INventory from NCAR (FINN): a high resolution global model to estimate the emissions from open burning, Geosci. Model Dev., 4, 625-641, doi:10.5194/gmd-4-625-2011, 2011.

Wesely, M. L.: Parameterization of surface resistances to gaseous dry deposition in regional-scale numerical models, Atmos. Environ., 23, 1293–1304, 1989.

Yu, H., A. Guenther, C. Warneke, J. de Gouw, S. Kemball-Cook, J. Jung, J. Johnson, Z. Liu, and G. Yarwood, 2015. "Improved Land Cover and Emission Factor Inputs for Estimating Biogenic Isoprene and Monoterpene Emissions for Texas Air Quality Simulations". Prepared for Texas Air Quality Research Program. (AQRP Project 14-016, September 2015).